2017-01-01

Evaluation Of Mechanical Parameters Of Contaminated Road Base And Railway Ballast

Prajwol Tamrakar
University of Texas at El Paso, ptamrakar@miners.utep.edu

EVALUATION OF MECHANICAL PARAMETERS OF CONTAMINATED ROAD BASE AND RAILWAY BALLAST

PRAJWOL TAMRAKAR

Doctoral Program in Civil Engineering

APPROVED:

Soheil Nazarian, Ph.D., Chair

Cesar Carrasco, Ph.D.

Vivek Tandon, Ph.D.

Diane I. Doser, Ph.D.

Charles Ambler, Ph.D.
Dean of the Graduate School

TO

EVERYONE

WHO IS ASSOCIATED

WITH

MY RESEARCH

EVALUATION OF MECHANICAL PARAMETERS OF CONTAMINATED ROAD BASE AND RAILWAY BALLAST

by

PRAJWOL TAMRAKAR, M.S.C.E

DISSERTATION

Presented to the Faculty of the Graduate School of
The University of Texas at El Paso
in Partial Fulfillment
of the Requirements
for the Degree of

DOCTOR OF PHILOSOPHY

Department of Civil Engineering
THE UNIVERSITY OF TEXAS AT EL PASO
May 2017

ACKNOWLEDGEMENTS

First and foremost, I would like to offer my sincerest gratitude to my advisor and graduate committee chair, Professor Soheil Nazarian, for his continuous advice, trust and encouragement during last four years of my doctoral degree. Professor Nazarian supported me throughout my research with his patience and knowledge whilst allowing me a room to work in my own way, taught me the techniques of critical thinking and analysis, and shaped my professional career. He introduced me several nondestructive techniques for evaluating highway pavements and railway tracks. As a result, I have increased my ability to learn and explore advancements in those areas.

My appreciation is also extended to graduate committee members, Professor Cesar Carrasco, Professor Vivek Tandon and Professor Diane I. Doser, for supporting, guiding and providing valuable comments and feedbacks to complete my dissertation.

A very special thanks to Dr. Deren Yuan, Senior Research Associate at the Center for Transportation Infrastructure Systems (CTIS). From the very first day at CTIS, Dr. Yuan guided me and explained me about the theoretical and experimental backgrounds of the researches related to nondestructive seismic testings. His expertise in analyzing the data for the Spectral Analysis of Surface Waves (SASW) test, Portable Seismic Property Analyzer (PSPA) test and Free-Free Resonant Column (FFRC) test helped to create building blocks of my dissertation. I would also like to thank Dr. Hoda Azari, NDE Program Manager at Federal Highway Administration, for teaching me to conduct the SASW tests on railway tracks.

I would also like to appreciate contributions of Dr. Imad Abdallah, Executive Director of CTIS, for providing technical suggestions to improve my dissertation; Mr. Jose Garibay, Laboratory Manager at CTIS for managing materials for the experiments and teaching several laboratory tests; Dr. Cesar Tirado, Research Associate at CTIS, for providing technical advices; Mr. Sergio Rocha, Research Associate at CTIS, for technical supports during field experiments.

I would like to thank my colleagues of CTIS- Jose Luis Ramirez, Aaron Arce, Yair Morales, Jose Luis, Jannet Hernandez, Miguel Antonio Perez, Uriel Rocha, Sarvesh Dhakal, Claudio Pereira, Jorge Velarde, Jorge Beltran, Victor Garcia, Paloma Zamarripa, Guilherme Barbosa de Castro, Pablo Cobos and others for their help and support for conducting laboratory and field experiments.

I am very much grateful toward my father Laxmi Narayan Tamrakar, mother Sharmistha Tamrakar, sister Pratistha Tamrakar, brother Prafulla Tamrakar and wife Smriti Rajkarnikar Tamrakar for their unconditional love, care, encouragement and support at the time of need.

Lastly, I would like to thank the research projects sponsored by the USDOT University Transportation Center Program and Federal Railroad Administration for supporting to purse my doctoral degree.

ABSTRACT

This dissertation comprises two topics in the area of transportation geotechnics that focus on the evaluation of stiffness parameters of contaminated road base and railway ballast. The abstracts of these two studies are provided in the following two paragraphs.

The performance of a flexible pavement depends on the mechanical characteristics of its unbound granular base layer. The mechanical characteristics such as stiffness and deformation resistance depend on many factors such as the material gradation, fines content, moisture content, physical properties of coarse aggregate and more. The base materials are often contaminated by the excessive fines that is caused by improper material handling, migration of fines from subgrade and the other reasons. The moisture content of base layers may alter during pavement construction and operation by exposure to excessive water and percolation of rainwater from pavement surfaces. In this research, the mechanical behaviors of contaminated base materials were evaluated to understand the effects on the performance of the pavements. Twelve different test sequences were performed with a combination of moisture contents from dry to wet of optimum moisture content and four different fines contents through laboratory and simulated field tests. An increase in moisture content was typically detrimental to the mechanical properties of the base material. However, the increase in the fines contents yielded mixed results.

One of the major challenges associated with railway systems is the degradation of the railway tracks with time. The ballast that forms the major supporting structure of the railway track degrades mainly due to the application of train dynamic loads, changes in climatic conditions and interaction of ballast and the underlying subgrade. The contamination of the ballast (also known as ballast fouling) due to the penetration of clay, rock dust, coal or any other agent accelerates track degradation, and affects the stability of the ballast in particular and the track in general. In this research, the roles of fouling agents and moisture content were evaluated to understand the effects on the mechanical characteristics of ballast. Thirteen different tests sequences were performed with a combination of two different fouling agents at three degrees of fouling and three

different moisture contents through simulated field tests. The fouling agents directly impacted the physical properties of ballast by replacing the void spaces in ballast by fine particles and disturbing the structural integrity of ballast particles. The effect of contamination on the performance of the ballast was highly dependent on the type of fouling agent. For clay-fouled specimens, the increase in the degree of fouling and the moisture resulted in significant reduction in the deformation resistance and load bearing strength.

TABLE OF CONTENTS

LIST OF TABLES

LIST OF FIGURES

CHAPTER 1 INTRODUCTION

This dissertation is comprised of two topics in the area of transportation geotechnics. The first topic is focused on the evaluation of the stiffness parameters of a contaminated road base through laboratory and simulated field tests. The second topic is associated with the evaluation of the stiffness parameters of a contaminated railway ballast through simulated field tests.

The following sections provide an overview of the two topics. The background information, research approach and testing procedures, and test results for those topics are provided in Chapters 2 and 3. Chapter 4 provides the summary and conclusions for both topics.

1.1. Overview of Research

1.1.1. Base Materials

Stresses and deformations within pavement layers due to vehicular loads decrease gradually with depth. The ability of the base layer to safely distribute the stresses from the surface course to the subgrade affects the performance and life span of the pavement. The amount of fines (aggregates passing sieve number 200 or smaller than 75 microns) and water content of the base play important roles in achieving satisfactory performance. National and state transportation agencies usually limit the amount of fines in the base materials. However, contamination with excessive fines may detrimentally affect the mechanical properties of the base layers. Although the moisture content is controlled during construction, the moisture level can vary during the pavement operation phase due to climatic changes. During the rainy season, the pavement layers are subjected to high moisture contents. After evaporation and drainage, the moisture content may drastically reduce below the optimum level. These variations in moisture content are likely to affect the material properties and pavement performance. The intrusion of excessive moisture into the geomaterials with plastic fines results in a softening behavior that affects the material

properties negatively. It is essential to understand the effects of fines and moisture content on the mechanical characteristics of base materials.

The mechanical characteristics of the geomaterials, such as Young's modulus and shear strength, depend on many factors such as the material gradation, fines content, moisture content, physical properties of coarse aggregates (e.g., surface roughness and hardness), type of aggregates (e.g., crushed or uncrushed), mineralogy of aggregates, plasticity of fines. In this study, the mechanical characteristics of the base materials are investigated through laboratory and small-scale tests. Laboratory tests include the index and mechanical tests that ensure the quality of the available material for pavement construction. Small-scale tests include the scenarios that resemble tests under controlled field conditions for quality control purposes.

1.1.2. Ballast

The rail network, an important part of the transport system in the US, is comprised of more than 160,000 miles of tracks. About two-fifths of the intercity freight and one-third of the nation's exports depend upon the railway industry (ASCE 2013). One of the major challenges associated with the railway systems is the degradation of the railway tracks with time. The ballast that forms the major supporting structure of the railway track degrades mainly due to the application of train dynamic loads, changes with climatic conditions and interaction of ballast and the underlying subgrade. The contamination of the ballast (also known as ballast fouling) due to the penetration of clay, rock dust, coal dust or any other agent accelerates track degradation, and affects the stability of the ballast in particular and the track in general.

In this research, the mechanical characteristics of clean and fouled ballast were investigated through small-scale experiments that simulated field conditions in the laboratory under controlled material properties, moisture conditions and applied loads on the specimens.

1.2. Statement of Problem

1.2.1. Base Materials

Historical data pertaining to the evaluation of pavement performance have shown that most pavement distresses originate from the underlying pavement layers. Table 1.1 provides a summary of these distresses as reported by Saeed et al. (2001). For example, one of the common distresses in flexible pavements is rutting (permanent deformation). Permanent deformation of the base layer may occur due to insufficient compaction, excessive moisture content and/or poor material quality (Fleming et al. 2000). Fine particles (fines) in an unbound aggregate base contribute to attaining sufficient compaction level, and hence, provide stability to the pavement system. Excessive fines can cause contamination in the base material resulting in increase in the moisture susceptibility and reduction of stiffness properties. The presence of excessive fines in unbound aggregate base can be due to segregation of material during pavement construction or contamination of material from underlying subgrade soil during pavement life.

The combined effects of excessive fines and moisture content can be detrimental in cold climates. Konrad and Lemieux (2005) studied the influence of fines on the frost susceptibility of geomaterials in the laboratory using freezing tests. The authors considered granitic (non-plastic) fines and kaolinite clay (plastic) fines. They found that the frost susceptibility of the aggregates increases with both types of fines.

A survey of the State Departments of Transportation (DOTs) in the US and transportation agencies in Canada by Tutumluer (2013) found that 33 out of 46 respondents limited the fines in the base to less than 12% while five respondents allow more than 15% fines. Some of respondents indicated that they did not differentiate between plastic and non-plastic fines. The degree of variation in the stiffness properties of the base materials should be assessed to determine the optimal amount of fines.

Table 1.1 Summary of Flexible Pavement Distress, Contributing Factors and Related Test Parameters (Saeed et al. 2001)

Type of Distress	Description of Distress	Base Failure Manifestation	Contributing Factors	Possible Related Test Parameter
Fatigue Cracking (Alligator Cracking)	Appears as fine, longitudinal hairline cracks parallel to one another in the wheel path in the direction of traffic. Progression of distress is signaled by interconnection of cracks forming many-sided, sharp angled pieces. As cracks become wider, spalling may occur.	High deflection/strain in the asphalt concrete surface due to lack of base stiffness. Alligator cracking only occurs in areas where repeated wheel loads are applied. High flexibility in the base or inadequate thickness of base allows for excessive bending strains in the asphalt concrete surface. Changes in base properties with time can render the base inadequate to support loads.	Low modulus Improper gradation High fines content High moisture level Lack of adequate particle angularity and surface texture. Degradation under repeated loads and freeze-thaw cycling.	Resilient Modulus Gradation & fines content Frost susceptibility Density
Rutting/ Corrugations	Long surface depressions in the wheel path that may not be noticeable except during and following rains. Pavement uplift may occur along the sides of the rut. Resulting from permanent deformation in one or more pavement layers or subgrade, usually caused by consolidation and/or lateral movement of the materials due to load.	Lateral displacement of particles with applications of wheel loads due to inadequate shear strength resulting in a decrease in the base layer thickness. Consolidation of the base due to inadequate initial density or changes in base properties with time due to poor durability or frost effects may also cause rutting.	Low shear strength Low density of base material Improper gradation High fines content High moisture level Lack of adequate particle angularity and surface texture. Degradation under repeated loads and freeze-thaw cycling.	Angle of internal friction Cohesion Gradation Fines content
Depressions	Depressions are localized low areas in the pavement surface caused by settlement of the foundation soil or consolidation in the subgrade or base/ subbase layers due to improper compaction.	Inadequate initial compaction or nonuniform material conditions results in additional reduction in volume with load applications. Changes in material conditions due to poor durability or frost effects may also result in localized densification with eventual fatigue failure.	Low density of base material	Density
Frost Heave	Frost heave appears as an upward bulge in the pavement surface and may be accompanied by surface cracking resulting in potholes. Freezing of underlying layers resulting in an increased volume of material causes the upheaval. An advanced stage of distortion mode of distress resulting from differential heave is surface cracking with random orientation and spacing.	Ice lenses are created within the base/subbase during freezing temperatures, particularly when freezing occurs slowly, as moisture is pulled from below by capillary action. During spring thaw large quantities of water are released from the frozen zone, which can include all unbound materials.	Freezing temperatures Source of water Permeability of material high enough to allow free moisture movement to the freezing zone.	Gradation Fines Content Fines Type

1.2.2. Ballast

Several well-documented railway incidents in the past have been attributed to unstable tracks caused by the fouled ballast. Huang et al. (2009) mentioned two incidents of derailment in Wyoming due to coal dust fouling. The Federal Railroad Administration (FRA) reported that the July 2013 accident in Bronx, NY was due to presence of fouled ballast sections in the railway track (NTSB 2013).

The fouling material usually interrupts the draining function of the track, and the accumulated excessive moisture results in an unstable track. Bailey et al. (2011) reported that the excessively settled tracks in Québec, Canada were due to a blockage in a drainage system within the track caused by the fouled ballast formed with clay and sand. Another consequence of fouled ballast is track settlement. Han and Selig (1997) evaluated the settlement behavior of ballast contaminated with clay and silt using a ballast box. The authors reported that the ballast settlement increased with the increase in the degree of fouling and moisture content.

The railway accidents due to fouling can be minimized if the tracks are regularly monitored for the loss of mechanical properties due to fouled ballast. In this research, several small-scale experiments were conducted to understand the role of fouled ballast on the stability of the track.

1.3. Objective and Scope

1.3.1. Base Material

Although the performance of pavements is influenced by multiple factors, this study is focused on understanding the role of the base layer to maintain the stability of pavement systems. The main factors influencing the responses of the base layer during construction and operation phases are vehicle loading characteristics, precipitation and ground water table, and the strength characteristics. The vehicle loading characteristics affect the magnitude of the stresses experienced by the base whereas the climatic conditions affect the variation in its moisture content and stiffness.

Due to combined effects of vehicle loading and climatic condition, it is desirable to evaluate the stiffness parameters (e.g., modulus, and permanent deformation resistance) of the base materials, and to model their effects on the pavement performance and the estimated life of pavements.

The objectives of this study can then be categorized in the following bullets:

- To evaluate the stiffness parameters of base materials with various fines contents and moisture contents;
- To understand the impact of the variations in fines content and moisture content of base materials on their performance;
- To develop a relationship among the stiffness parameters, fines content and moisture content; and
- To correlate the stiffness parameters obtained from the laboratory and field methods.

1.3.2. Ballast

As some of the characteristics of rail tracks and pavements, such as the layering mechanism of the materials, the distribution of stresses and the use of geomaterials, are common, the material characterization techniques used for pavements can be potentially adopted for rail tracks with appropriate modifications. The nondestructive testing (NDT) devices such as a Light-Weight Deflectometer (LWD) and a Portable Seismic Property Analyzer (PSPA) used in pavements can be implemented to measure the moduli of ballast specimens. The Spectral Analysis of Surface Waves, Impulse Response and Load-Deformation tests can also be conducted.

In this study, several specimens were prepared with known degree of fouling with two common types of fouling agents, clay and rock dust, to evaluate mechanical properties of fouled ballast. The degrees of fouling considered were 0%, 20% and 50% by weight of the total ballast. The 50% fouled ballast represented the heavily-fouled specimen whereas the 20% fouled ballast represented the moderately-fouled specimen. The specimens were prepared at three different moisture conditions — dry, saturated and wet. The saturated specimens represented the condition

of ballast after heavy rain whereas the wet specimens represented the partially dried specimens after saturation.

The objectives of this research can be categorized as:

- To evaluate the impacts of two types of fouling agents, clay and rock dust, on the mechanical properties of ballast;
- To measure the stiffness parameters of clean and fouled ballast at various degrees of fouling and moisture contents, and;
- To understand the effects of fouling on the performance of rail tracks.

1.4. Organization of Dissertation

Aside from this chapter, the dissertation contains 3 chapters. Chapter 2 is dedicated to the research associated with the base materials. That chapter contains three sections. Section 2.1 provides background information and review of the literature related to the characteristics of unbound granular materials used as road base and methods for characterizing those materials. Section 2.2 describes the research approach and testing procedures. It explains the procedure of preparing different aggregate mixes for testing. The mixes are differentiated by the percentage of fines content. That section also explains the ranges for varying the moisture contents of the mixes. The types and procedures of different tests for the laboratory and the small-scale tests are also explained in that section. Section 2.3 presents the results from the laboratory and small-scale tests. In addition, that chapter provides comparisons of the laboratory and small-scale test results to understand how the outcomes of the laboratory tests reflect on the field performance.

Chapter 3, which is dedicated to ballast fouling, consists of three sections as well. Section 3.1 provides background information and review of the literature related to the effects of ballast fouling, characterization techniques of clean and fouled ballast in the laboratory and in the field, and the proposed nondestructive techniques for determining the mechanical properties of the clean and fouled ballast. Section 3.2 describes the research approach and testing procedures. The

procedure for preparing the fouled ballast specimens from two types of fouling agents is also described. That section also explains the procedures for conducting different tests for the small-scale experiments. Section 3.3 presents the results from the small-scale experiments. In addition, the outputs from different small-scale experiments are compared to show the relationships among different stiffness parameters.

Chapter 4, which is the last chapter of the dissertation, summarizes both studies in two sections. Section 4.1 provides the summary of the research associated with the base materials. The research outcomes and the lessons learned are also provided as the concluding remarks of the research. On the same way, section 4.2 provides the summary and concluding remarks.

CHAPTER 2 EVALUATION OF STIFFNESS PARAMETERS OF CONTAMINATED ROAD BASE

2.1. Background

This section focuses on the review of the literature with an emphasis on the behavior of the base materials, the role of fines content and moisture content on mechanical characteristic of bases, various challenges associated with base materials during design and constructions, and the methods for characterizing base materials.

2.1.1. Factors Affecting Stiffness of Base Materials

The load distribution mechanism in mechanically stabilized bases depends on particle interlocking and particle friction. The stresses experienced by the base layer mainly due to the moving vehicles are not uniform; rather the stresses are concentrated along load carrying particle chains formed by the coarse aggregates. Mechanical behavior of unbound granular bases is influenced by parameters such as stress sensitivity, nonlinearity, and anisotropy (Karasahin et al. 1993).

Stress sensitivity is associated with hardening and softening behaviors of material under repeated vehicle loads (Von Quintus and Killingsworth 1998). The hardening behavior results in a greater strength and stiffness under the repeated loads. Similarly, the softening behavior results in the reduction in the material strength or stiffness. The repeated load triaxial (e.g., resilient modulus) tests can be used to characterize the hardening and softening behaviors of base materials.

Nonlinearity refers to the response of the material in terms of strain due to an applied stress. A base layer has a linear response for small strains and nonlinear response at higher strains. Ishihara (1996) mentioned that soils exhibit linear elastic behavior below a strain of 10^{-2}% and nonlinear elasto-plastic behavior in the strain range of 10^{-2}% to 1%. The magnitude of the strain experienced by a base layer is a function of the applied load and mechanical characteristics of the

pavement layers. Sawangsuriya et al. (2006) stated that a typical range of strains experienced by bases was 10^{-2}% to 1% that fell under a nonlinear response range.

Anisotropy relates to the differences in the behavior of a material in different directions. The anisotropy can be either inherent or load induced (Salehi et al. 2008). The inherent anisotropy is due to the orientation of coarse aggregates in the base layer; whereas the load-induced anisotropy is related to the magnitude of stress or strain in various orientations at a location within the base layer due to moving vehicle load.

Gradation, moisture content and degree of compaction of base materials affect their constitutive models, and hence, their stiffness. Richter (2006) and Cary and Zapata (2010) discussed the impact of moisture content on the in-situ moduli of the pavement materials. The other factors that can also affect the stiffness of the base materials are surface roughness, angularity and asperity of the aggregates. Pan et al. (2006) studied the aggregate morphological indices of pavement geomaterials with an image analysis approach. They observed that the resilient modulus noticeably increased when the aggregate angularity and surface roughness increased.

2.1.2. Roles of Fines Content, Gradation and Moisture Contents of Base Materials

Thompson and Smith (1990) and Tian et al. (1998) showed that fines content can affect the strength of road construction materials. The alternation of fines content in a base material may result in a different packing order and void distribution and packing density. Other factors, such as the maximum aggregate size, particle size distribution of coarse aggregate and shape of coarse aggregate, also play important roles in the achieved packing density. One of the methods of estimating the packing density is by measuring the "fine fraction porosity" that is a ratio between the total voids in the aggregate matrix and the total voids if the entire matrix comprised of the coarse particles only (Bilodeau et al. 2009). The change in the material gradation due to the variation in the fines content has the potential to replace the contact spaces between the aggregates by the fines. This phenomenon may alter the load carrying capacity through particle-to-particle contacts in an aggregate matrix. The permeability of a material decreases, and its frost

susceptibility and moisture susceptibility increase with an increase in the material packing density. As such, base materials with high fines contents are not suitable for drainage and frost-protection purposes.

Hicks and Monismith (1971) reported that the resilient modulus of partially crushed aggregates with fines contents in excess of 10% was lower than the fully crushed aggregates with the same amount of fines. They indicated that crushed aggregates with more surface contact points contributed to the increased resilient modulus behavior. However, this effect on the resilient modulus was minimal when the fines contents were in the range of 2% to 10%. Jorenby and Hicks (1986), Kamal et al. (1993) and Lekarp et al. (2000) reported that the voids in the aggregate mix prepared from well-graded aggregates were usually replaced by fines to a certain level, and that this phenomenon attributed to an increase in the resilient modulus. On the contrary, Barskale and Itani (1989) observed a significant reduction in the resilient modulus when the fines content increased from 0% to 10%.

Yideti et al. (2014) studied the role of particle size and shape of granular materials and their impacts on the resilient behavior of the base materials. The authors adopted a packing theory approach to understand the influence of the porosity of the material posed by the granular materials on the deformational behavior of the entire pavement structure. The following three key parameters were used for studying the resilient behavior:

- Primary structure (coarse grain particles that form the load-carrying network of unbound granular materials),
- Primary structure porosity (the fraction of the volume of voids in the primary structure over the total volume of granular mix) and
- Coordination number (the average number of contact points per particle of primary structure as a function of porosity).

The authors observed an increase in the resilient modulus of the materials with primary structure porosities between 32% and 47% (coordination number between 9.6 and 6.4) and a

decrease in the resilient modulus for primary structure porosities greater than 50% (coordination number less than 6). They concluded that the fines that filled the pore spaces and decreased the primary structure porosity could contribute to the increment of resilient modulus of the base.

The variation in the material gradation impacts the pavement design and construction procedures (Thom and Brown 1988; Dawson et al. 1996; and Lekarp 1999). The studies performed by Kolisoja (1997) using aggregates with similar grain size distributions and fines contents showed that the resilient modulus increased with increasing the maximum particle size. An increase in the particle size decreased the particle-to-particle contact resulting in a lower total deformation and consequently a higher stiffness.

Santha (1994); Malla and Joshi (2008); and Yau and Quintus (2002) estimated the resilient modulus of granular materials based on their gradations. Those studies demonstrated that the resilient behaviors of the base materials measured with the resilient modulus testing method were influenced by the fines content. Gidel et al. (2001) stated that the permanent deformation of pavement layers could be controlled by adopting a well-graded gradation of the unbound granular materials and introducing about 6% to 10% fines to achieve a high density.

The variation in the moisture content of the base material results in the alternation of the degree of saturation that ultimately impacts the pore water pressure or the suction properties of the materials (Dawson et al. 2000). The mechanical parameters of the materials may vary with changes in the suction properties. Several authors (e.g., Raad et al. 1992; Yuan and Nazarian 2003; Richter 2006; and Cary and Zapata 2010) studied the impact of the moisture content on the strength and stiffness of the base materials. The amount of moisture present in most granular materials has been found to influence the resilient response of the materials in both the laboratory and in-situ conditions. Lekarp et al. (2000) reported that the resilient modulus of the base material showed a drastic decrease as the saturation level reached 100%. Similarly, Ekblad and Isacsson (2006) measured the resilient moduli of the coarse granular materials at various moisture contents up to saturation. The authors reported that the materials with high fines contents showed a significant

reduction in their resilient moduli whereas the materials with less fines contents showed a minor reduction in their resilient moduli even when the moisture content increased up to saturation.

2.1.3. Base Material Characterization for Design and Construction

The variation of particle size in the mix contributes to the heterogeneous nature of the base, and the orientation of course particles contributes to the anisotropic behavior of the base. Although heterogeneity and anisotropy are simplified for pavement design purposes, the modeling and construction process of base course encounter many constraints posed by the fines content, material handling, contamination of material, methods use for construction, approaches for quality control and more.

2.1.3.1 Variation of Fines Content

The stability of the aggregate matrix of the base material depends on the amount of fines available to fill the void spaces (Ghabchi et al. 2013). The deficiency of the fines in the mix may result in an unstable matrix due to excessive movement of the coarse particles with respect to one another. Excessive fines may also result in an unstable matrix due to the replacement of the contact points of the granular materials by fines. In both of these scenarios, the materials exhibit a lower shear strength and resilient modulus possibly resulting in excess permanent deformation. Several researchers have proposed the optimum fines contents (Gray 1962; and Tutumluer and Seyhan 2000) or optimum gradation (Brown and Chan 1996) in order to obtain the maximum strength parameters. The optimum fines content depends on several factors including the type of coarse aggregates, the shape and size of the coarse aggregates, and the type of fines.

2.1.3.2 Improper Material Handling

Although it is possible to control the material gradation and moisture content in the laboratory, it is not feasible to control these parameters accurately in the field during construction. Improper material handling may lead to aggregate segregation resulting in a non-uniform

distribution of the fines in the aggregate mix (Nohl and Domnick 2000; Rauch et al. 2000). The aggregate segregation may contribute to the variation in the degree of compaction and may cause the reduction in the shear strength, stiffness and deformation resistance throughout the pavement sections (Tutumluer 2013).

2.1.3.3 Contamination of Unbound Aggregates

The contamination of the unbound aggregate layer during the pavement operational phase may influence the pavement performance. The migration of fines from the subgrade can contaminate the base (Alobaidi and Hoare 1996; Chapuis et al. 1996). The possibility of the migration of the fines is exaggerated by a) high water table during the rainy season, b) the lack of a separating layer between the base and subgrade, and c) the degrading subgrade or the use of a poor quality subgrade.

2.1.3.4 Variation in Methods of Compaction

The impact methods are typically used in the laboratory to compact the materials whereas the vibratory methods are adopted in the field to compact the layers of geomaterials. The mechanical responses of the granular materials after compaction may be different due to the differences in the compaction methods. Kaya et al. (2012) performed a comparative study between the impact and vibratory compaction methods on the unbound granular materials. The authors found that the impact method changed the gradations of the materials due to crushing and breakage of the particles. The change in the gradation of the materials resulted in an alteration of the optimum moisture content (OMC). The authors reported that higher California Bearing Ratios (CBR) were achieved for the materials compacted with the vibratory methods but higher resilient moduli were obtained for the materials compacted with the impact method.

2.1.3.5 Differences in Quality Control Approaches

One of the crucial steps in the construction of pavements is proper quality control and quality assurance to ensure the constructed pavements meet the design requirements. The Proctor tests are performed in the laboratory to attain the maximum density and the optimum degree of compaction, whereas the nuclear density tests are conducted in the field to estimate the density as a quality measure (White et al. 2006). In this scenario, a gap between the laboratory and field tests exists that may result in undesirable outcomes in the context of the quality control. Moreover, a clear relationship between the material performance in the laboratory and in the field is required to validate the test results obtained from the pavement construction sites.

2.1.4. Methodology for Characterization for Design and Construction

The elasto-plastic behavior of the unbound aggregate bases affects the strength characteristics of that layer (Habiballah and Chazallon 2005; Huang et al. 2010). Although the stress-strain response of the bases for short-term loading may be linear, the responses for long-term loading posed by a large number of repeated vehicle loads could be nonlinear. In other words, the design methods based on the elasticity of the materials cannot be used to estimate the plastic strains accumulating in the granular layer of pavement systems.

A comprehensive review of the common test methods applied to the unbound granular materials for determining the pavement performance is provided by Saeed et al. (2001). During the early developmental period of the pavement design procedure, the soil strength parameters such as the CBR value, Hveem R-value, and Soil Support Value (SSV) were used. These parameters were adopted with the assumption that the failure in the pavement occurred in the weakest pavement layers, i.e. the subgrade. However, the failure of the flexible pavement may occur due to the excessive rutting or cracking of the pavement layers, and the softening caused by the surface layer cracking (Brown and Chan 1996). The 1993 AASHTO pavement design guide recommended the use of the resilient modulus instead of the parameters such as CBR and SSV.

The resilient modulus tests allow for the characterization and modeling of the elasto-plastic and the softening and hardening behaviors of the granular materials in the pavement materials.

In general, the strength and stiffness tests are conducted for characterizing the strength, modulus, and permanent deformation behaviors of the unbound aggregate materials in pavement systems. The strength and stiffness tests listed by Saeed et al. (2001) are provided in Table 2.1. Out of these tests, the triaxial tests are the most common strength tests and the resilient modulus tests are the most common stiffness tests.

Table 2.1. Tests for Unbound Granular Materials (from Saeed et al. 2001)

Property Measured	Test
Shear Strength	Static Triaxial Shear Repeated Load Triaxial Unconfined Compression Direct Shear CBR Hveem Stabilometer
Stiffness	Resilient Modulus Resonant Column

2.1.4.1 Traditional Tests for Unbound Granular Materials

Out of many available tests for the unbound granular materials, three types of tests – unconfined compressive test, resilient modulus test and permanent deformation test, are discussed below.

Unconfined Compression Test

The unconfined compression tests are common methods to determine the unconfined compressive strength (UCS) of granular materials used in pavements (Schnaid et al. 2001; Piratheepan et al. 2010; Wen et al. 2010). TXDOT follows test procedure Tex-117-E for determining UCS of granular materials. The testing system consists of a loading frame with a crosshead mounted hydraulic actuator to measure applied load and induced deflection, and a data acquisition system Figure 2.1a. A typical result of the unconfined compression test is shown in

Figure 2.1b. The maximum stress experienced by the specimen (or the stress at failure of specimen) is the UCS.

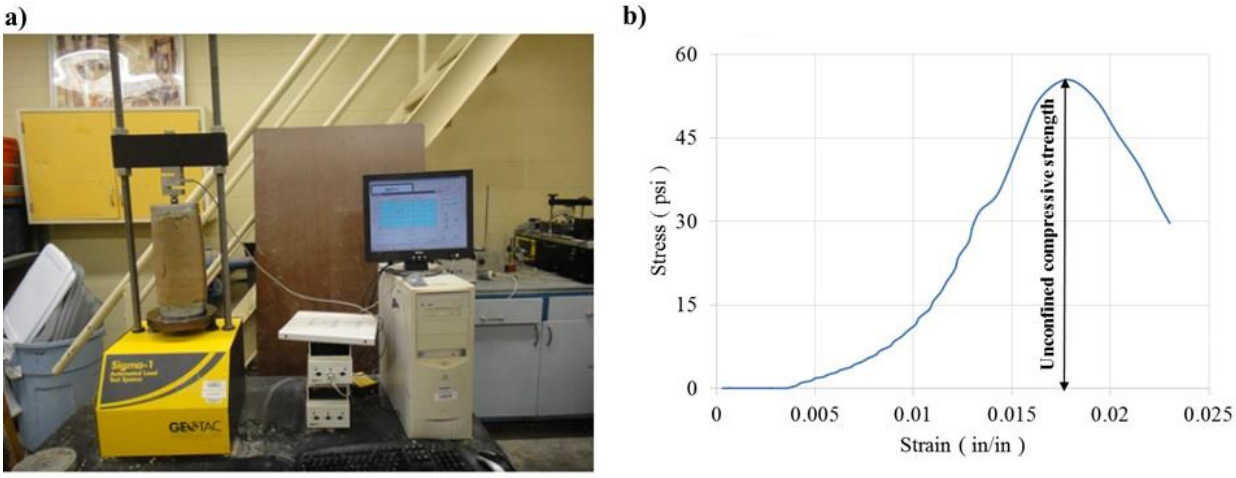

Figure 2.1. Unconfined compression test: a) Test setup and b) Typical output

Resilient Modulus Test and Permanent Deformation Test

One of laboratory methods advocated for determining these two parameters is the repeated load triaxial test as per AASHTO T-307. The testing system consists of a loading frame with a crosshead mounted hydraulic actuator (Figure 2.2a). A load cell is attached to the actuator to measure the applied load. The specimen is housed in a triaxial cell where a confining pressure is applied. As the actuator applies the repeated load, specimen deformation is measured by a set of linear variable differential transducers (LVDTs) or noncontact sensors. A data acquisition system records all data during testing.

The resilient modulus determined from the repeated load triaxial test is defined as the ratio of the repeated axial deviator stress to the recoverable or resilient axial strain:

$$M_r = \frac{\sigma_d}{\varepsilon_r} \qquad \textbf{Equation 2.1}$$

where M_r is the resilient modulus, $\sigma_d = (\sigma_1 - \sigma_3)$ is the deviator stress, and ε_r is the resilient (recoverable) strain in the vertical direction (see Figure 2.2b).

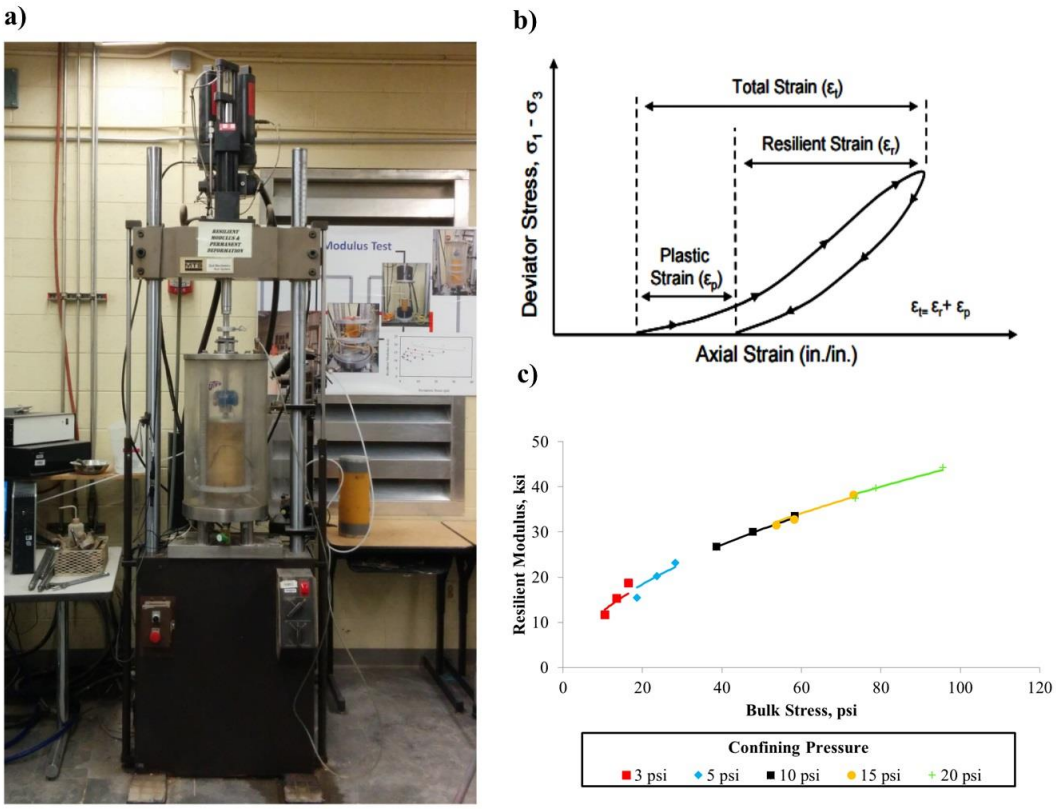

Figure 2.2. Resilient Modulus and Permanent Deformation Test: a) Test setup, b) Specimen response during Resilient Modulus Test (From Buchanan 2007) and c) Typical result obtained from Resilient Modulus Test

The load cycle duration is 1 second that includes a 0.1 second load duration and a 0.9 second rest period. The test is started by applying 1000 repetitions of a load equivalent to a maximum axial stress of 15 psi at a confining pressure of 15 psi. This is followed by a sequence of loadings with varying confining pressures and deviator stresses as tabulated in Table 2.2. These loading cycles are slightly modified from AASHTO T-307 in that the specimen is subjected to 25 repeated axial loads for each sequence instead of 100 cycles. A typical result obtained on a base material is shown in Figure 2.2c. Tutumluer (2013) provided a comprehensive review of the resilient modulus models for determining model parameters from the measured data. The Mechanistic Empirical Pavement Design Guide (MEPDG) recommended the following relationship to compute the representative resilient modulus (M_R) of unbound aggregates and fine-grained soils.

$$M_R = K_1\, p_a \left(\frac{\theta}{p_a}\right)^{K_2} \left(\frac{\tau_{oct}}{p_a} + 1\right)^{K_3} \qquad \textbf{Equation 2.2}$$

where θ is the bulk stress = $\sigma_1 + \sigma_2 + \sigma_3$, τ_{oct} is octahedral shear stress = $1/3[(\sigma_1 - \sigma_2)^2 + (\sigma_1 - \sigma_3)^2 + (\sigma_2 - \sigma_3)^2]^{1/2}$, p_a is atmospheric pressure, and K_1, K_2, *and* K_3 are constants obtained from experimental data.

Table 2.2. Loading sequences for Resilient Modulus (MR) and Permanent Deformation (PD) Tests (From Gandara 2004)

Sequence	Confining Pressure		Contact Stress		Cyclic Stress		Maximum Stress		N_{rep}	Tests
	kPa	psi	kPa	psi	kPa	psi	kPa	psi		
Conditioning	103.5	15	10.4	1.5	93.1	13.5	103.5	15	1000	PD
1	20.7	3	2.1	0.3	18.6	2.7	20.7	3	25	MR
2					41.4	6	41.4	6		
3					62.1	9	62.1	9		
4	34.5	5	3.4	0.5	31.1	4.5	34.5	5	25	
5					69	10	69	10		
6					103.5	15	103.5	15		
7	69	10	6.9	1	62.1	9	69	10	25	
8					138	20	138	20		
9					207	30	207	30		
10	103.5	15	10.3	1.5	58.6	8.5	69	10	25	
11					103.5	15	103.5	15		
12					207	30	207	30		
13	138	20	13.8	2	89.7	13	103.5	15	25	
14					138	20	138	20		
15					276	40	276	40		

The deformation responses of a base due to the repeated applied loads contains resilient and plastic or non-recoverable deformations (Figure 2.2b). The measure of cumulative non-recoverable deformations up to the end of the loading cycles, which provides the information about the plastic deformation of the base, is essential to understanding its rutting behavior. The conditioning phase of the resilient modulus test can be utilized for determining the permanent deformation of a specimen.

2.1.4.2 Nondestructive Tests for Unbound Granular Materials

The common nondestructive test methods of characterizing the base materials are the Free-Free Resonant Column (FFRC, Celaya et al. 2006; Williams and Nazarian 2007; Mazari et al. 2014), the Portable Seismic Property Analyzer (PSPA, Celaya et al. 2006) and the Light Weight Deflectometer (LWD, Von Quintus et al. 2009; Mazari et al. 2014).

Free-Free Resonant Column (FFRC) Test

The FFRC test was originally developed for the concrete specimens (ASTM C215). The test was modified for base and subgrade materials through hardware and software modifications (Stokoe et al. 1994; Nazarian et al. 2003). The FFRC test uses an instrumented hammer as an impulse source for generating impulsive waves over a range of frequencies, an accelerometer to capture the generated waves, and a data acquisition and data processing system. The propagated waves have one or more resonating frequency(ies) that depends upon the dimensions and stiffness of the specimen. The resonant frequencies (longitudinal and possibly shear resonant frequencies) are identified. Figure 2.3 shows the FFRC test and the output of test in form of frequency response.

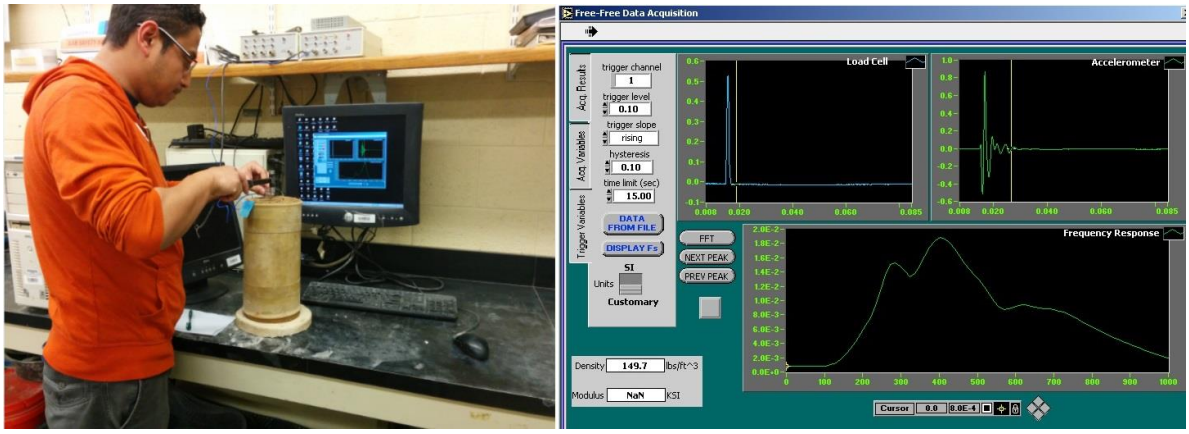

Figure 2.3 The FFRC test (left) and output of the test (right)

The modulus (E) of the specimen is provided by (Richart et al. 1970):

$$E = \rho (2f_c L)^2 \qquad \text{Equation 2.3}$$

where L is the length of the specimen, fc is the fundamental mode frequency related to the specimen vibration and ρ is the mass-density of the specimen.

Portable Seismic Property Analyzer (PSPA) Test

The PSPA consists of two accelerometers and a source packaged into a hand-portable system (Figure 2.4). The source produces an impulsive impact on the material surface that generates stress waves. The signals of the stress waves are captured by two accelerometers. The fast Fourier analysis of the signals are performed to compute the average shear wave velocity (V_s) of the material with an appropriately assumed Poisson's ratio. The low-strain or linear elastic modulus (E) (also termed as a seismic modulus; Nazarian et al. 2003) of a layer is, then, derived with the Poisson's ratio (υ) and mass-density(ρ) of the material using following equation:

$$E=2\,\rho\,V_s^2\,(1+\upsilon) \qquad \text{Equation 2.4}$$

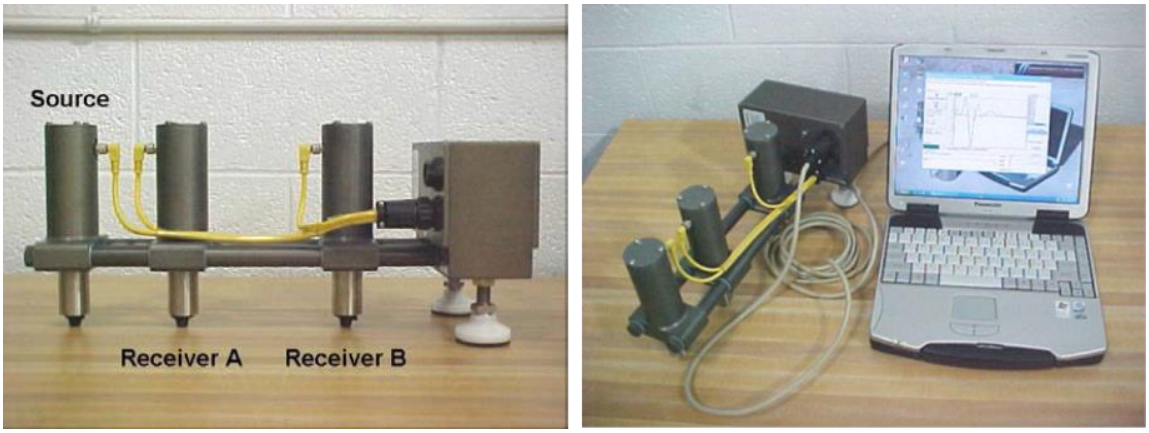

Figure 2.4 Portable Seismic Property Analyzer

Light Weight Deflectometer (LWD) Test

The LWD is a portable device (Figure 2.5) that measures the surface deflection under a given load and computes an effective modulus of a pavement system. The LWD test assumes that the material is a single elastic layer. The effective modulus, E_{eff}, is computed from

$$E_{eff}=[(1-\nu^2)\,F/(\pi\,a\,d_{LWD})]\,f \qquad \text{Equation 2.5}$$

where ν = Poisson's ratio of geomaterial, a = radius of load plate, F = LWD load, d_{LWD} = LWD surface deflection, and f = shape factor which is a function of the plate rigidity and soil type.

Figure 2.5 Light Weight Deflectometer

2.1.4.3 Performance Tests for Unbound Granular Materials

To understand the behavior of the geomaterials, various performance tests are used. The plate load test has been used by many investigators (e.g., Sweere 1990; DeMerchant et al. 2002; Alshibli et al. 2005; and Li and Baus 2005) to characterize the load-deformation characteristics of the geomaterials. The schematic of the plate load test apparatus is shown in Figure 2.6. The plate load test set up consists of a hydraulic actuator mounted on a heavy truck to apply load, a load cell to measure the load, a steel plate to impose the load on the road surface and one or more LVDTs to measure the vertical displacements. The concept of stiffness measurement is based on determining the ratio of the applied load and measured deformation under the plate. As the deformations are related to the combined effects of multiple layers below the plate, this type of in situ tests offers opportunities to measure a combined stiffness of the target pavement layer (the layer on which plate load test is conducted) and other layers below them. However, one of the

drawbacks of the plate load test is that the deformations of individual layers cannot be measured quantitatively.

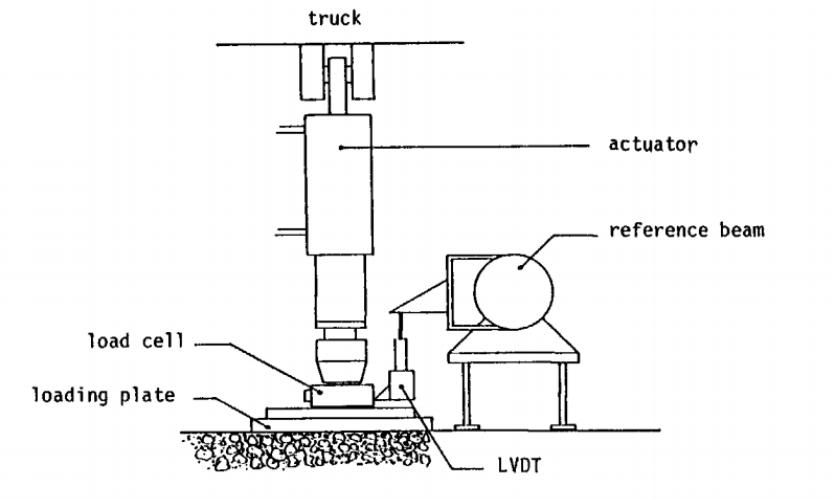

Figure 2.6 Principle of Plate Load Test Apparatus (from Sweere 1990)

Alshibli et al. (2005) used the plate load test on compacted layers of base and subgrade to measure their stiffness characteristics and correlate them with the measured stiffness from other devices such as the Geogauge, Light Weight Deflectometer and Dynamic Cone Penetrometer. The authors conducted tests on a test box that measured 5 ft long, 3 ft wide and 3 ft deep. The test box consisted of a 12-in. thick subgrade layer and a 16-in. thick base. The plate load tests were performed according to the ASTM D1195-93. The authors reported good statistical correlations between the modulus from the plate load test and the corresponding moduli from the other devices.

2.1.4.4 Previous Studies at UTEP

The Center for Transportation Infrastructure Systems (CTIS) at The University of Texas at El Paso (UTEP) has a 300-kip Material Testing and Simulation (MTS) system that is used for characterizing geomaterials under different load magnitudes and frequencies. Gandara and Nazarian (2006), Amiri et al. (2009), Gautam et al. (2009) and Mazari et al. (2014) conducted plate load tests at UTEP to measure the performance of pavement systems with large (36 in. in diameter)

specimens. The wall of the mold is made with 1-in. thick polyethylene, and the height of the mold is 28 in.

Gandara and Nazarian (2006) performed a series of load-deformation tests on large specimens prepared with three different base materials. A 6-in. thick base layer was prepared at the OMC over a 14-in. thick subgrade layer. The tests were performed on the specimens after construction, after the saturation of the subgrade and after the saturation of the base and subgrade. Up to 2000 haversine pulse loads with the durations of 0.1 sec followed by 0.9 sec of rest periods were applied to the specimens. The magnitude of the peak load was 2000 lb with a seating load of 200 lb. The resilient deformation of the base layer was computed at the end of the 200th cycle and the permanent deformation after the last cycle. In addition to those experiments, a series of numerical simulation with VESYS model was performed to obtain the theoretical deformations. It was found that the average deformation of the base when the base and subgrade were saturated was 10 times more than the condition when the base and subgrade were placed at the OMC. It was also noted that the predicted deformations from the numerical models and the measured deformations from the laboratory experiments did not favorably match.

Amiri et al. (2009) studied the performance of one base placed over two different types of subgrade. The authors conducted numerical simulations, as well as small-scale tests and full-scale tests with the same materials. A 5-in. thick layer of base was prepared on top of the subgrades for the small-scale tests. For full-scale tests, a 10-in. thick base layer was compacted in a road section with the same materials used in the small-scale tests. The vertical dimension of the full-scale test model was twice the small-scale tests. Moisture content of the specimens were varied as discussed in Gandara and Nazarian (2006). The numerical simulations were conducted with finite element models of the base, subgrade and the mold body using ABAQUS. In the case of the small-scale tests, a cyclic ramp load at a rate of 500 lb/min was applied to the specimens. The ramp load was increased in such a way that the peak loads varied from 500 lb to 5000 lb. In the case of the full-scale tests, plate load tests were carried at different road sections. The load tests were carried out

with a continuous loading pattern, and the peak load was 30 kips. The load-deformation characteristics measured from the small-scale and full-scale tests were similar. The authors also reported that the responses from the numerical simulation were similar to the experimental results after applying appropriate transfer functions.

Gautam et al. (2009) studied the mechanical properties of five different base materials. The authors prepared guidelines and test protocols to use locally available materials not meeting the material specification of TXDOT by adding chemical additives or modified gradation for construction of low-volume roads. Small-scale tests were one type of tests conducted to measure the field performance of bases at various moisture levels. A 6-in. thick base layer was prepared over a subgrade in the mold. The moisture contents of the materials were varied as discussed in Gandara and Nazarian (2006). Two types of loading, cyclic ramp and sinusoidal, were applied to the specimens. In the case of the cyclic ramp loading, loads were applied at a rate of 500 lb/min as mentioned by Amiri et al. (2009). The peak load was varied from 700 lb to 11000 lb. The loads in the case of the sinusoidal loading were applied with an amplitude of 2000 lbs and a frequency of 1 Hz. The corresponding deflections were measured in both loadings for the treated and non-treated bases. The authors observed that the permanent and resilient deformations of the treated bases were less than non-treated base and concluded that the use of the additives on the locally available materials could be a viable option for a better-performing pavement.

Mazari et al. (2014) performed several small-scale tests to compare the numerical and experimental responses of pavements using different loads, loading areas and moisture conditions. The pavement performance related parameters such as the deformation of the pavement layers were predicted after analyzing the results of the resilient modulus tests and the numerical models. The authors used one granular base and four kinds of fine-grained soils. Each specimen had a layer of 6-in. thick geomaterial over the subgrade. The cyclic plate loads with nominal contact stresses of 30 psi to 90 psi were applied to the specimens, and the corresponding deformations were measured. To perform the numerical simulations, the authors adopted finite element models of the

geomaterials and applied circular loads similar to the small-scale tests. The authors found the deflections of the geomaterials of various specimens were comparable to the deflections predicted by the numerical models with proper transfer functions.

2.2. Research Approach and Testing Procedure

Previous research has shown that the amount of fines content and moisture content present in the material affect the performance of the pavement systems. However, the allowable amount of fines for base materials is not strictly specified. In spite of implementation of a strict material specification for pavement construction, the gradation of material could change due to various reasons such as improper material handling, contamination of base material by subgrade. Similarly, the moisture content of a base material may alter during pavement construction and operation by exposure to excessive water and percolation of rainwater from pavement surface. To understand the effects of fines content and moisture content, 12 different series of tests were performed at four different fines contents and three different moisture contents as tabulated in Table 2.3. The nominal fines contents of 5% to 20% were used. The amount of moisture in the base materials was varied by OMC, OMC-1% and OMC+1% to capture the behavior of base materials at optimum, dry and wet conditions.

Table 2.3 Overall tests of base materials at different fines contents and moisture contents

Test No.	Nominal Fines Content (% by weight)	Nominal Moisture Content (% by weight)
1	5	OMC-1
2		OMC
3		OMC+1
4	10	OMC-1
5		OMC
6		OMC+1
7	15	OMC-1
8		OMC
9		OMC+1
10	20	OMC-1

11	OMC
12	OMC+1

2.2.1. Materials for Tests

A local producer provided a ready-to-deliver base material for this research. The material met the gradation specification for TxDOT Grade 1 (high quality) base. As shown in Figure 2.7, the base material contained about 2% fines. An additional material that primarily contained fines was also received from the same source to prepare contaminated specimens.

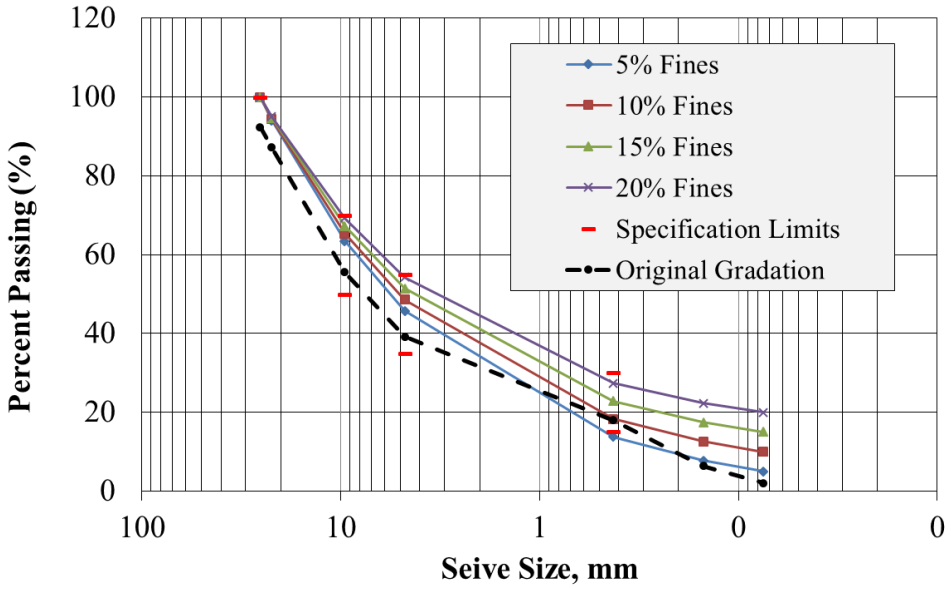

Figure 2.7. Particle size distribution for material mixes of different fines contents

Cooper et al. (1985) provided a relationship for maintaining the structural stability of a granular material when the percentage of fines is changed. Cooper et al.'s relationship, which was used in this study, is in the form of

$$\mathbf{P = \frac{(100-F)(d^n-0.075^n)}{(D^n-0.075^n)} + F} \qquad \textbf{Equation 2.6}$$

where P = percentage passing a sieve of size d in mm, F = percentage of material passing through a 0.075 mm sieve (i.e., fines content), d = sieve size (mm), D = maximum particle size (mm), and n = power relationship (typically 0.45).

The gradations for the four different bases formulated using Equation 2.6 are shown in Figure 2.7 and Table 2.4. Soil classifications of these bases as per AASHTO and USCS and their OMCs and maximum dry densities for bases with different fines contents are tabulated in Table 2.5.

Table 2.4. Particle size distribution of mixes

Standard Sieve Size	Nominal Sieve Opening (mm)	(% Passing)						
		Acceptance Limits		Original Gradation	5%	10%	15%	20%
		Low	High					
1"	25.4	100	100	92.3	100.0	100.0	100.0	100.0
7/8"	22.22	65	90	87.2	94.0	94.3	94.7	95.0
3/8"	9.52	50	70	55.6	63.4	65.4	67.3	69.2
#4	4.75	35	55	39.2	45.7	48.6	51.4	54.3
#40	0.42	15	30	17.9	13.8	18.3	22.9	27.4
#100	0.15	-	-	6.4	7.7	12.6	17.4	22.3
#200	0.075	-	-	2.0	5.0	10.0	15.0	20.0

Table 2.5 Soil classifications for base materials

Material	Atterberg Limits		Proctor Tests		Classification	
	LL	PI	OMC, %	MDD, pcf	AASHTO	USCS
Original	22	10	--	--	A-2-4(0)	GW
5% Fines	23	10	6.3	145	A-2-4(0)	GW-GC
10% Fines	24	9	6.4	144	A-2-4(0)	GP-GC
15% Fines	26	9	7.2	142	A-2-4(0)	SC
20% Fines	28	9	7.2	139	A-2-4(0)	SC

2.2.2. Test Procedures

The test procedures to conduct laboratory and small-scale tests are explained in the following subsections.

2.2.2.1 Moisture-Density and Moisture-Modulus Relationships

The maximum dry density (MDD) and optimum moisture content (OMC) were determined for each of the four mixes as per Tex-113-E. The results are shown in Figure 2.8 and summarized in Table 2.5. The MDD decreases and the OMC increases with the increase in fines content. The specimens used to determine the moisture-density relationship were also used to determine the

seismic modulus with FFRC tests. A typical relationship between moisture vs density and moisture vs modulus for the mix of 20% fines content is shown in Figure 2.9. Although maximum dry density occurs at optimum moisture content, the maximum modulus occurs at a moisture content less than OMC. In other words, the modulus at the OMC is less than the maximum modulus.

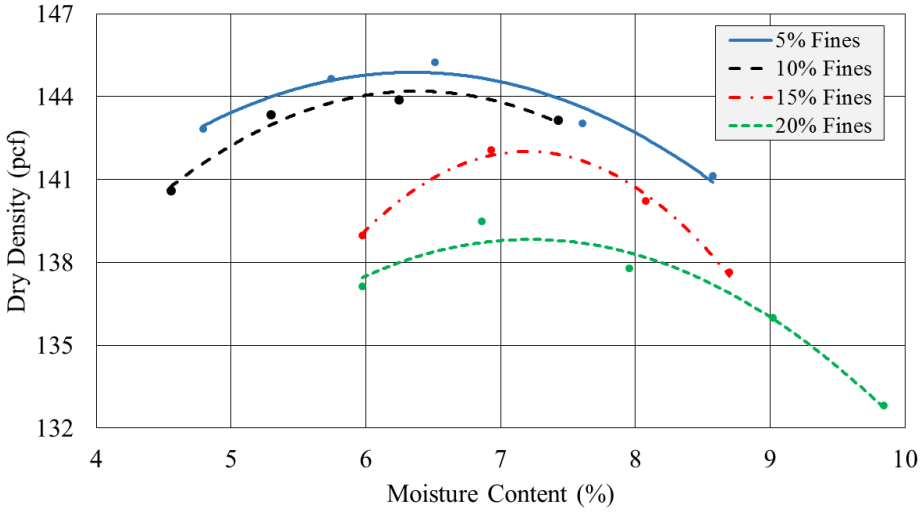

Figure 2.8 Moisture-density relationships for bases various fines contents

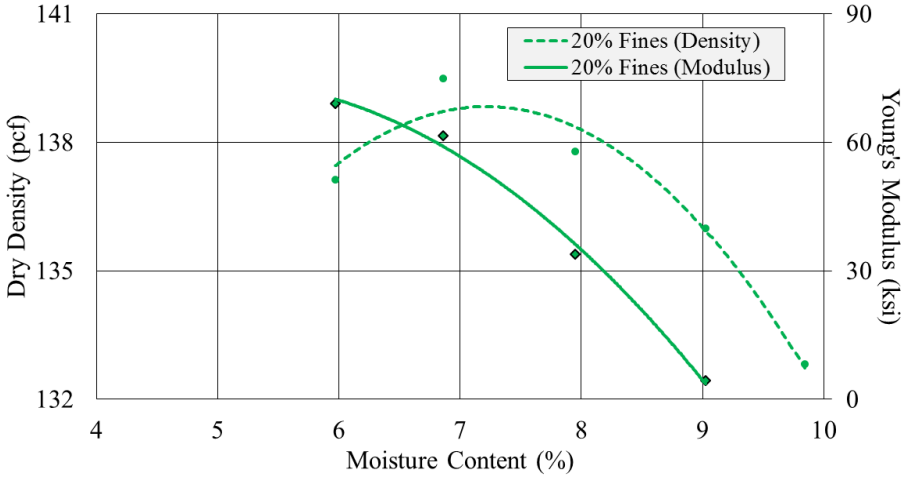

Figure 2.9 Typical moisture-density and moisture-modulus relationships

2.2.2.2 Laboratory Mechanical Properties

Aside from index tests, the laboratory tests consist of the strength tests and stiffness tests. The strength tests consisted of the unconfined compression tests. The stiffness tests included the

FFRC, permanent deformation and resilient modulus (MR) tests, as discussed in Section 2.1. To perform these laboratory tests, four standard (6 in. in diameter and 12 in. in height) specimens were prepared for a specified fines content and moisture content, and tested about 24 hours after compaction. After completion of each test, the actual moisture content of the material was measured by breaking the specimen and drying it in the oven.

2.2.2.3 Small-Scale Test

Small-scale tests, as a substitute for controlled field tests, were carried out on the large (36 in. in diameter and 6 in. in height) specimens for each fines content and moisture content as mentioned in Table 2.3. The mold and the loading system used by previous researchers at UTEP (Gandara and Nazarian 2006, Amiri et al. 2009, Gautam et al. 2009 and Mazari et al. 2014) were adapted for the small-scale tests.

The schematic of the mold with the layers of geomaterials for a small-scale test is shown in Figure 2.10. The mold was made from a polyethylene sewage pipe with one closed end. The

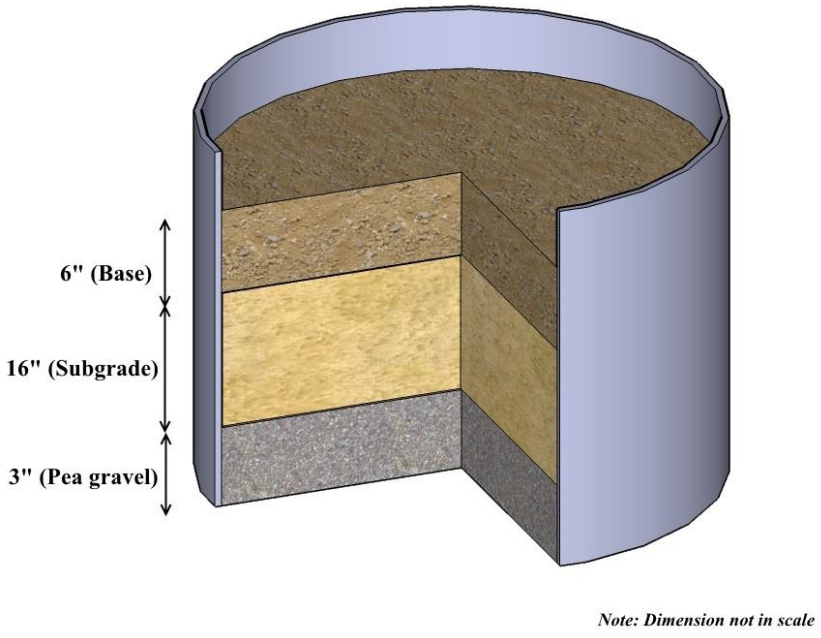

Figure 2.10 Schematic for mold cross-section for a small-scale test

mold had an inner diameter of 36 in., height of 28 in. and thickness of 1 in. The bottom and the inner wall of the mold were lined with 6-mil thick polyethylene sheet. The soil profile for each specimen consisted of 3 in. of pea gravel at the bottom, 16 in. of subgrade over the layer of pea gravel and 6 in. of base over the subgrade as shown in Figure 2.10.

The subgrade and the configuration of layers were adopted from Mazari et al. (2014). The subgrade material was designated as SM material as per USCS soil classification. The MDD and OMC of the subgrade were 112 pcf and 15.2%, respectively. The subgrade layer was compacted in 2 in. lifts. Plate load tests as well as LWD and PSPA tests were conducted on each specimen 24 hours after the preparation of the base layer.

The plate load test can be divided into two categories: a) Cyclic modulus test and b) Cyclic stage test. Both tests were conducted with an MTS system. The cyclic modulus tests were conducted with three different plates with diameters of 4 in., 8 in. and 12 in. (Figure 2.11).

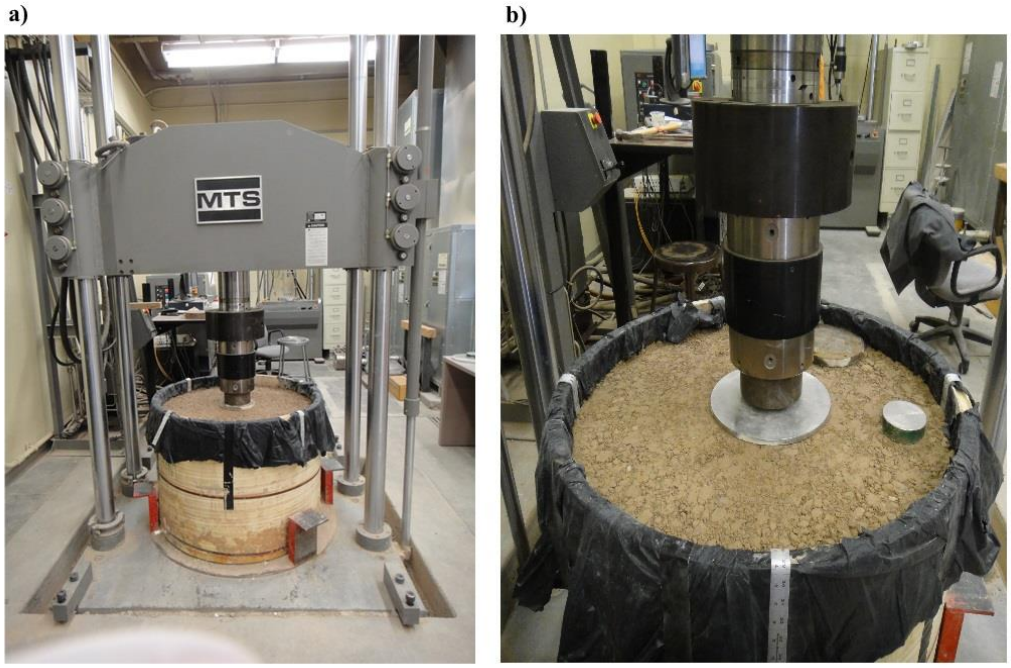

Figure 2.11 Small-scale test with a MTS system- a) Plate load test, and b) Three different plates for plate load tests

Haversine loads with peak contact pressures of 30 psi, 50 psi, 70 psi and 90 psi were applied on the specimen using the different plates. Ten load pulses with loading and resting periods of 0.1 sec

and 0.9 sec, respectively, were applied for each test regime. The typical applied loads and corresponding plate deformations from cyclic modulus test are shown in Figure 2.12. For each set of load, the modulus (termed as a cyclic modulus) of the material was computed using the average vertical stress and the average recoverable strain.

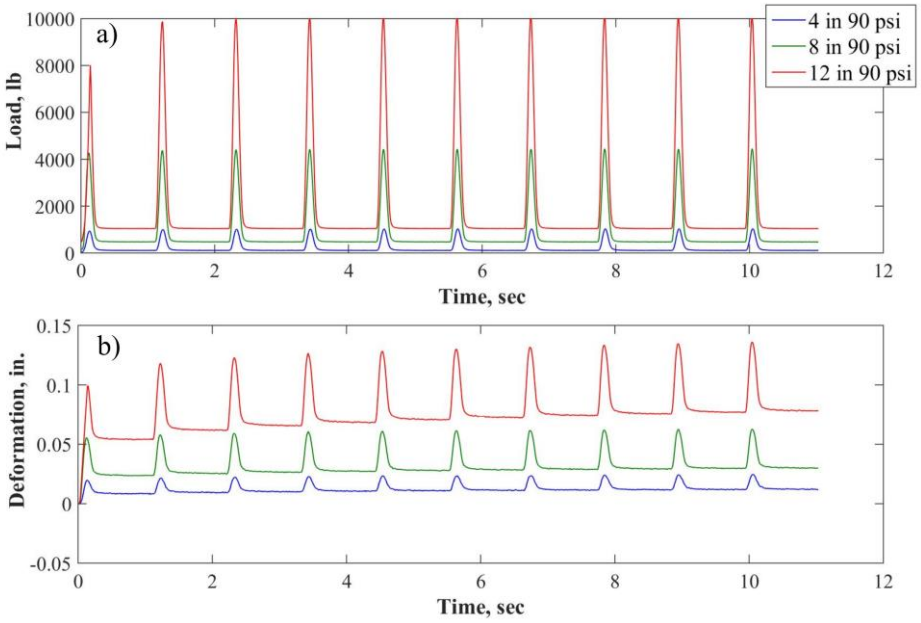

Figure 2.12 Typical load-deformation responses from the cyclic-modulus test: a) applied loads and b) measured deformations

The cyclic stage tests were conducted after the cyclic modulus tests by using only the 8 in. plate. Two different loading patterns, cyclic ramp load and continuous load, were used for these tests. The loading rate for both loading patterns was 500 lb/min. In the case of the cyclic ramp load, the peak load was increased from 500 lb to 5000 lb in 500 lb increments. After reaching each peak load, the specimen was unloaded at an unloading rate of 500 lb/min, and allowed to rest for one minute before starting the next load. In the case of the continuous load, the load increased continuously from 0 lb up to 5000 lb, and unloaded in one minute. The typical load-deformation response of cyclic stage tests are shown in Figure 2.13. The outcomes of the cyclic stage test were i) load-deformation responses of cyclic ramp load and continuous load, ii) permanent deformation of material under the continuous load, and iii) stiffness of material measured using the slopes of

the load-deformation curve for the continuous load and the backbone curve for the cyclic ramp load.

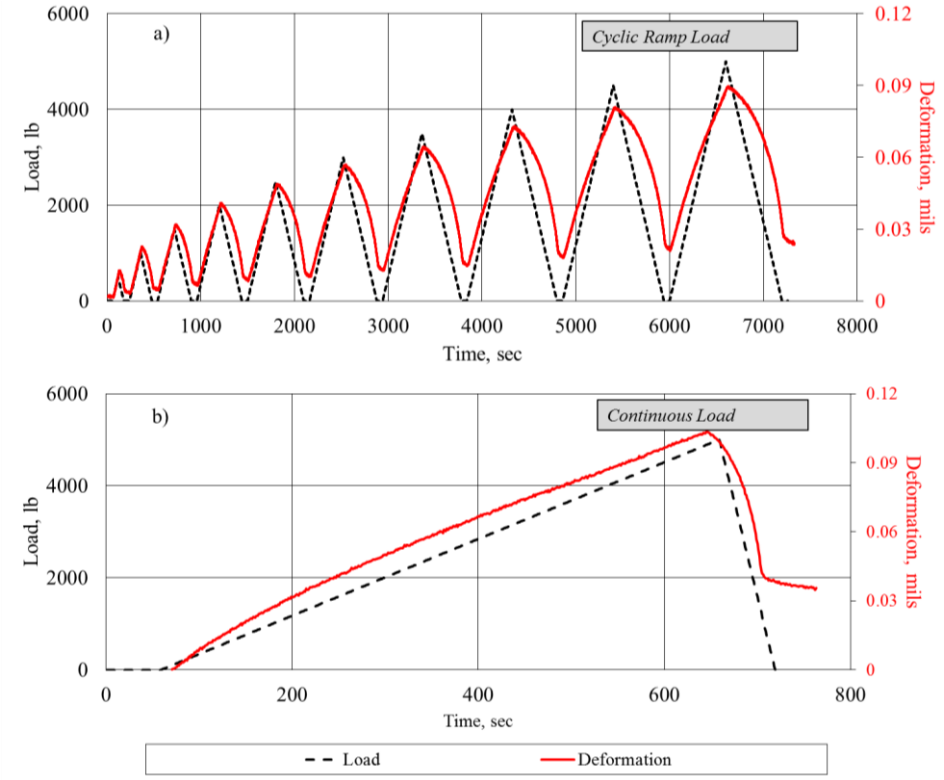

Figure 2.13 Typical load-deformation responses from the cyclic-stage test for a) cyclic ramp load and b) continuous load

An LWD manufactured by Zorn Instruments was adopted (Figure 2.14). The LWD tests were performed as per ASTM E2583. The effective modulus (termed as a LWD modulus) given in Equation 2.2 was computed assuming a Poisson's ratio of 0.4, the radius of load plate as 4 in., LWD load as 1700 lb, and shape factor of 2. For each specimen, three spots were chosen to conduct the LWD tests and measure deflections under the load plate (Figure 2.14). The PSPA tests were conducted to measure seismic modulus (termed as PSPA modulus) at 24 different locations on the specimen's surface as shown in Figure 2.15.

Figure 2.14 Small-scale test with LWD

Figure 2.15 Small-scale test with PSPA

2.3. Results from Laboratory and Small-Scale Tests

This section presents the results from the laboratory tests on standard (6 in. in diameter and 12 in. in height) specimens and small-scale tests on large (36 in. in diameter and 6 in. in height)

specimens. Twelve different tests sequences (see Table 2.3) were performed with a combination of moisture contents (OMC-1%, OMC and OMC+1%) and fines contents (5%, 10%, 15% and 20%).

2.3.1. Laboratory Tests

Four standard specimens were used for performing each of the laboratory tests, as discussed in Section 2.2. The first two specimens were used for conducting FFRC and unconfined compression tests and the other two specimens were used for conducting permanent deformation and resilient modulus tests. The results of these tests are presented in the following subsections.

2.3.1.1 Unconfined Compression Tests

The unconfined compressive strength (UCS) of standard specimens from unconfined compression tests are presented in Figure 2.16. Figure 2.16a shows the variations in strengths at different moisture contents for a specific fines content, i.e., the results grouped by fines content.

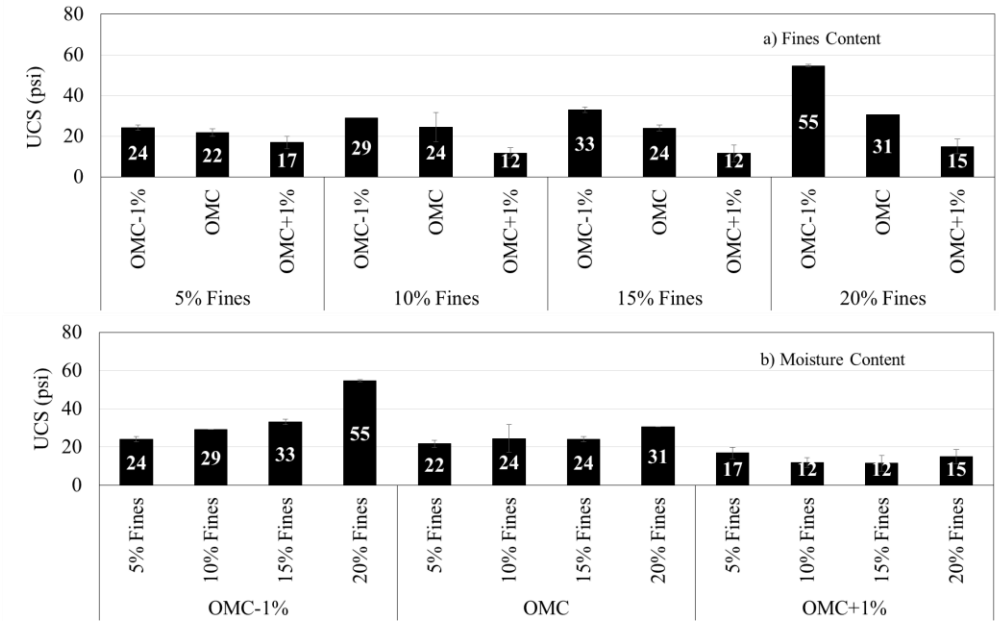

Figure 2.16. Unconfined compressive strength (USC) of standard specimens: a) grouped by fines content and b) grouped by moisture content

Similarly, Figure 2.16b shows the results grouped by moisture content. The UCS decreases with increase in moisture content. The results in Figure 2.16a also imply that the rate of reduction in strength increases with increase in fines content. In other words, for each fines content, the highest UCS occurs at OMC-1%. Figure 2.16b shows that the UCS increases with fines content when the nominal moisture content is either OMC-1% or OMC. The strengths for the OMC+1% specimens are less impacted by the variation in fines content.

2.3.1.2 FFRC Tests

Figure 2.17 shows the variations in the FFRC modulus of standard specimens with fines content and moisture content. As shown in Figure 2.17a, the FFRC modulus decreases with

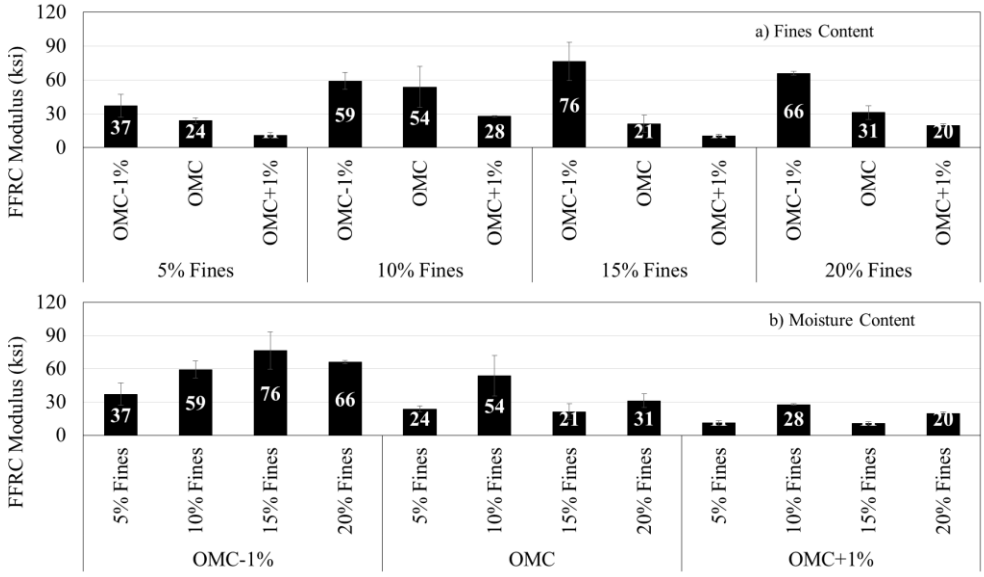

Figure 2.17 FFRC modulus of standard specimens: a) grouped by fines content and b) grouped by moisture content

increase in moisture content for all fines contents. The results also show that a significant reduction in the FFRC modulus occurs for the specimens prepared with 15% fines content, especially between the moisture contents of OMC-1% and OMC. Figure 2.17b shows that the moduli for specimens prepared at OMC-1% are greater than the moduli at OMC and OMC+1%. In addition, the maximum moduli are achieved between 10% to 15% fines contents for all moisture contents.

2.3.1.3 Permanent Deformation Tests

Figure 2.18 shows the variations in permanent strain of standard specimens with the number of loading cycles. The resilient (permanent strain after 200 cycle) and permanent strains after the last cycle are summarized in Figure 2.19. The results for specimens prepared at OMC+1% are not included because the specimens were too wet to withstand the loads during the tests. The increase in the moisture content results in an increase in the resilient and permanent deformations, and hence resilient and permanent strains. As the fines content increases from 10% to 20%, the permanent strain typically decreases at OMC-1% and OMC. The specimens prepared with 10% fines content show more permanent deformation at OMC-1% and OMC as compared to the specimens prepared with other fines contents.

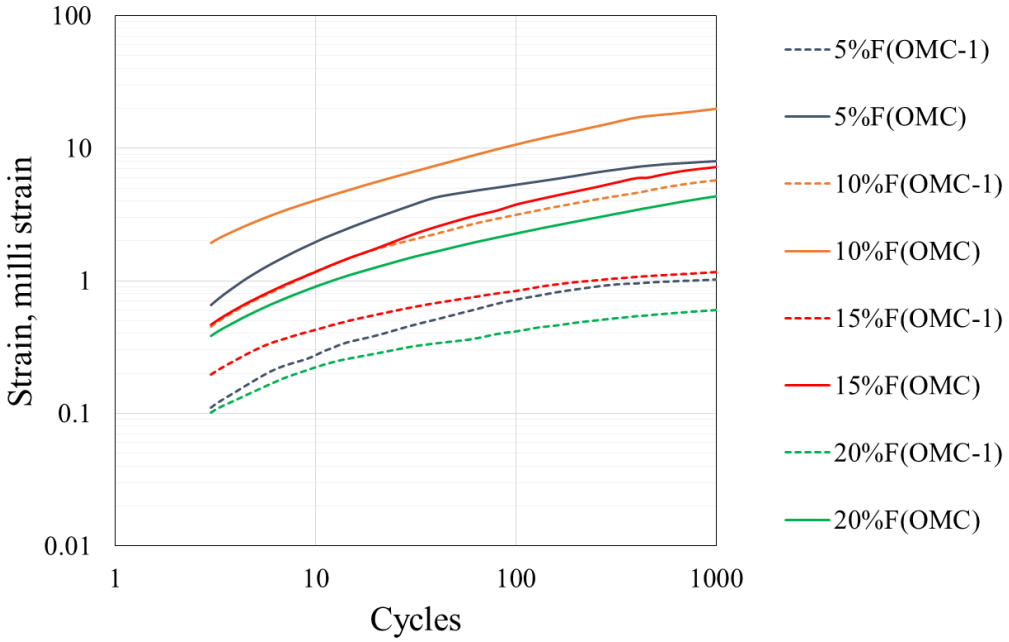

Figure 2.18. Strains measured at different loading cycles on standard specimens in permanent deformation tests

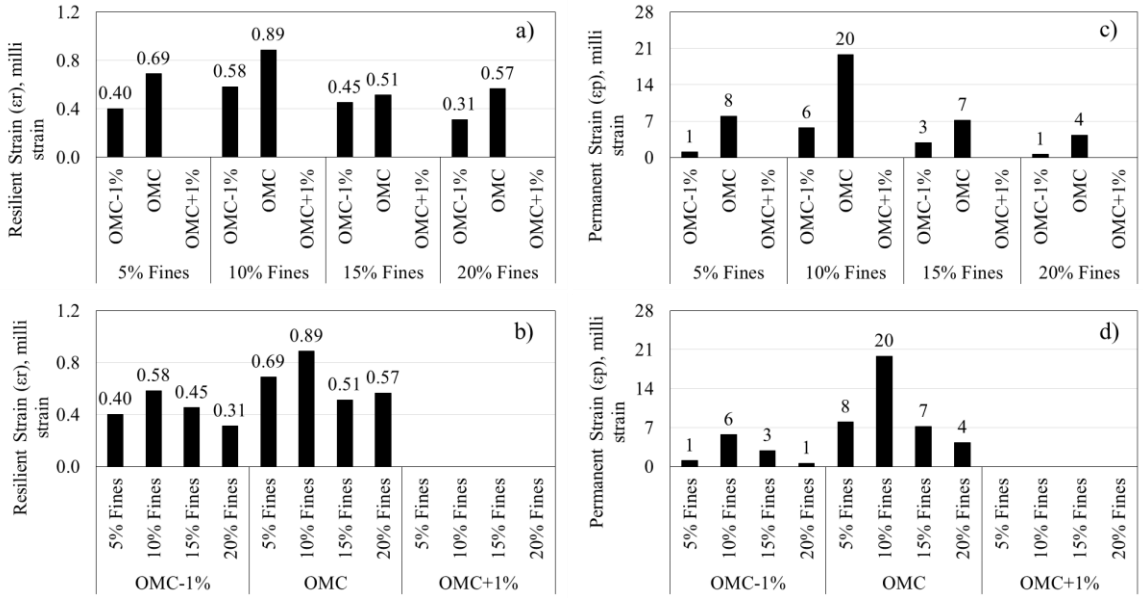

Figure 2.19 Resilient strains of standard specimens: a) grouped by fines content and b) grouped by moisture content. Permanent strains: c) grouped by fines content and d) grouped by moisture content.

2.3.1.4 Resilient Modulus (MR) Tests

The representative resilient moduli of specimens are presented in Figure 2.20. The results for the specimens prepared at OMC+1% are not available because the specimens were too wet to

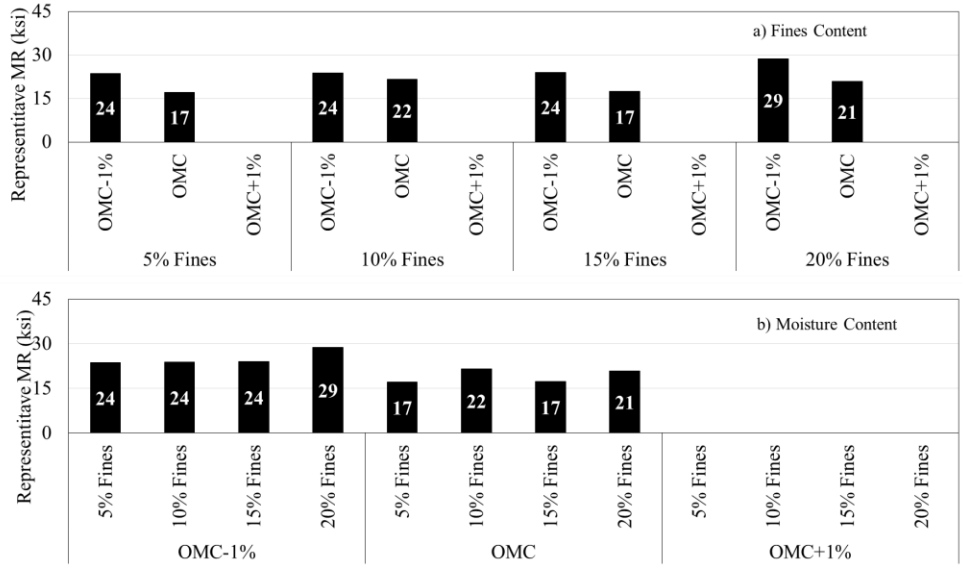

Figure 2.20 Representative resilient modulus (MR) of standard specimens: a) grouped by fines content and b) grouped by moisture content

withstand the loads during the tests. The representative resilient moduli were computed using a bulk stress of 31 psi and an octahedral shear stress of 7.5 psi in Equation 2.2. The resilient moduli of specimens slightly decrease with increase in moisture content for all fines contents. From Figure 2.20b, the resilient modulus is not considerably influenced by the change in fines content at OMC-1% and OMC.

2.3.2. Small-Scale Tests

One large specimen was used for performing each of the small-scale tests, as discussed in Section 2.2. The results of the tests are presented in the following subsections.

2.3.2.1 PSPA Tests

Figure 2.21 shows the variations in the PSPA modulus of the base on large specimens with fines content and moisture content. The PSPA moduli for the specimens prepared at OMC+1% are not reported because the specimens were too wet and too soft to couple seismic energy. Figure 2.21a shows that the PSPA modulus decreases with increase in moisture content. The PSPA

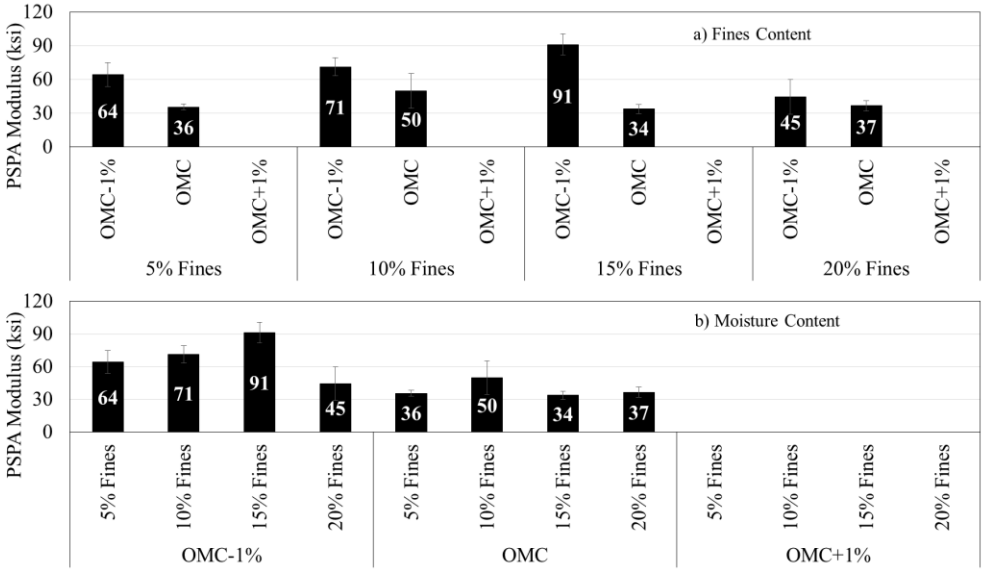

Figure 2.21 PSPA modulus of large specimens: a) grouped by fines content and b) grouped by moisture content

moduli of the specimens prepared with 15% fines content decrease more as compared to the other specimens when the moisture content increases from OMC-1% to OMC. The trends in Figure 2.21a for specimens prepared from 5% to 15% fines contents are similar to those for the FFRC tests. From Figure 2.21b, the PSPA modulus generally increases with increase in fines content from 5% to 15% for the specimens prepared at OMC-1%. The results also show that the maximum moduli are typically achieved between 10% to 15% fines contents.

Figure 2.22 shows the PSPA modulus on top of the subgrade for each specimen before constructing the base layer. The modulus of subgrade varied from 24 ksi to 35 ksi throughout the tests with an average modulus of 28 ksi and a COV of 10%. This result shows that the mechanical properties of the subgrade for different specimens were similar throughout the tests.

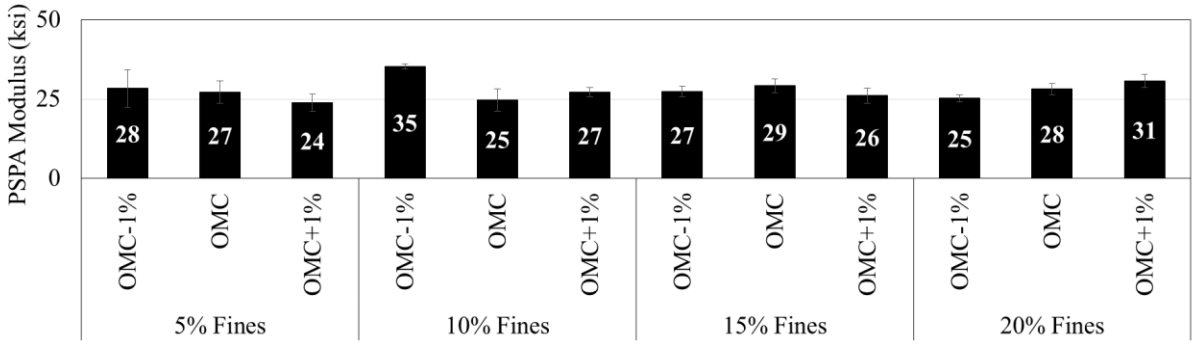

Figure 2.22 PSPA modulus of subgrade

2.3.2.2 LWD Tests

Figure 2.23 shows the variations in the LWD modulus of base on large specimens with fines content and moisture content. The LWD modulus typically decreases with increase in moisture content (Figure 2.23a). The rate of reduction in the modulus is higher for the specimens prepared with 10% and 15% fines contents as compared to the specimens prepared with 5% and 20% fines contents. Figure 2.23b shows that the LWD moduli for specimens prepared at OMC-1% are greater than the moduli at OMC and OMC+1%. The maximum moduli of the specimens are typically achieved with 10% fines content at OMC-1% and OMC. The results with LWD are

influenced by the modulus parameters of the subgrade layer because the thickness of base layer is only 6 in.

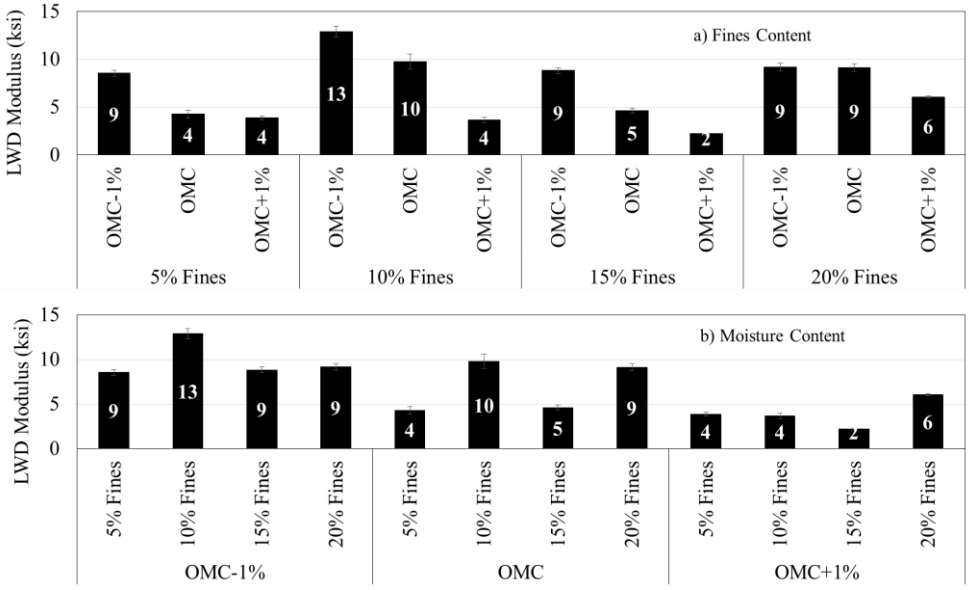

Figure 2.23 LWD modulus of large specimens: a) grouped by fines content and b) grouped by moisture content

Figure 2.24 shows the LWD modulus on top of the subgrade for each specimen before constructing the base. The modulus of subgrade varied from 4 ksi to 6 ksi with an average modulus of 5 ksi and a COV of 15%. This result again shows the reasonably uniform nature of the mechanical properties of the subgrade.

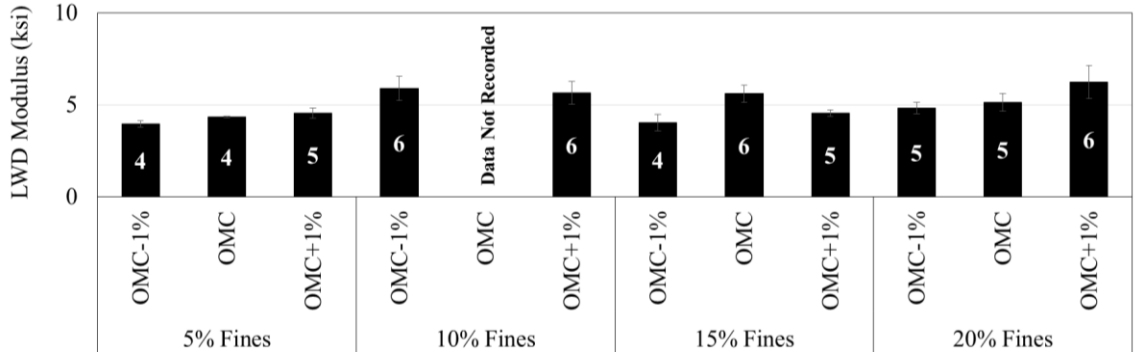

Figure 2.24 LWD modulus of subgrade

2.3.2.3 Cyclic Modulus Tests

Figure 2.25 through Figure 2.27 show the variations in the cyclic modulus (i.e., the ratio of the measured average vertical stress and the average recoverable strain in a cyclic modulus test as discussed in Section 2.2) of the base in the large specimens with fines content and moisture content. These figures also show the variations in the cyclic modulus for various contract pressures and plate diameters. The cyclic modulus typically increases with increase in contact pressure for the 4 in. diameter plate for the specimens prepared with 10% to 20% fines contents.

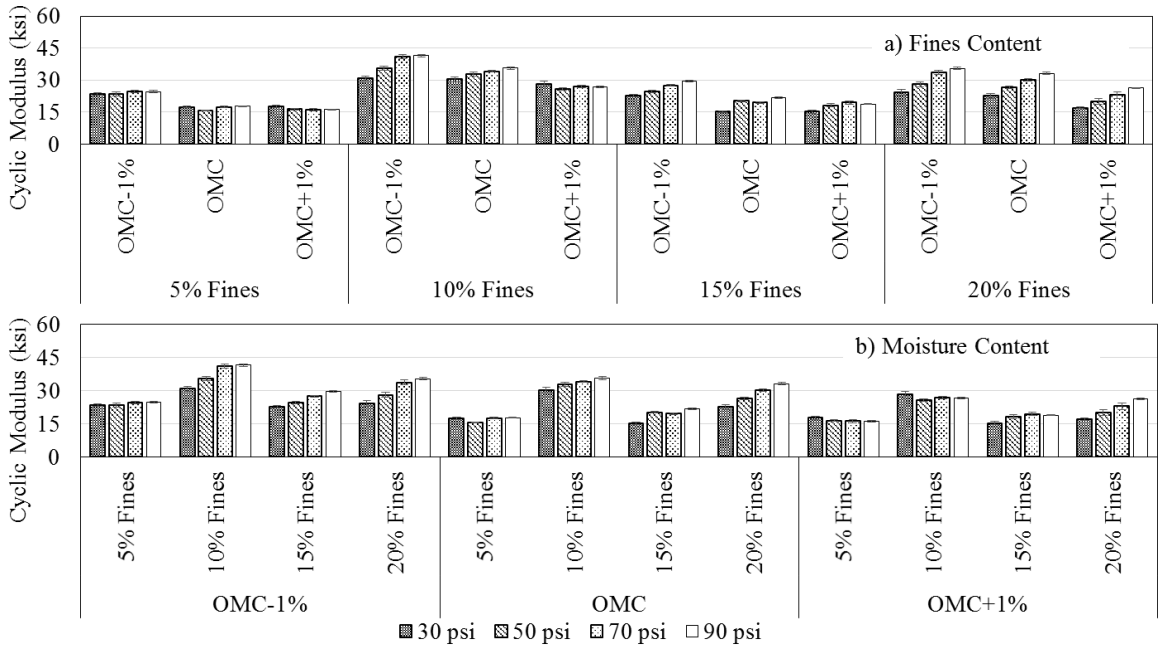

Figure 2.25 Cyclic modulus of large specimens from cyclic modulus test using 4" diameter plate: a) grouped by fines content and b) grouped by moisture content

The cyclic modulus decreases with increase in moisture content in most instances. In the cases of test results with 8 in. and 12 in. diameter plates, the moduli increase with increase in contact pressure and slightly decrease or remain constant with increase in moisture content (Figure 2.26 and Figure 2.27). Figure 2.25 through Figure 2.27 also show that the modulus of the specimen decreases with increase in the plate diameter. The decrease in the modulus is possibly due to the influence of the subgrade in the experiments. Furthermore, the maximum moduli were achieved with the specimens prepared at 10% fines content for all moisture contents.

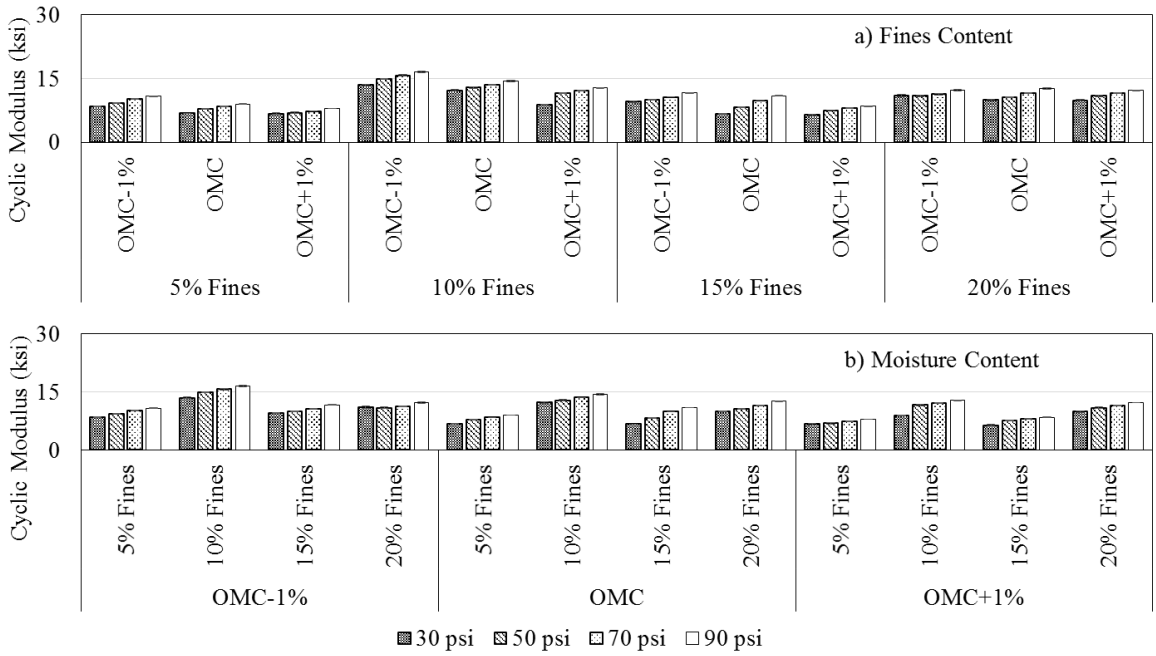

Figure 2.26 Cyclic modulus of large specimens from cyclic modulus test using 8" diameter plate: a) grouped by fines content and b) grouped by moisture content

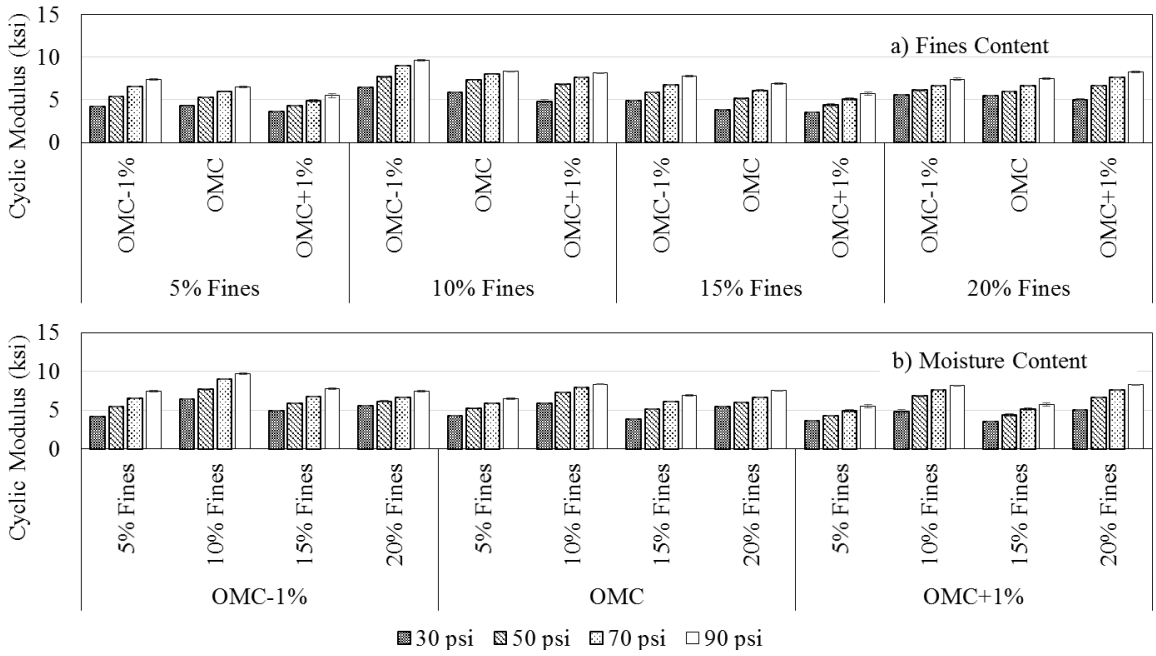

Figure 2.27. Cyclic modulus of large specimens from cyclic modulus test using 12" diameter plate: a) grouped by fines content and b) grouped by moisture content

2.3.2.4 Cyclic Stage Tests

Figure 2.28 shows the load-deformation responses of the base in the large specimens with the cyclic stage tests using various fines contents, moisture contents and loading conditions (cyclic-ramp load vs. continuous load). The deformation of the specimens increases with increase in moisture content. The specimens prepared with 15% fines content deform significantly more at OMC+1% as compared to the other specimens prepared with different fines content and the same

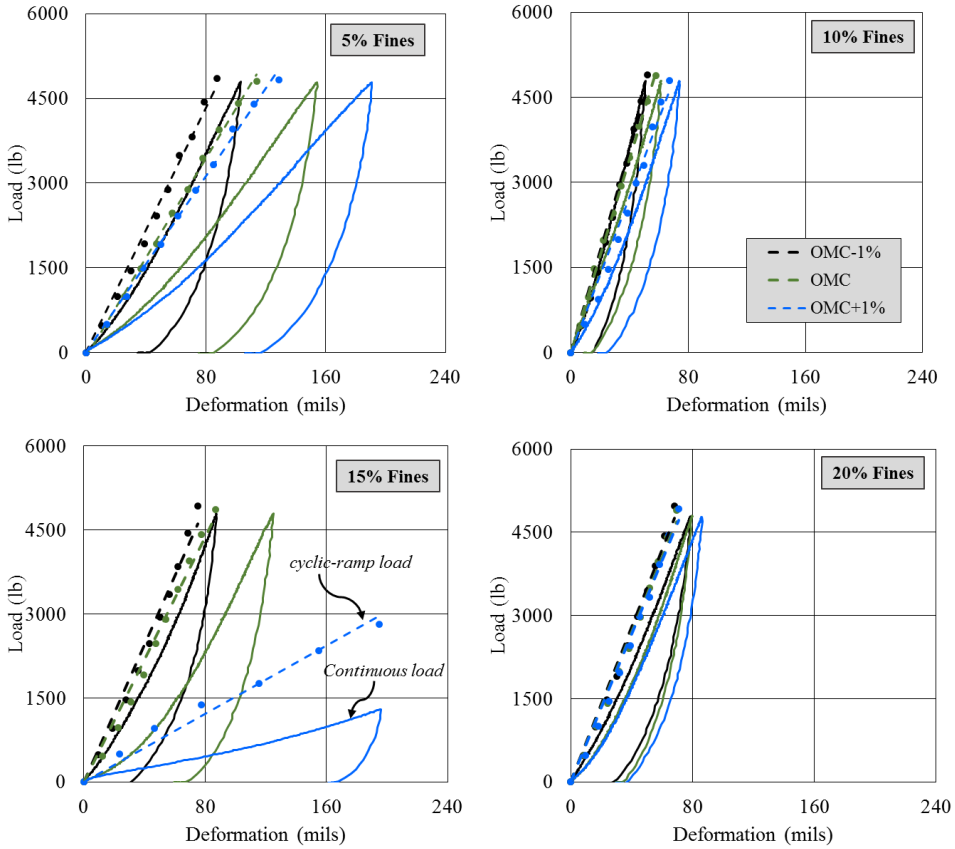

Figure 2.28 Load-deformation response of large specimens from cyclic stage test

moisture content. The specimen prepared with 15% fines content and moisture content of OMC+1% seemed highly wet as compared to all other specimens at OMC+1%. This is perhaps the reason for observing a high deformation. A clear trend in deformation with respect to the change in the fines content cannot be observed. The peak deformations of the specimens prepared with 10% and 20% fines contents are less than 80 mils and around 80 mils, respectively. However,

the peak deformations for the specimens prepared with 5% and 15% fines contents are more than 80 mils.

To better understand these unusual deformational behaviors of bases with various moisture contents and fines contents, one must understand the soil-water-interaction of material at microscopic levels. In all tests, the continuous loads result in more deformations than the cyclic-ramp loads of the same magnitude. Furthermore, the difference in the deformation responses due these two types of loads increases with increase in moisture content for the specimens prepared with 5% and 15% fines contents.

Figure 2.29 shows the variations of stiffness (measured using the slopes of the load-deformation curve for the continuous load and the backbone curve for the cyclic ramp load) of the bases with fines content and moisture content. As the deformation due to the continuous load is greater than the cyclic-ramp load (Figure 2.28), the stiffness due to the continuous load is less than that of the cyclic-ramp load. The stiffness decreases with increase in moisture content for all fines

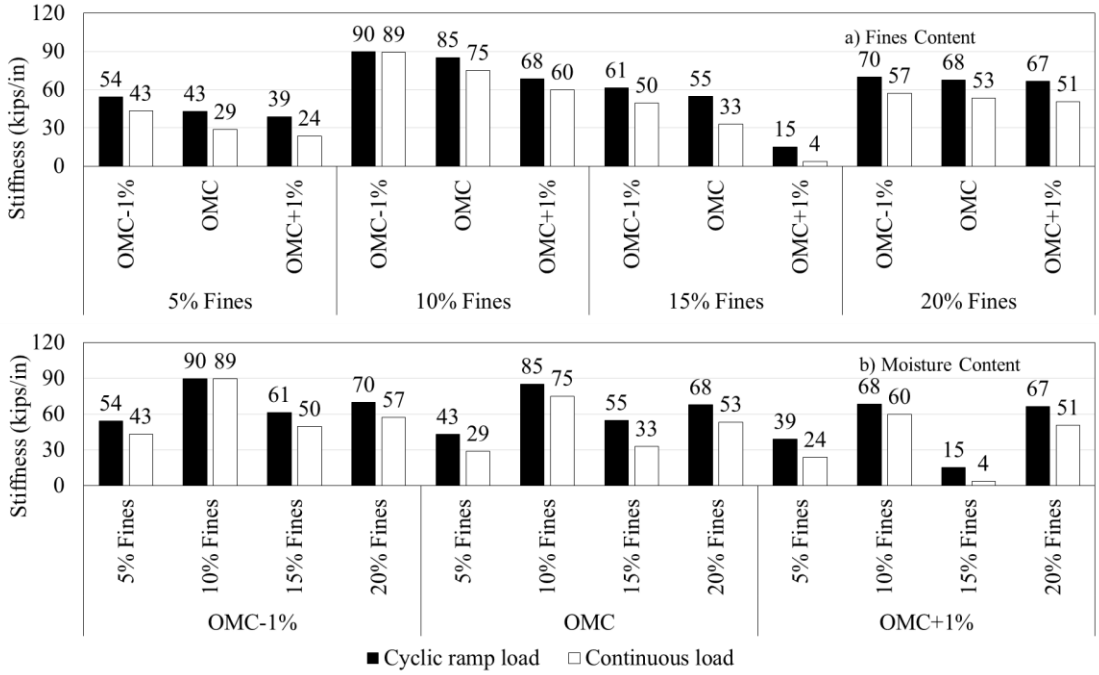

Figure 2.29 Stiffness of large specimens from cyclic stage test: a) grouped by fines content and b) grouped by moisture content

content. The specimens prepared with 15% fines content are sensitive to change in moisture content, especially when the moisture content increases from OMC to OMC+1%. On the other hand, a reverse trend is evident for the specimens prepared with 20% fines content. From Figure 2.29b, the maximum stiffness is achieved for the specimens prepared with 10% fines contents at all moisture contents.

The variations in the permanent deformation (under the continuous load) of the large specimens with various fines content and moisture content are presented in Figure 2.30. The permanent deformation increases with increase in moisture content for all fines contents. The specimens prepared with 5% and 15% fines deform more significantly at OMC and OMC+1% as compared to the other specimens prepared at 10% and 20% fines contents. In general, the specimens prepared at 15% fines content are more sensitive to changes in the moisture content

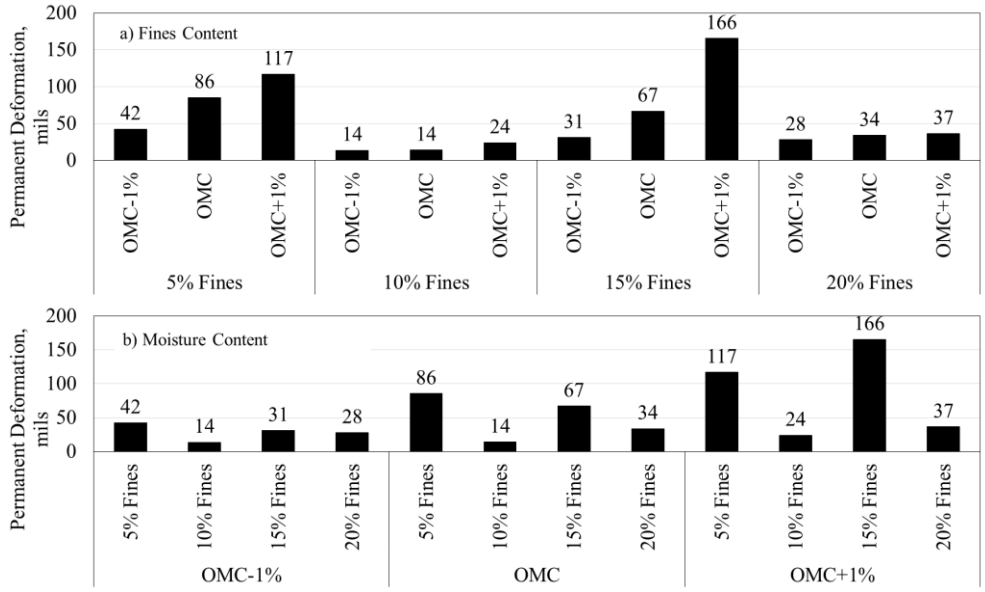

Figure 2.30 Permanent deformation of large specimens from cyclic stage tests: a) grouped by fines content and b) grouped by moisture content

while a reverse behavior is observed for the specimens prepared at 20% fines content. Furthermore, the permanent deformations of the specimens prepared at 15% fines content are only comparable with that of the standard specimens of the laboratory tests. The deformations in these specimens doubled when the moisture content increased from OMC-1% to OMC.

2.3.3. Comparison of Laboratory and Small-Scale Tests

This section deals with the comparisons of the test results obtained from the laboratory and small-scale tests. These results are also correlated to understand the impact of the fines content and moisture content on the laboratory tests and small-scale tests.

2.3.3.1 Effect of Moisture Content on Laboratory Tests

The relationships between the normalized moduli, UCS and permanent deformation with the normalized moisture content of standard specimens are shown in Figure 2.31. The normalized modulus is defined as the ratio of the measured modulus at a given moisture content and the

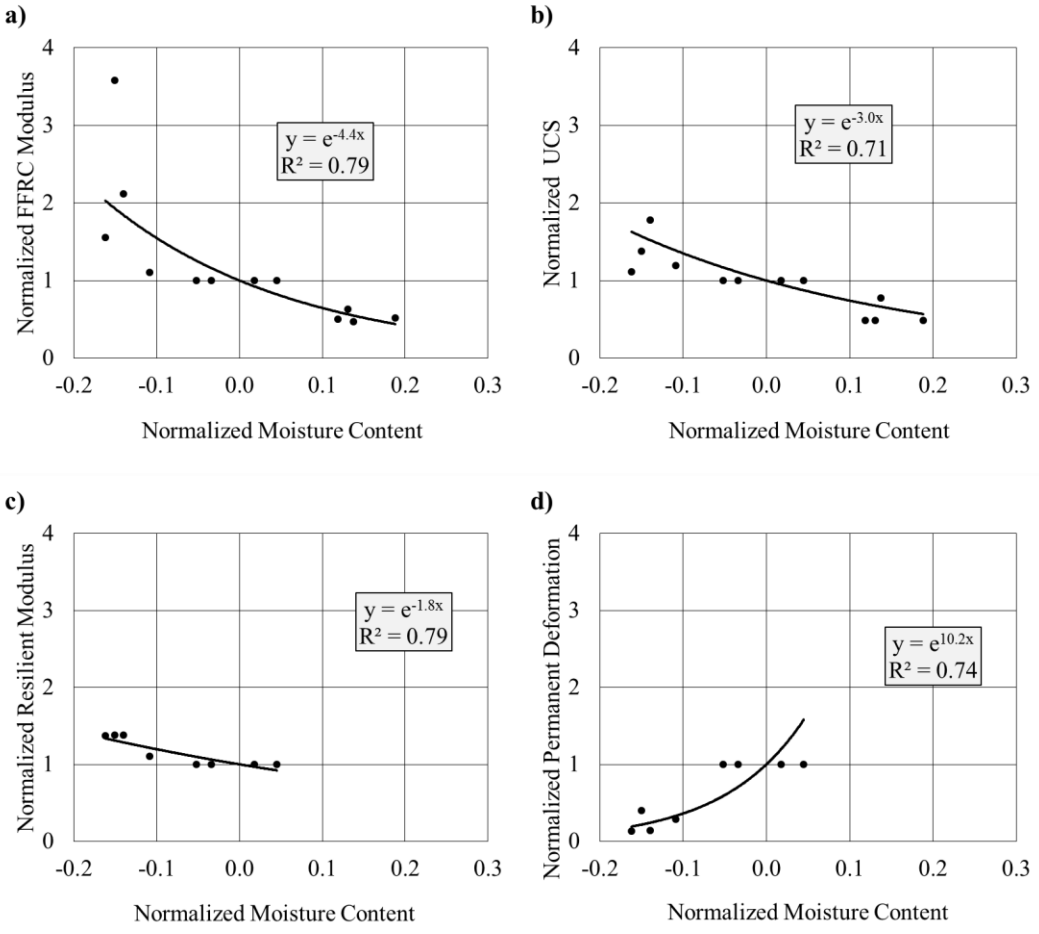

Figure 2.31. Variations in normalized moduli, UCS and permanent deformation with normalized moisture content in laboratory tests: a) FFRC Test, b) Unconfined Compression Test, c) Resilient Modulus Test and d) Permanent Deformation Test

modulus at OMC. The UCS and permanent deformation are also normalized in a similar way. The normalized moisture content is the difference between the measured moisture content and OMC divided by OMC. As the resilient modulus and permanent deformation tests were conducted only at OMC-1% and OMC, few data are available for analyses (Figure 2.31c and Figure 2.31d). The normalized FFRC modulus, resilient modulus and UCS decrease with increase in moisture content. The FFRC modulus is more sensitive to the changes in the moisture content as compared to the resilient modulus and UCS.

Figure 2.31d shows that the normalized permanent deformation increases with increase in moisture content. The correlation coefficients (R^2) for all cases are greater than 70% that indicate reasonably strong correlations between each test results and moisture content.

2.3.3.2 Effect of Moisture Content on Small-Scale Tests

Figure 2.32 shows the variations in normalized modulus, stiffness and permanent deformation with the normalized moisture content of the large specimens (for small-scale tests). The stiffness is measured from the maximum load and corresponding deformation from the continuous load in the cyclic stage tests. As the PSPA tests were conducted only at OMC-1% and OMC, few data are available for analyses (Figure 2.32b). The increase in the moisture content results in decrease in the LWD and PSPA moduli (Figure 2.32a, Figure 2.32b). Both of these test results correlate reasonably well with the moisture content. However, these relationships do not seem to be appropriate below a certain moisture content. Further, the stiffness values of the large specimens due to the continuous and cyclic ramp loads decrease with increase in the moisture content (Figure 2.32c). The stiffness values measured by the two loading methods at OMC are similar. However, the variations in the stiffness with moisture content are not as pronounced and well-defined as for the LWD and PSPA. Figure 2.32d shows that the permanent deformation increases with increase in the moisture content. The result provides a reasonable correlation between the deformation and moisture content.

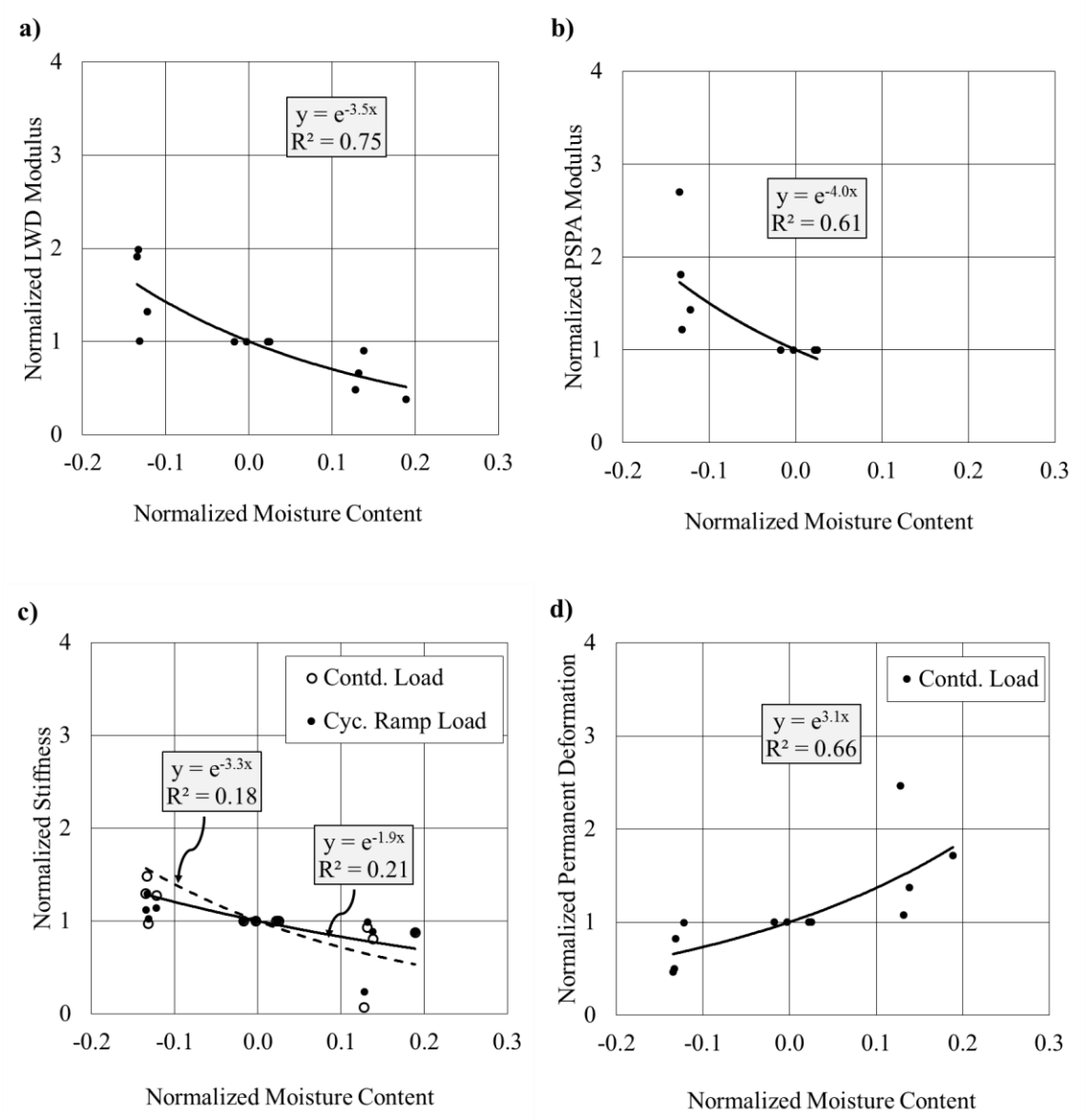

Figure 2.32 Variations in normalized modulus, permanent strain and stiffness with measured moisture content in small-scale tests: a) LWD Test, b) PSPA Test, c) Cyclic Modulus Test (CST) showing stiffness and d) CST showing permanent strain

2.3.3.3 Correlation of Laboratory Tests

The test results from the three types of laboratory tests (MR, FFRC and UCS) are correlated in Figure 2.33. The resilient moduli are reasonably correlated with the FFRC moduli and UCS values. A weaker correlation is observed between the FFRC modulus and UCS. The relationship

between the resilient modulus and the FFRC modulus of geomaterials reported by Nazarian et al. (2014) is also superimposed in Figure 2.33a. The two relationships differ only slightly from one another.

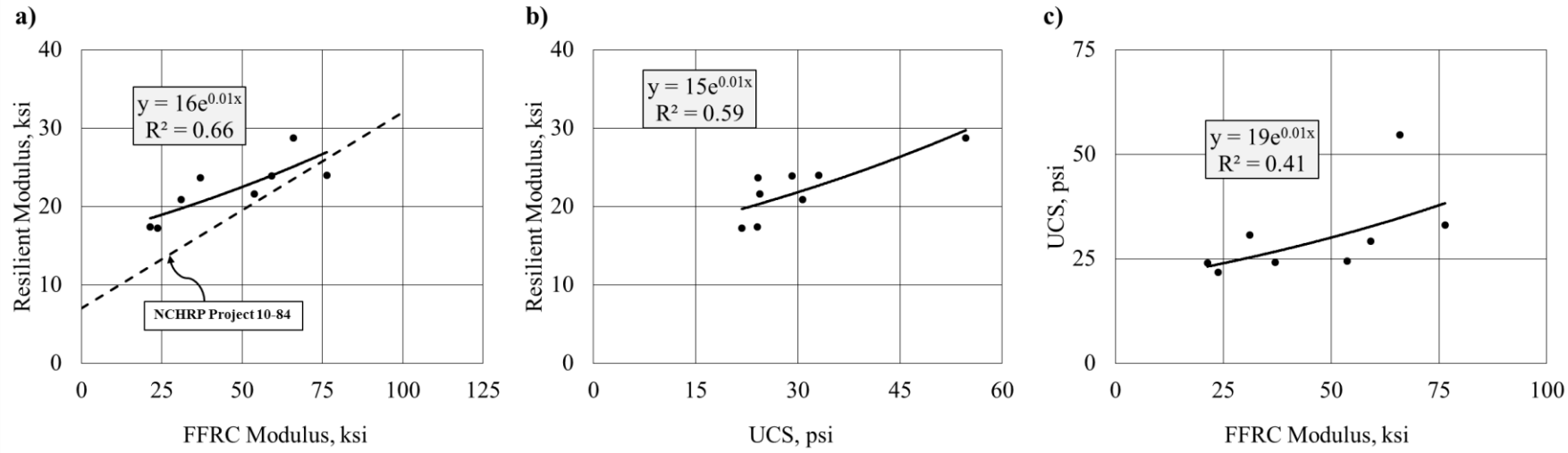

Figure 2.33 Variation in moduli and UCS of specimens in laboratory tests: a) Resilient Modulus (MR) Test and FFRC Test, b) MR Test and Unconfined Compression Test (UCT), and c) UCT and FFRC Test

2.3.3.4 Correlation of Small-Scale Tests

The relations of the test results from the LWD and cyclic plate load tests are shown in Figure 2.34. As cyclic plate load tests were carried out with three different plate diameters (diameters of 4 in., 8 in. and 12 in.) using four different peak contact pressures (30 psi, 50 psi, 70 psi and 90 psi), a combination of twelves different relationships between the LWD modulus and the cyclic modulus are

obtained. The R^2 typically increases with decrease in the plate diameter, except at the peak contact pressure of 30 psi. Further, the R^2 also typically increase with increase in the peak contact pressure from 50 psi to 90 psi. The results also indicate that the LWD moduli correlate reasonably well with the cyclic moduli measured with the largest plate (12 in. diameter) and the highest peak contact pressure (90 psi).

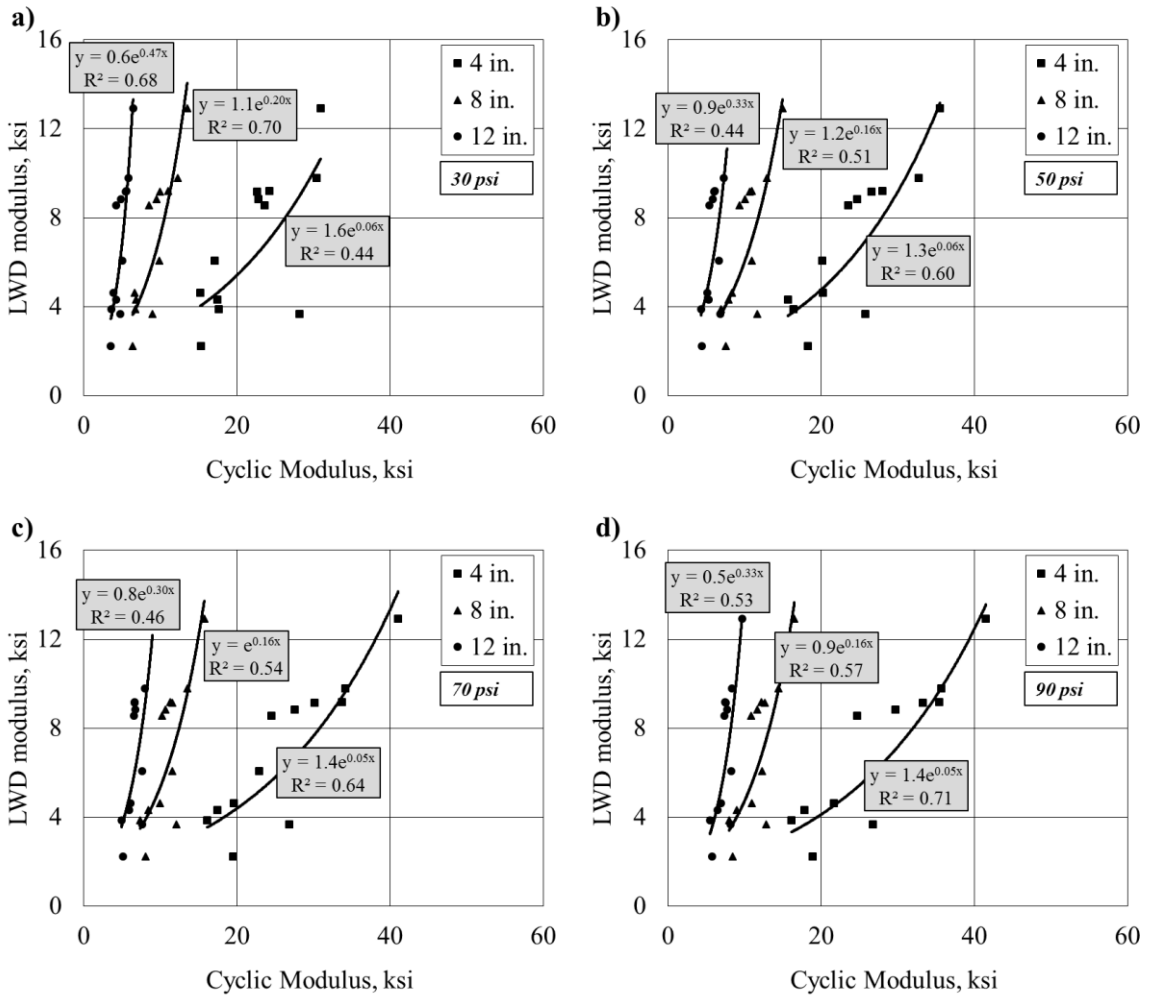

Figure 2.34 Variations in modulus of large specimens in small-scale tests with different loading plates at different peak contact pressures: a) 30 psi, b) 50 psi, c) 70 psi and d) 90 psi

The LWD used for the tests has an 8 in. diameter plate and the peak contact pressure under the plate during the LWD test is approximately 34 psi. The cyclic modulus test with 8 in. diameter plate and 30 psi peak contact pressure is comparable with the LWD test. The LWD test results

yielded the highest R^2 of 70% (see Figure 2.34a) with the cyclic modulus test conducted with 8 in. diameter plate at the peak contact pressure of 30 psi.

Figure 2.35 shows the variations in the LWD modulus with the stiffness measured on the large specimens in the cyclic stage tests. Based on the R^2 values, the results from the two plate load tests are reasonably correlated to the LWD modulus.

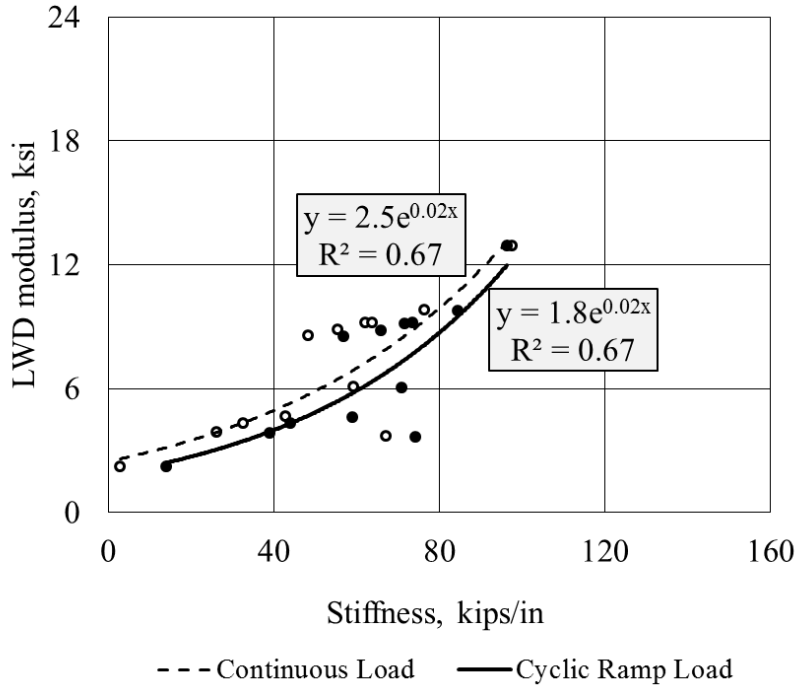

Figure 2.35 Variations in the LWD modulus and stiffness of large specimens measured through cyclic stage test in small-scale tests

2.3.3.5 Correlation of Laboratory Test and Small-Scale Tests

Figure 2.36 compares the permanent strains on the standard specimens from the laboratory tests with that of the large specimens from the small-scale tests. As permanent deformation tests on the standard specimens were conducted only at OMC-1% and OMC, few data points are available The large specimens typically experience more permanent strains than the standard specimens. The permanent strains from the laboratory tests are poorly correlated (R^2=.008) with the small-scale tests.

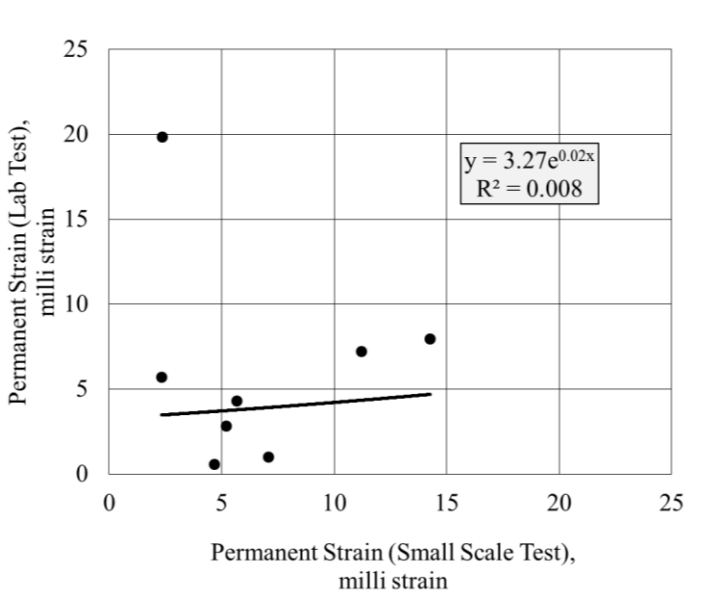

Figure 2.36 Variations in permanent strains of laboratory tests and small-scale tests

Figure 2.37 shows the correlations between the k-parameters from the resilient modulus tests on the standard specimens and the permanent strains from the permanent deformation tests on the standard and large specimens. The k_2 and k_3 parameters have comparatively good correlation with the permanent strains from the standard laboratory specimens than those of the small-scale tests ($R^2 < 0.01$). On the other hand, the k_1 parameters are better correlated with the permanent strains of the large specimens. The permanent strains from the standard and large specimens gradually decrease with increase in the magnitude of k_1 parameter.

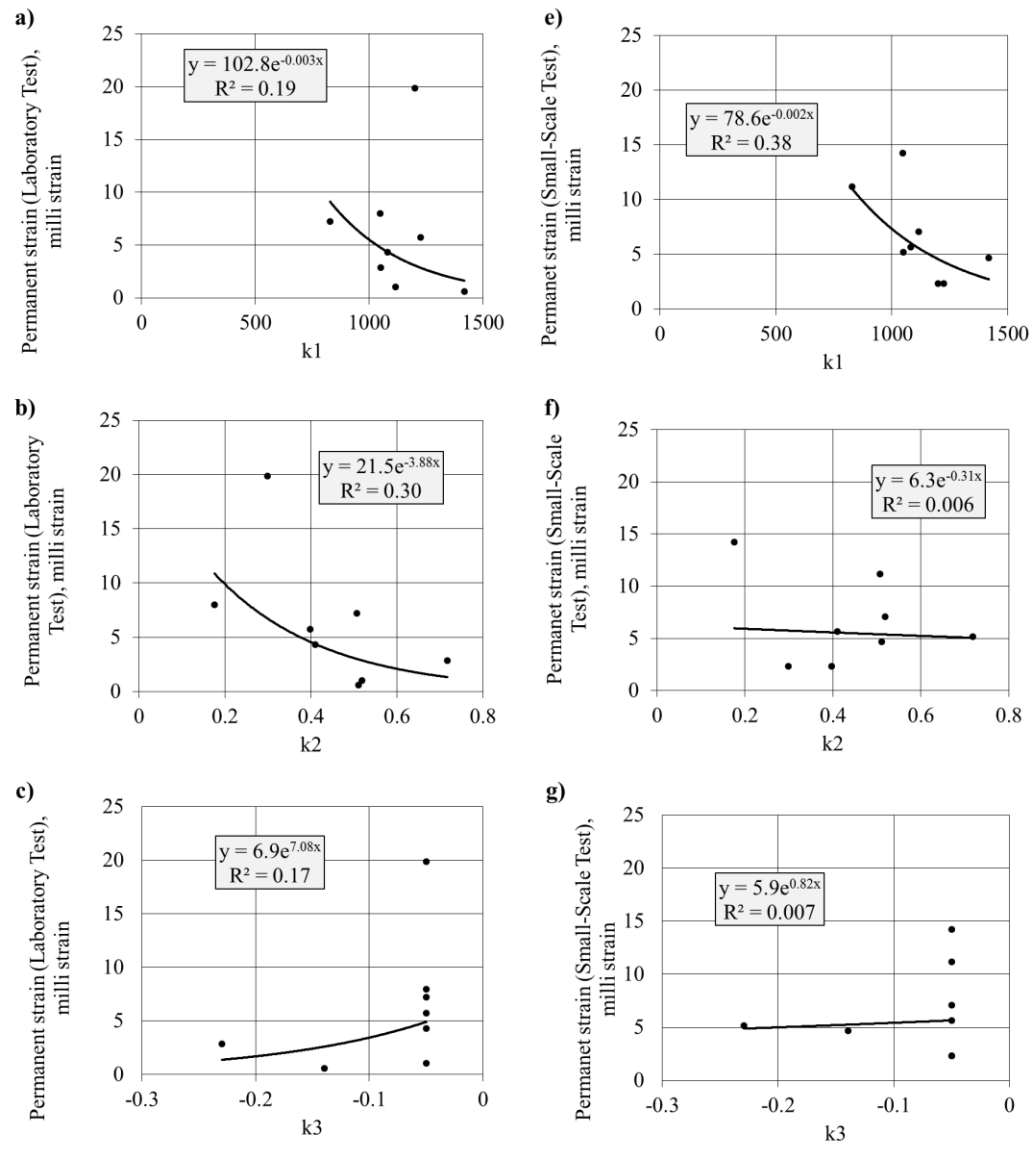

Figure 2.37 Variation of k-parameters with permanent strain measured from laboratory test (a, b and c). Variation of k-parameters with permanent strain measured in small-scale test (e, f and g)

Figure 2.38 compares the FFRC moduli of the standard specimens with the PSPA moduli of the large specimens. A good correlation between the two parameters are observed with the PSPA modulus being about 10% greater than the FFRC modulus.

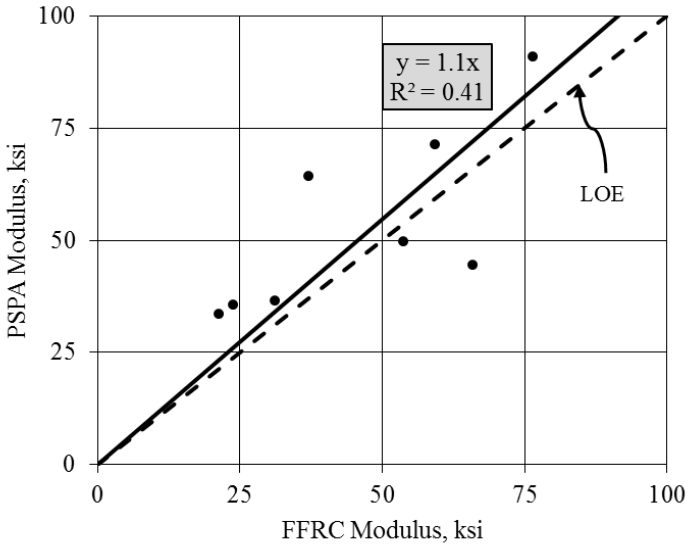

Figure 2.38 Variations in the PSPA modulus from small-scale test with the FFRC modulus from the laboratory test

CHAPTER 3 EVALUATION OF STIFFNESS PARAMETERS OF CONTAMINATED RAILWAY BALLAST

3.1. Background

This section focuses on the review of the literature with an emphasis on the effects of ballast fouling, characterization techniques of the clean and fouled ballast in the laboratory and in the field, and the proposed nondestructive techniques for determining the mechanical properties of the clean and fouled ballast.

3.1.1. Railway Track

A railway track is usually composed of a layer of ballast placed over a natural compacted soil or subgrade (Figure 3.1). Sometimes, a layer of sub-ballast is also introduced between the ballast layer and subgrade. The ballast layer, forming the top-most layer of geomaterials in a railway track, consists of coarse and angular aggregates. The aggregate particle size in the ballast usually ranges from 2.5 in. to 0.375 in. For example, the ballast designated by the American Railway Engineering and Maintenance-of-Way (AREMA) as AREMA 24 has a maximum aggregate size of 2.5 in. and minimum aggregate size of 0.5 in. whereas the ballast gradation of AREMA 4 has maximum aggregate size of 1.5 in. and minimum aggregate size of 0.375 in. (see Table 3.1). In the case of sub-ballast, the aggregate size varies from 0.375 in. to less than 0.003 in.

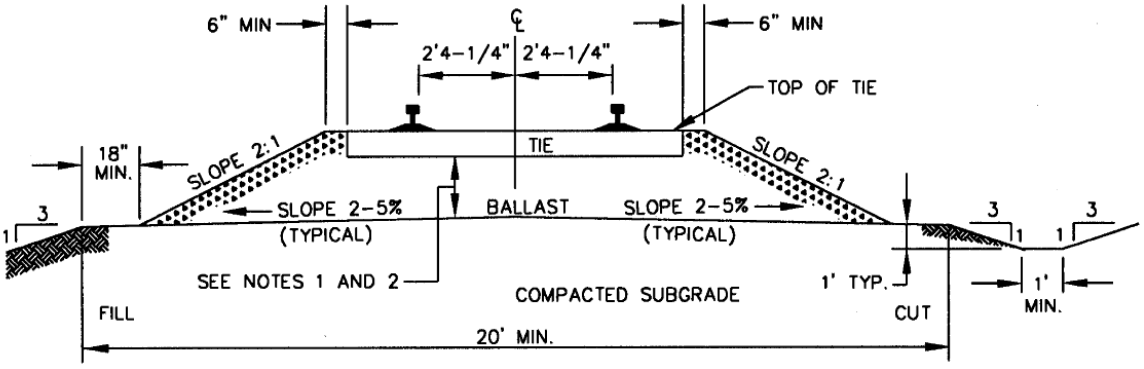

Figure 3.1. A typical railway track section (from USACE 2014)

The sub-ballast layer also functions as a filter medium between the ballast and fine-grained subgrade that restricts migration of fines from the subgrade to the ballast.

Table 3.1. Recommended Ballast Gradations (from AREMA 2012)

Size No. (See Note 1)	Nominal Size Square Opening	Percent Passing									
		3″	2½″	2″	1½″	1″	¾″	½″	d″	No.4	No. 8
24	2½″- ¾″	100	90-100		25-60		0-10	0-5	–	–	–
25	2½″ - d″	100	80-100	60-85	50-70	25-50	–	5-20	0-10	0-3	–
3	2″ - 1″	–	100	95-100	35-70	0-15	–	0-5	–	–	–
4A	2″ - ¾″	–	100	90-100	60-90	10-35	0-10	–	0-3	–	–
4	1½″ - ¾″	–	–	100	90-100	20-55	0-15	–	0-5	–	–
5	1″ - d″	–	–	–	100	90-100	40-75	15-35	0-15	0-5	–
57	1″ - No. 4	–	–	–	100	95-100	–	25-60	–	0-10	0-5

Note 1: Gradation Numbers 24, 25, 3, 4A and 4 are main line ballast materials. Gradation Numbers 5 and 57 are yard ballast materials.

As no binding material is used for preparing the ballast layer, the load distribution mechanism is by particle interlocking and particle friction. A proper selection of suitable ballast gradation is required for acquiring a proper density, draining excessive water, maintaining a uniform support to ties (structures supporting rails) and reducing deformations due to the train dynamic loads.

The track operation and the variation in the climatic condition affect the mechanical properties of the layers of ballast, sub-ballast and subgrade. Excessive moisture in most geomaterials results in a reduction in the shear strength or stiffness. In addition, the contamination of the ballast with fines from the deterioration of ballast and migration of subgrade can lead to the degradation of the shear strength of the ballast (Anderson and Rose 2008; Parsons et al. 2012).

3.1.2. Ballast Fouling

Huang et al. (2009) discussed different phases of fouling in the ballast (see Figure 3.2). The clean ballast is formed by contacts within aggregates that results in void spaces (Figure 3.2a). During the process of fouling, the void spaces are filled with the contaminating agents (Figure 3.2b). With the increase in fouling, the voids filled with fouled materials expand and result in the

loss of contact among aggregates (Figure 3.2c). The major consequence of a fouled ballast is track deformation due to train loads. An increase in the moisture content of the fouled ballast causes significant reduction in the shear strength since the fouled material acts as a lubricant.

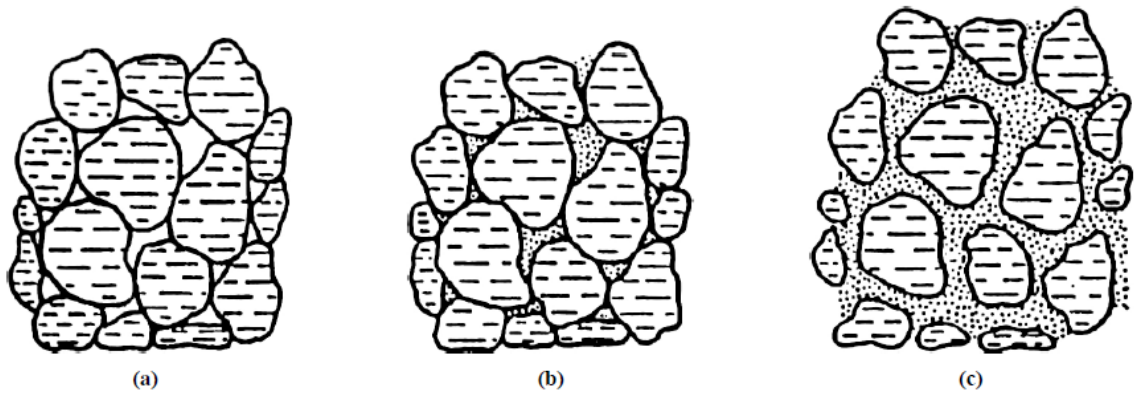

Figure 3.2. Different phases of fouling: a) clean ballast, b) partially fouled ballast, and c) fully fouled ballast (from Huang et al. 2009)

Selig and Waters (1994) mentioned that 76% of fouling was caused by ballast breakdown, 13% by infiltration from sub-ballast, 7% by infiltration from the ballast surface, 3% from subgrade intrusion, and 1% is related to tie wear. The authors proposed the following two methods for quantifying ballast fouling:

a. Fouling percentage, the ratio of the dry weight of the material passing the 0.374 in. sieve to the dry weight of total sample
b. Fouling index, the sum of percentage of materials passing through the 0.187 in. sieve and 0.003 in. sieve

Some other methods of quantifying ballast fouling based on the volumetric method are Percentage Void Contamination (PVC; Feldman et al. 2002) and Void Contamination Index (VCI; Indraratna et al. 2010). The PVC is a ratio of volume of fouling material to the initial volume of voids in the ballast. The concept of VCI is similar to PVC with consideration of void ratio, specific gravity and gradation of ballast and fouling material.

3.1.3. Characterization of Fouled Ballast

Several researchers have studied the characteristics of fouled ballast using laboratory tests (Han and Selig 1997; Huang et al. 2009; Parsons et al. 2012) or field performance tests (Roberts et al. 2006). The presence of coarser ballast particles and the composite arrangements of railway structures, such as rails and ties, pose a problem in field characterization of ballast. De Bold et al. (2010) mentioned the use of the Falling Weight Deflectometer for evaluating in situ stiffness of ballast required time consuming and expensive disassembling of rails and ties from the ballast.

Huang et al. (2009) used a shear box to determine the shear strength of clean and fouled ballast prepared with coal dust, plastic clayey soil, and mineral filler. They varied the amount of the fouling agents and conducted tests under the dry, wet and optimum moisture conditions. The authors reported the highest shear strength for the clean ballast. The addition of the fouling material resulted in a decrease in shear strength, while the ballast fouled with coal showed a significant loss of strength. The loss in strength accelerated with the increase in the moisture content for all cases.

Parsons et al. (2012) conducted a soil resistivity survey using the Wenner configuration to measure the level of ballast contamination. A test box was used for modeling the fouled ballast with contamination levels between 20% and 50%. The test box consisted of water inlet and outlet ports to alter the moisture content. The authors observed that the resistivity and the permeability of the fouled ballast decreased with the increase in the degree of fouling and moisture content. The rate of reduction in the permeability of the fouled ballast was found to be proportional to the increase in the percentage of contamination level.

Roberts et al. (2006) illustrated the use of the Ground Penetrating Radar (GPR) to determine the fouling conditions in the railway tracks. The authors found that the fouled ballast had a minimum scattering of the GPR signal compared to the clean ballast.

3.1.4. Nondestructive Techniques

Several nondestructive testing (NDT) techniques implemented in characterizing pavements have been proposed to evaluate the mechanical properties of the clean and fouled ballast. Each technique is introduced briefly in the following sub-sections.

3.1.4.1 Spectral Analysis of Surface Waves (SASW) Test

The Spectral Analysis of Surface Waves (SASW) method have been used in geotechnical site investigation and pavement evaluation (Nazarian and Stokoe 1985; Yuan and Nazarian 1992; Stokoe et al. 1994; Calderón-Macías and Luke 2010; Nazarian 2012). The fundamental principle of the SASW method is based on the measurement of surface wave velocity propagating through the material to estimate the shear wave velocity profile. The equipment required are impact energy sources, two or more receivers (geophones or accelerometers) placed on the ground surface, and a computer-based data acquisition/analysis system. A complete procedure with the SASW approach consists of the following three steps:

1. conducting field measurements to obtain the time domain signals from the receivers,
2. interpreting the time signals to construct a dispersion curve, and
3. analyzing the dispersion curve through a back calculation or inversion process to derive a representative shear wave velocity profile and, hence, a modulus profile showing the distribution of stiffness of subsurface.

3.1.4.2 Portable Seismic Property Analyzer (PSPA) Test

The Portable Seismic Property Analyzer (PSPA) consists of two accelerometers (receivers) and a source packaged into a hand-portable system (see Figure 3.3a). The source produces an impulsive impact on the material surface that generates stress waves. The signals of the stress waves are captured by two accelerometers. The spectral analysis of the signals are performed to compute the average shear wave velocity (Vs) of the material. The low-strain or linear elastic

modulus (E) (Nazarian et al. 2003) of a layer (see Figure 3.3b) is, then, derived with the Poisson's ratio (υ) and mass-density (ρ) of the material using the following equation:

$$E = 2 \rho V_{s2} (1 + \upsilon) \qquad \text{Equation 3.1}$$

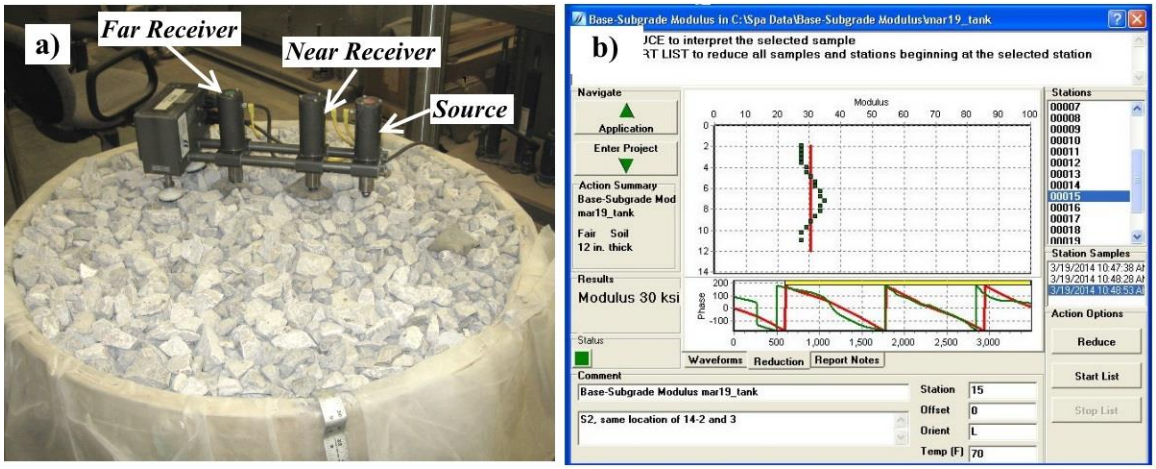

Figure 3.3 PSPA Test on a ballast specimen (a) and analysis of PSPA data

3.1.4.3 Light Weight Deflectometer (LWD) Test

The LWD is a portable device (see Figure 3.4a) that measures the surface deflection under

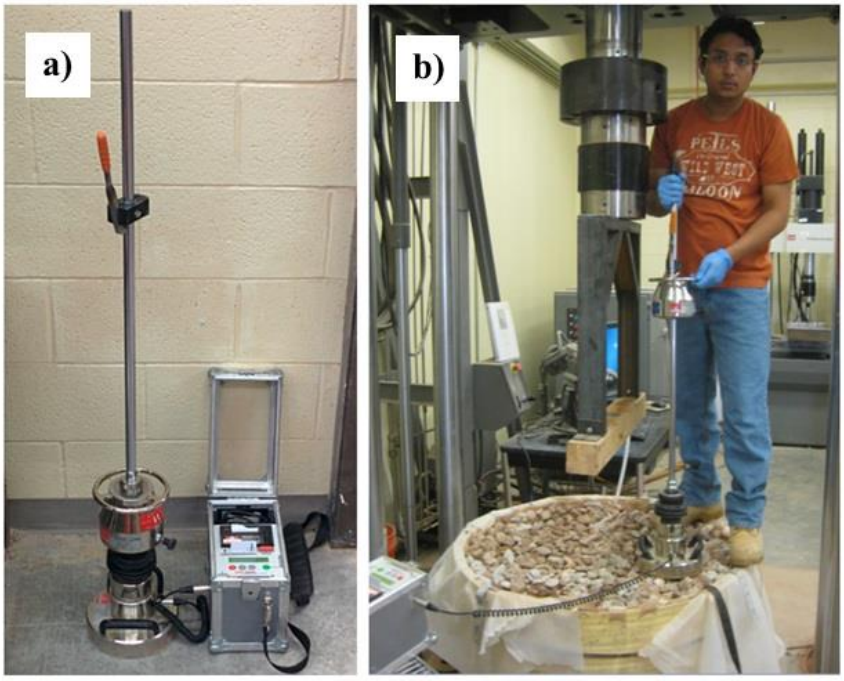

Figure 3.4. LWD (a) and LWD test on a ballast specimen (b)

a given load and computes an effective modulus. The LWD test assumes that the material is a single elastic layer. The LWD test has an advantage of determining in-situ stiffness of pavement base and subgrade rapidly for quality management (Fleming et al. 2007; Nazarian et al. 2014). The effective modulus, E_{eff}, is computed from the following equation

$$E_{eff}=[(1-\nu^2)F/(\pi\, a\, d_{lwd})]f \qquad \text{Equation 3.2}$$

where ν = Poisson's ratio of the geomaterial, a = radius of load plate, F = LWD load, d_{lwd} = LWD surface deflection, and f = shape factor which is a function of the plate rigidity and soil type.

3.1.4.4 Load-deformation Test

The load-deformation test (a.k.a., plate load test) has been used by many investigators (e.g., Sweere 1990; DeMerchant et al. 2002; Alshibli et al. 2005; Li and Baus 2005) to understand the deformation characteristics of the geomaterials under compressive loads. The schematic of typical load-deformation test apparatus is shown in Figure 3.5. The test set up consists of a hydraulic actuator mounted on a heavy truck to apply load, a load cell to measure the load, a steel plate to impose the load on the road surface and one or more Linear Variable Displacement Transformers (LVDTs) to measure the vertical displacements.

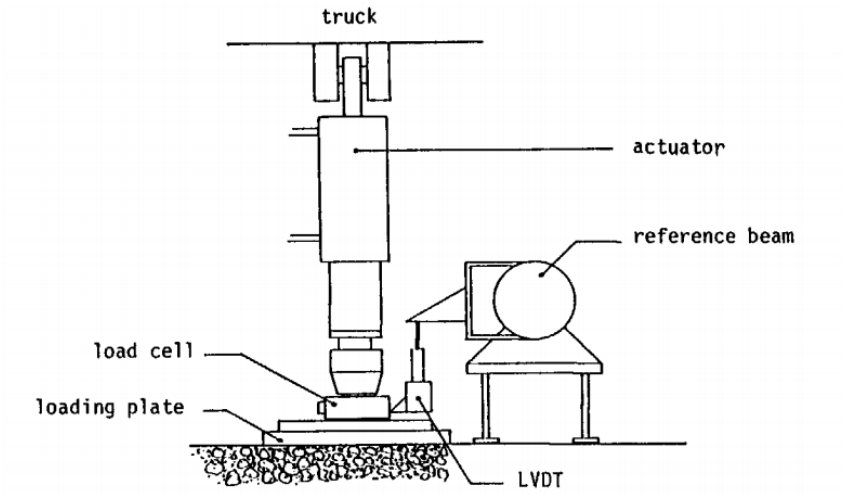

Figure 3.5. Load-Deformation test apparatus (from Sweere 1990)

3.1.4.5 Impulse Response (IR) Test

The Impulse Response method has been adopted for several applications such as the detection of defects under rigid pavement (Nazarian et al. 1994; Nazarian and Reddy 1996) and assessment of the condition of bridge decks (Gucunski et al. 2013). The Impulse Response method has also been used for the health monitoring of railway structures such as rail, tie and ballast (Kaewunruen and Remennikov 2006; De Bold et al. 2010; De Bold 2011). The fundamental principle of the impulse response test is based on the excitation of a structure by an instrumented hammer and the measurement of the vibration of the structure. The hammer response and the structure response are usually measured in the time-domain, and are transformed to the frequency domain using fast Fourier transform. The ratio of the structure response to the hammer response in the frequency domain is known as the frequency response function (FRF) which is required to understand the dynamic behaviors the system. When the structure responses are measured with the velocity transducers (e.g., geophones), the FRF measures mobility of the system (Ewins 1984). De Bold et al. (2010) presented typical FRF responses for honeycomb and sound concretes (see Figure 3.6). The authors mentioned that the air voids in the honeycomb concrete are responsible for the higher mobility that corresponds to the lower stiffness.

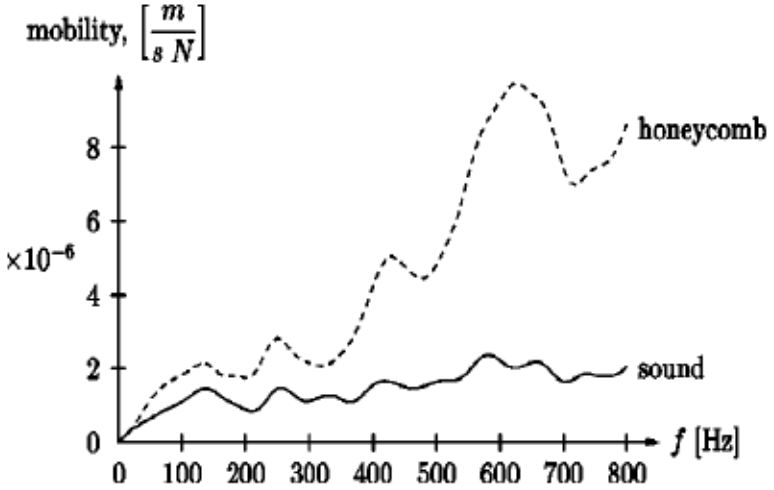

Figure 3.6. Typical FRF of honeycombed and sound concrete specimens (from De Bold et al. 2010)

3.2. Research Approach and Testing Procedure

This section describes the type of the ballast and fouling agents used for preparing the specimens, and the testing protocols for conducting the small-scale experiments.

3.2.1. Experiment Design and Construction of Fouled Ballast Specimens

The schematic of a ballast specimen is shown in Figure 3.7. The mold, which was made from a polyethylene pipe, had an inner diameter of 36 in., height of 28 in. and thickness of 1 in. The material profile for each specimen consisted of 3 in. of pea gravel at the bottom, 12 in. of subgrade in the middle and 12 in. of ballast on the top. The bottom and the inner walls of the mold were lined with 6-mil thick polyethylene sheet to minimize the interaction between the geomaterials and the mold walls. Based on a finite element analysis, Amiri (2004) found the dimensions of this specimen is appropriate for the type of tests carried out in this study.

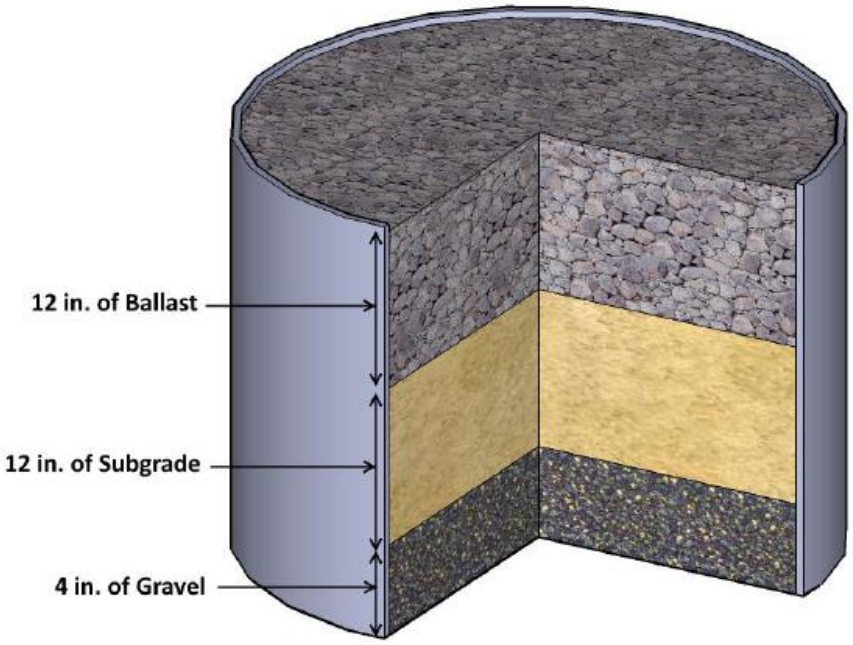

Figure 3.7. Schematic of a mold filled with pea-gravel, subgrade and ballast

The subgrade, which was common to all specimens, was designated as SM as per USCS soil classification with maximum dry density (MDD) and the optimum moisture content (OMC) of 112 pcf and 15.2%, respectively.

The clean ballast, designated as AREMA 4, was obtained from a local quarry in El Paso. Using ASTM C29 procedure, the bulk dry density of the clean ballast was found to be 108 pcf. Two types of fouling agents, rock dust and clay, were used. The rock dust particles were finer than 0.750 in. and contained 1.5% fines (particles finer than 0.003 in.) whereas the clay particles were finer than 0.047 in. and contained 97% fines. The rock dust was obtained from the same quarry that produced the ballast. The clay was a high-plasticity clay obtained from Minnesota. As per Unified Soil Classification System (USCS), the rock dust was classified as "SW" and the clay as "CH." The plasticity indices (PIs) of clay and rock dust were 53 and 10, respectively.

To fabricate the fouled ballast specimens, the clean ballast was mixed with the appropriate fouling agents in the proportion of 20% (moderately-fouled) or 50% (heavily-fouled) by weight of clean ballast; and then compacted to the nominal bulk densities reported in Table 3.2. The gradations for the clean and fouled ballast specimens are shown in Figure 3.8. The classifications of the fouled ballast specimens as per Selig and Waters (1994) are tabulated in Table 3.3. Even though the fouling percentages for the moderately-fouled and heavily-fouled specimens fouled with clay and rock dust are similar (see Table 3.3), their fouling indices are quite different.

Table 3.2. Dry densities and moisture contents of fouled ballast specimens prepared with clay and rock dust

Degree of Fouling	Moisture Condition	Dry Density* (pcf)		Moisture Content (%)	
		Clay	Rock Dust	Clay	Rock Dust
Moderately-Fouled	Dry	116	122	0	0
	Sat.			33	28
	Wet			17	22
Heavily-Fouled	Dry	129	137	0	0
	Sat.			28	23
	Wet			18	20

** Dry density of clean ballast specimen is 108 pcf*

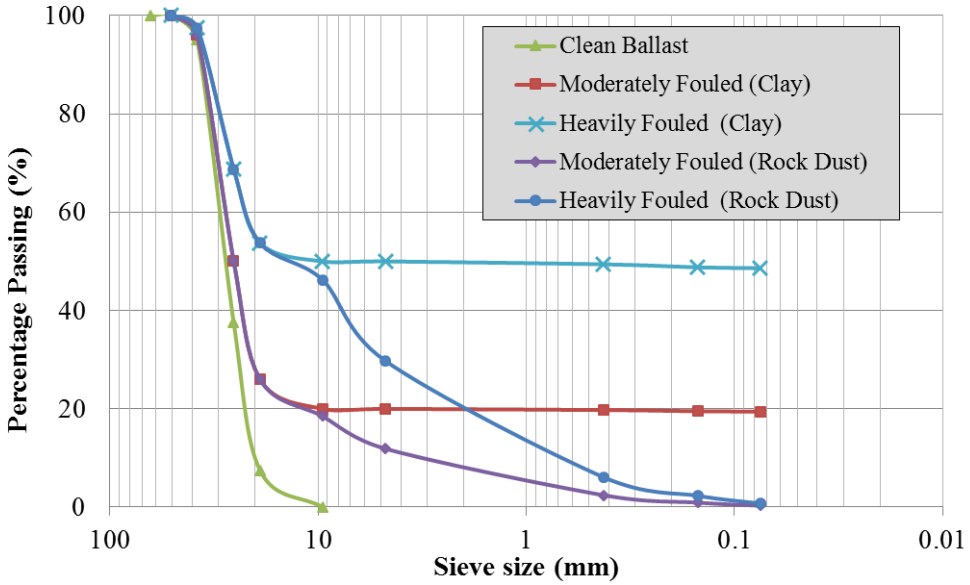

Figure 3.8. Gradations for clean and fouled ballast specimens

Table 3.3. Classification of fouled ballast specimens as per Selig and Waters (1994)

Degree of Fouling	Fouling Percentage		Fouling Index	
	Clay	Rock Dust	Clay	Rock Dust
Moderately-Fouled	20%	18%	39%	12%
Heavily-Fouled	50%	46%	99%	30%

3.2.2. Testing Protocols and Processes

Each specimen was tested under three moisture conditions: dry, saturated and wet (i.e., partially dried after saturation) conditions. The clean ballast was first mixed uniformly with the appropriate amount of oven-dried fouling materials in a concrete mixer to simulate a fouled specimen under the dry condition. After the completion of the tests in the dry condition, the fouled ballast was saturated by introducing water from soaker hoses placed on top of the specimen in the mold. The tests were subsequently repeated in the saturated condition. The saturated ballast was left to dry after the second set of tests for three days, and the tests were repeated in the wet condition. After completion of tests, about 10 lb of the material was extracted from the specimen to measure the moisture content. The measured moisture contents of the fouled ballast specimens are presented in Table 3.2.

3.2.3. Small-Scale Experiments

Several NDT tests, as described in section 3.1, were performed for estimating the mechanical properties of the clean and fouled ballast specimens. These tests included the SASW test, PSPA test, LWD test, Load-Deformation test and Impulse Response test.

3.2.3.1 SASW Test

The SASW tests were conducted to measure shear-wave velocity of ballast. A 3-oz ball peen hammer was used to generate signals and two accelerometers with the frequency range between 2.5 Hz to 3000 Hz and sensitivity of 1000 mV/g were used to record the generated signals. The source offset (the distance between the source and the first accelerometer) of 12 in. and receiver spacing (the distance between the two accelerometers) of 12 in. were adopted. Eighteen SASW tests were performed on each specimen.

3.2.3.2 PSPA Test

The PSPA tests were conducted to measure the elastic modulus (referred as a PSPA modulus hereafter) at 24 different locations of the mold surface as shown in Figure 3.3b.

3.2.3.1 LWD Test

An LWD manufactured by Zorn Instruments was adopted. The LWD tests were performed as per ASTM E2583. The effective modulus (referred as a LWD modulus hereafter) given in Equation 2.2 was computed assuming a Poisson's ratio of 0.4, the radius of load plate as 4 in., LWD load as 1700 lb, and shape factor of 2. For each specimen, three spots were chosen to conduct the LWD tests and measure deflections under the load plate (Figure 3.4b).

3.2.3.1 Load-deformation Test

In a typical load-deformation test (a.k.a. plate load tests), a circular plate is used for imposing the load as the contact area between the vehicle tire and the pavement surface is assumed

to be circular (Huang 2004). The circular plate usually used for the plate load tests was replaced with a tie with dimensions equivalent to half of a standard tie (36 in. length, 4 in. width and 4 in. height.) to simulate the train loads better.

To characterize the geomaterials under different loading magnitudes and frequencies, a Material Testing and Simulation (MTS) system was used for loading the tie using a steel bracket as shown in Figure 3.9a. A continuous load, up to 3500 lb, was applied at a loading rate of 500 lb/min (see Figure 3.9b). After reaching the peak load, the specimen was unloaded in one minute. During these tests, the deformation of the specimen was measured during the loading and unloading stages. A typical load-deformation response is shown in Figure 3.9c. The stiffness of the simulated track bed and the permanent deformation (the total deformation after removal of the load) were determined from the load-deformation response.

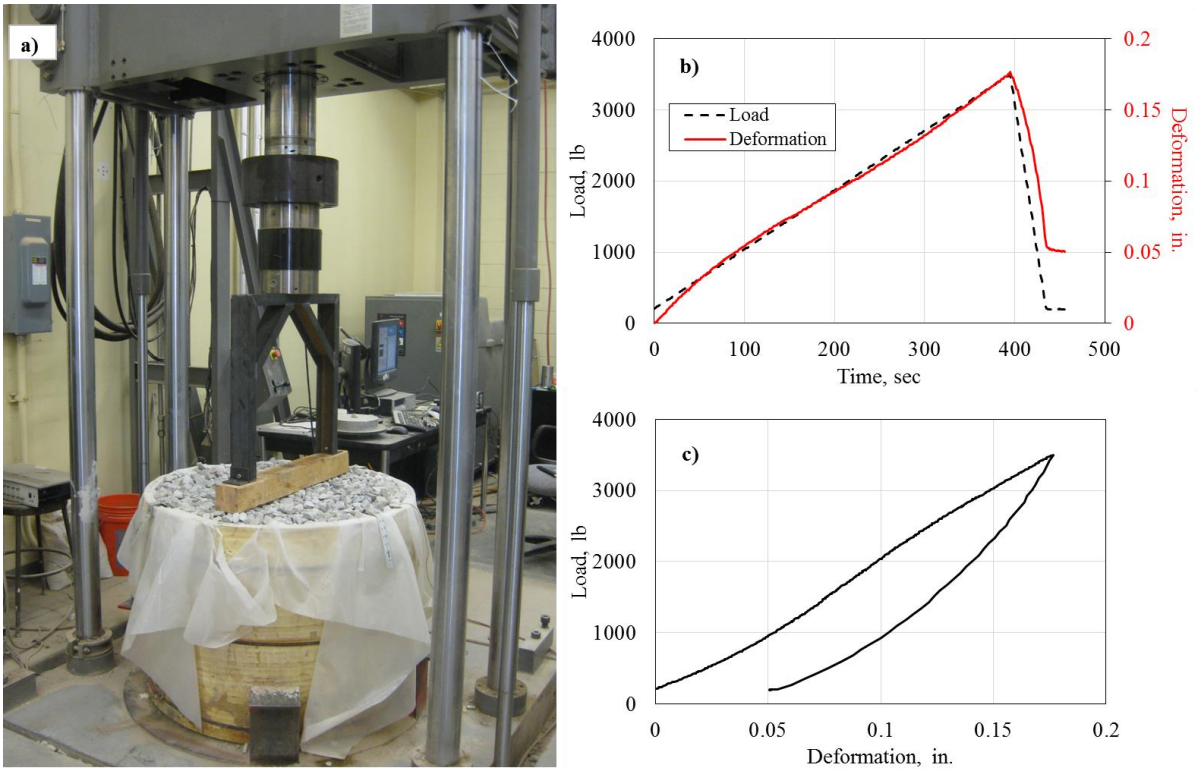

Figure 3.9. Load-Deformation Test (a), load and deformation vs time plot (b) and load vs deformation plot (c)

3.2.3.1 IR Test

A schematic of the impulse response (IR) test as shown Figure 3.10a is similar to the technique described by De Bold et al. (2010) with a few differences summarized in Table 3.4. Two geophones (with resonant frequency of 4.5Hz and sensitivity of 1000 mV/in./sec) and one instrumented hammer (with sensitivity of 1 kip/V) were used for the test. One geophone was fixed to the tie and the other to the ballast. The instrumented hammer was used to impact either the tie or the ballast to measure the responses of both the tie and ballast simultaneously with the two geophones. With this test configuration, four different FRFs were obtained as detailed in Table 3.4.

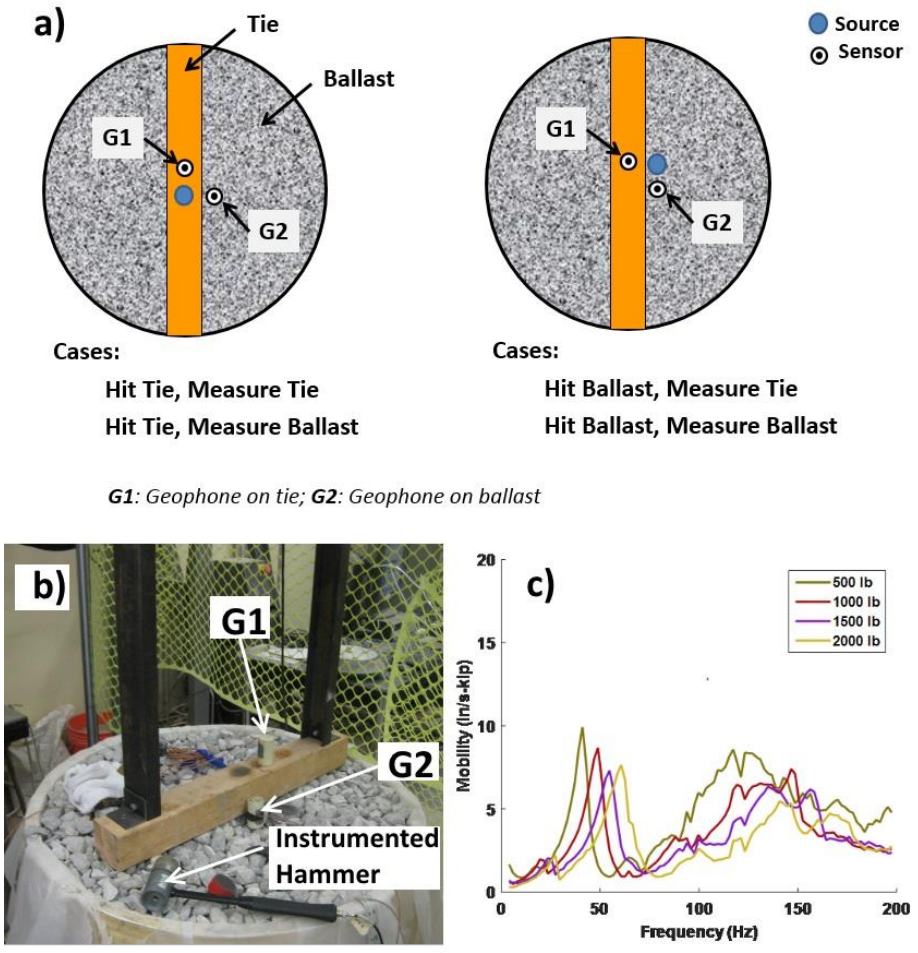

Figure 3.10. Schematic of Impulse Response tests for different source-sensor configurations mentioned in Table 3.5 (a), Impulse Response test (b) and typical FRFs at different external loads as mentioned in Table 3.4 (c)

Table 3.4. Impulse Response Test

	De Bold et al. (2010)	This Research
Geophones	One	Two: one on tie and the other on ballast
External Load	No load	The tie was loaded with vertical loads (the preloading forces) of 500 lb, 1000 lb, 1500 lb and 2000 lb
Hammer excitation	On tie, ballast and rail	On tie and ballast
Measurements	Initial slope of FRF and average mobility	Slope from origin to first peak in FRF

The IR tests were repeated at several preloading forces to simulate the impact of the intensity of the load applied on the stiffness of the ballast. For this purpose, the tie was preloaded between 500 lb and 2000 lb (in increments of 500 lb) with the MTS through the tie and steel bracket. Typical frequency response functions (FRFs) obtained from the IR test are shown in Figure 3.4c. The results of the IR tests were presented in terms of the stiffness of specimens measured from the FRFs (called IR stiffness hereafter). The inverse of the slope of a line that connects the first peak and the origin of the FRF was used to compute the IR stiffness. Figure 3.11 shows an example for computing the IR stiffness. The first peak in the FRF is used to compute IR stiffness for simplifying the results.

Table 3.5 Source-sensor Configurations of Impulse Response Test

Cases	Description	Code
Hit tie, measure tie	The hammer is excited on the tie and the geophone on the tie measures the responses	HTMT
Hit tie, measure ballast	The hammer is excited on the tie and the geophone on the ballast measures the responses	HTMB
Hit ballast, measure tie	The hammer is excited on the ballast and the geophone on the tie measures the responses	HBMT
Hit ballast, measure ballast	The hammer is excited on the ballast and the geophone on the ballast measures the responses	HBMB

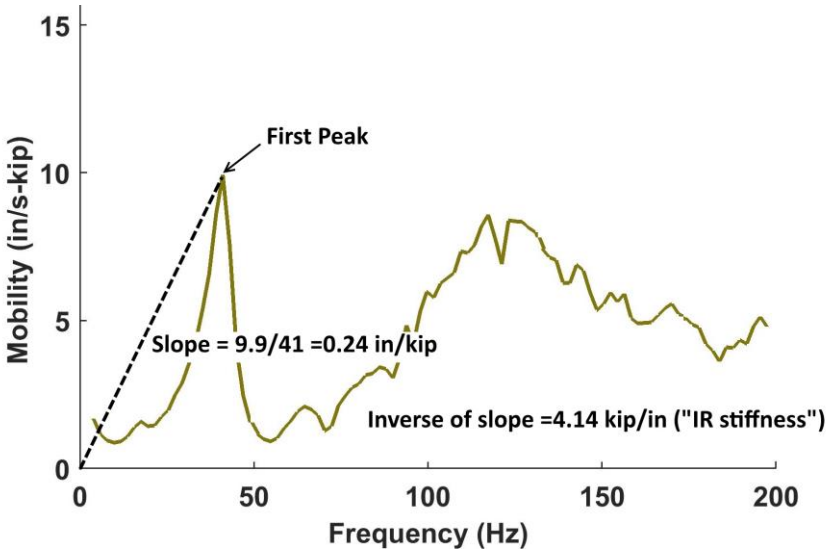

Figure 3.11. Computation of IR stiffness

3.3. Results from Small-Scale Experiments

This section presents the results from thirteen different small-scale experiments (see Table 3.2) conducted on the clean and fouled ballast specimens. The relationships among different test results are also provided.

3.3.1. SASW Tests

The phase spectra, and as such the dispersion data and shear-wave velocity profiles from the SASW tests, were often not of high quality. The limited space to place accelerometers, the lack intimate contact between the receivers and the ballast, and the excessive scattering of the signals from the coarse ballast particles were the anticipated causes for not obtaining the high quality data.

3.3.2. PSPA Tests

The PSPA moduli of the clean, and clay- and rock dust-fouled ballast specimens are presented in Figure 3.12. The heights of the error bars correspond to one standard deviation that were typically about 5 ksi but always less that than 8 ksi. These standard deviations that correspond to coefficients of variation of 10% to 26% demonstrate the non-homogenous nature of the ballast, and point out to the need for more than one measurement for characterizing such materials.

The PSPA tests of the clean ballast were only conducted under the dry condition because the free-draining nature of the material did not lend itself to saturation. However, past experience showed that the impact of the moisture on the modulus of clean ballast was minimal. For the moderately fouled specimens, irrespective of the fouling agent, the saturated moduli are less than the corresponding dry conditions. However, as the materials dry out to the wet condition, the moduli increase significantly. For the heavily fouled conditions, the trend is somewhat different. Even though the saturated moduli are less than the dry ones, the moduli after subsequent drying do not increase, significantly. Comparing the moduli under the dry conditions, the dry moduli increase as the degree of fouling increases. This indicates that under the dry condition, fouling might help in stiffening the track foundation. On the other hand, as soon as the fouled ballast becomes saturated it will lose its bearing capacity to some extent.

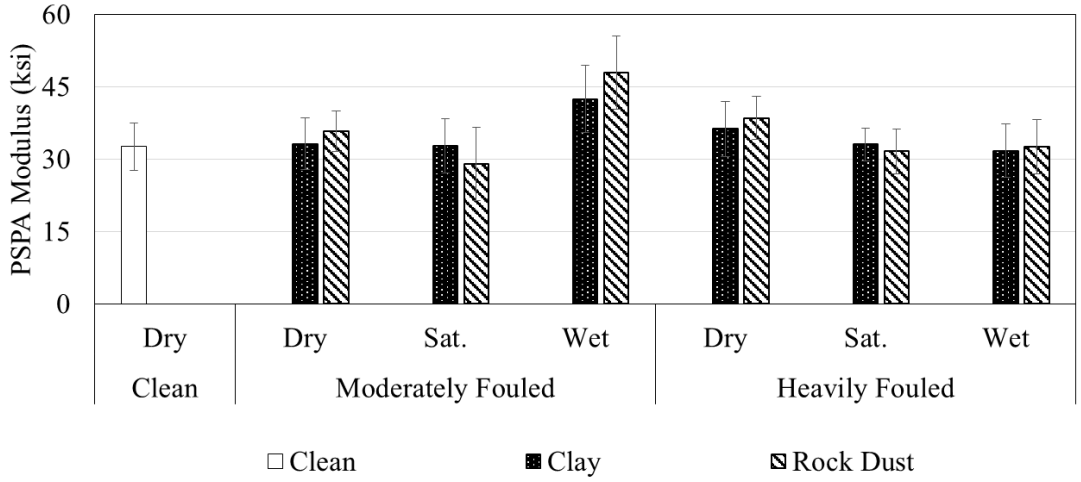

Figure 3.12. PSPA modulus of clean, and clay- and rock dust-fouled ballast specimens

3.3.3. LWD Tests

Figure 3.13 presents the variation in the LWD moduli of the clean and fouled ballast specimens with moisture content and degree of fouling. The average LWD modulus of the clean ballast is 6 ksi, which is significantly less than the corresponding PSPA modulus. The differences can be attributed to the fact that the PSPA moduli are the small-strain moduli of the ballast layer,

whereas the LWD moduli are the high-strain moduli of the combination of the ballast and the softer subgrade layer below it.

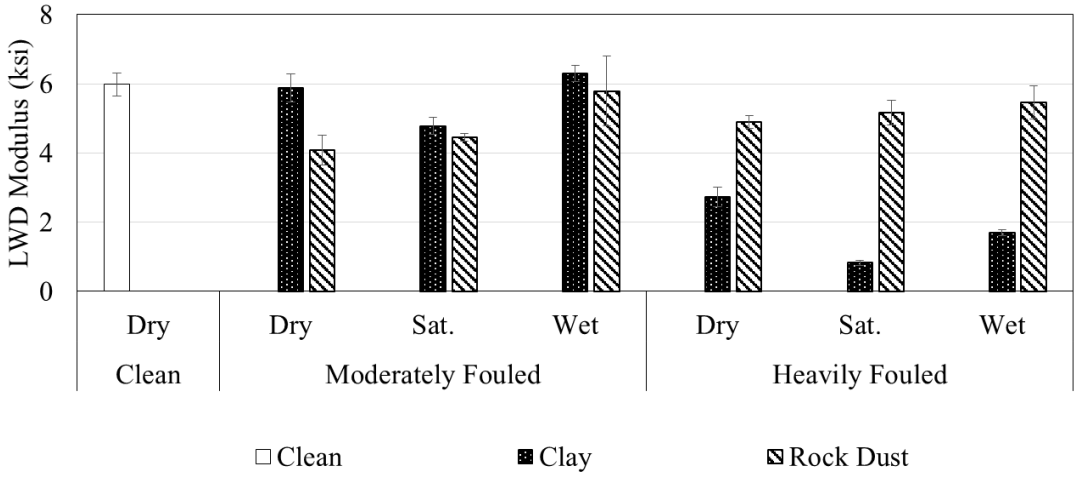

Figure 3.13 LWD modulus of clean, and clay- and rock dust-fouled ballast specimens

The moduli for the specimens moderately fouled with clay demonstrate a pattern that are somewhat similar to the PSPA; whereas the moduli of the dry and saturated specimens moderately fouled with rock dust-fouled specimens are similar. The moduli of the specimens heavily fouled with rock dust are almost independent of the moisture condition. On the contrary, the moduli of the specimens heavily fouled with clay demonstrate sensitivity to moisture condition. Even though the moduli of the specimens moderately fouled with rock dust and clay are similar under similar moisture conditions, the moduli of the specimens heavily fouled are significantly different. Unlike the PSPA moduli from the dry conditions, a consistent pattern between the modulus and degree of fouling is not apparent.

3.3.4. Load-deformation Tests

The load-deformation behaviors of the clean and fouled ballast specimens at dry, saturated and wet conditions are presented in Figure 3.14 for the clay-fouled specimens, and in Figure 3.15 for the rock dust-fouled specimens. The black dotted curves in those figures represent the response of the clean ballast specimen. Unfortunately, only the loading response was available for the clean

ballast. In all cases, the fouled specimens, at least initially, exhibit less deformation than the clean specimen does. The heavily fouled saturated specimen with clay exhibited excessive deformation. The load deformation curves for the rock dust-fouled specimens is essentially independent of the moisture condition, as shown in Figure 3.15

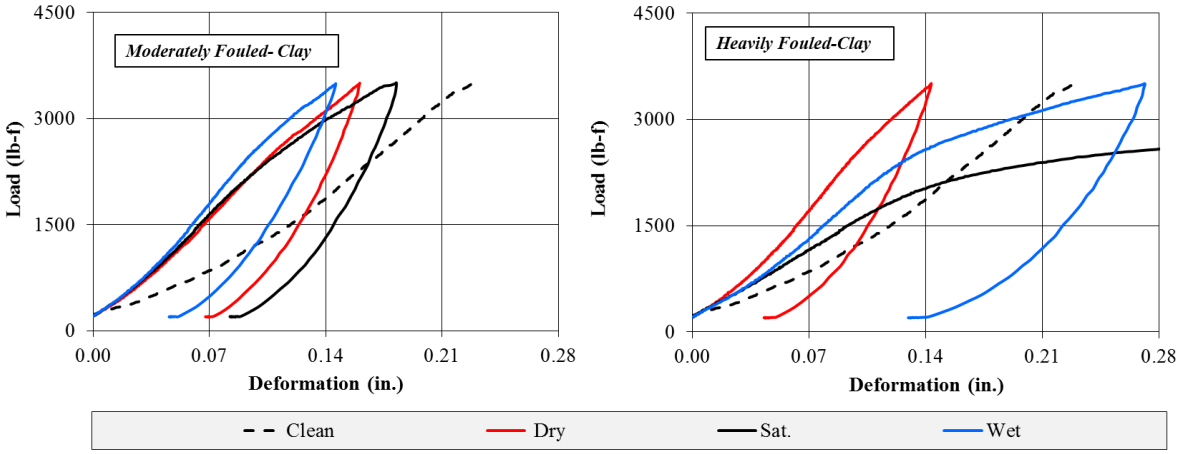

Figure 3.14. Load-Deformation response of clean and clay-fouled ballast specimens

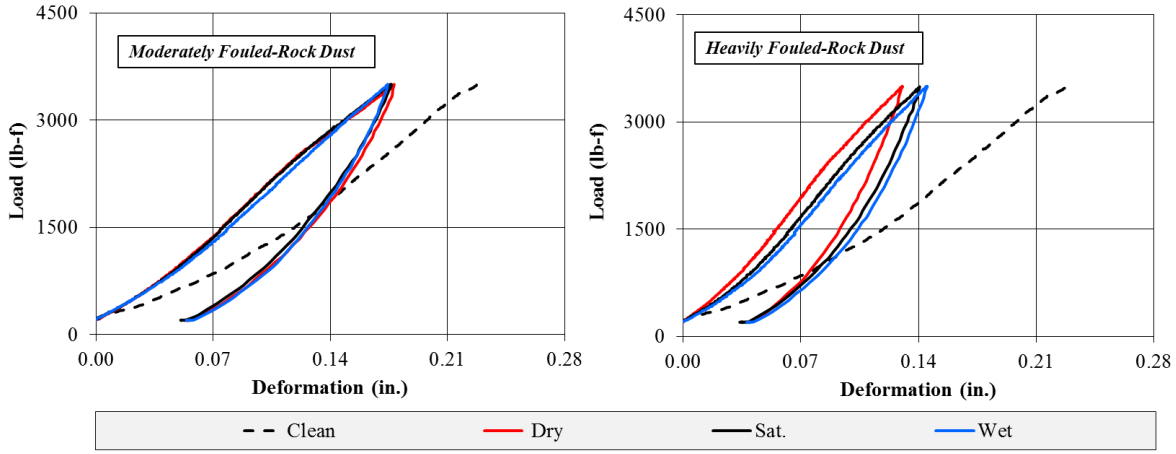

Figure 3.15. Load-Deformation response of clean and rock dust-fouled ballast specimens

Table 3.6 compares the permanent deformations measured on the fouled specimens. The highest permanent deformation of 794 mils is observed for the saturated heavily-fouled specimens prepared with clay. Except for the saturated and wet clay-fouled specimens, the permanent deformations of specimens decrease with the increase in the degree of fouling.

Table 3.6. Permanent deformation of clay- and rock dust-fouled ballast specimens

Degree of Fouling	Permanent Deformation (mils)					
	Clay			Rock Dust		
	Dry	Sat.	Wet	Dry	Sat.	Wet
Moderately-Fouled	68	83	46	52	50	54
Heavily-Fouled	43	794	130	37	34	38

The load-deformation responses presented in Figure 3.14 and Figure 3.15 were further analyzed to compute the stiffness of each specimen (called LD stiffness hereafter). The LD stiffness is defined as the slope of the load-deformation curve during loading. Figure 3.16 shows the variation in the LD stiffness of the clean and fouled ballast specimens with moisture content and degree of fouling. Except for the saturated heavily-fouled specimens prepared with clay, the fouled specimens exhibit greater LD stiffness than that of the clean ballast. The LD stiffness of the heavily fouled specimens prepared with clay are highly sensitive to change in the moisture condition. The LD stiffness of the rock dust-fouled specimens seems to be independent of the moisture content for a given degree of fouling, and similar to the PSPA, increasing with the increase in the degree of fouling under the dry condition.

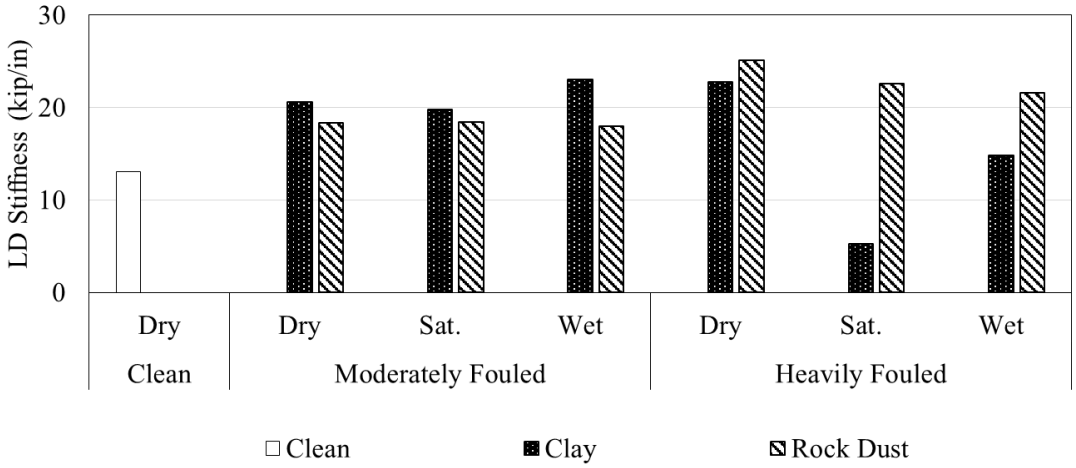

Figure 3.16 Stiffness of clean, and clay- and rock dust-fouled ballast specimens measured through Load-Deformation test

3.3.5. IR Tests

Typical examples of the HTMT (hit tie, measure on tie) IR stiffness for the clay- and rock dust-fouled specimens are provided in Figure 3.17. The IR stiffness values for all source-sensor configurations are reported in Appendix A. In these series of tests, the impact of the preloading force on the results are presented in addition to the impact of the moisture content and the degree of fouling. The IR stiffness in the HTMT configuration increases as the preloading force increases.

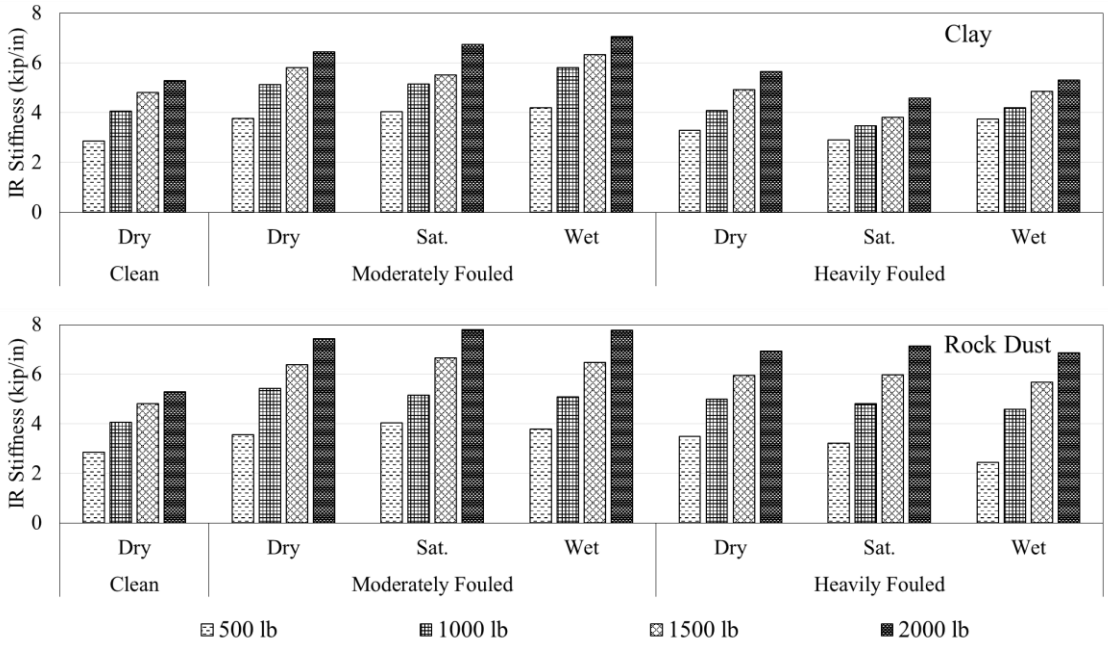

Figure 3.17 Stiffness of clean, and clay- and rock dust-fouled ballast specimens measured through Impulse Response test for the HTMT case

Given the number of parameters and configurations involved in the IR tests, a statistical analysis was carried out to understand the impacts of all of these parameters on the IR stiffness. The results from a correlation analysis showing the relationship between the IR stiffness and the test parameters are shown in Table 3.7. These relationships depend upon the source-sensor configurations. For example, the correlation coefficient for the preloading force varies between 0.51 and 0.82 whereas the correlation coefficient for the dry density varies between 0.01 and -0.58. This indicates that the source-sensor configuration, i.e. the locations of the source and geophone should be carefully considered. In general, the preloading force has strong correlations with the IR

stiffness, the fouling agent PI has weak correlation with the IR stiffness and the other parameters have moderate correlations.

Table 3.7. Correlation coefficients of IR stiffness with the test parameters

Source-sensor configuration	Preloading Force, kips	Fouling Agent PI	Fouling Percent, %	Fouling Index, %	Moisture Content, %	Dry Density, pcf
HTMT	0.82	-0.07	-0.11	-0.23	0.08	0.01
HTMB	0.66	0.09	-0.38	-0.17	-0.33	-0.45
HBMT	0.51	-0.08	-0.62	-0.50	-0.26	-0.58
HBMB	0.53	0.13	-0.31	-0.09	-0.21	-0.36

Based on the results in Table 3.7, multiple linear regression analyses were carried out to understand the influences of several test parameters on the IR stiffness of the specimens and develop appropriate prediction models. The major outputs of these analyses are the standardized and unstandardized β coefficients, t-stat, p-value, global coefficient of determination (R^2) and the standard error of estimate (SEE). The standardized β coefficients provide the relative contributions of each of independent variable in predicting the dependent variable. On the other hand, the unstandardized β coefficients are the regression coefficients for developing the prediction model. The t-stat and p-value are required for quantifying the evidence of the test. The R^2 and SEE measure the goodness and accuracy of the prediction model.

Table A1 in Appendix A shows the standardized β coefficient and p-value for all test parameters for each source-sensor configuration. As the fouling index and fouling percentage represent the same degree of fouling and the fouling percentage has more influence (higher rank and lower p-value) than that of the fouling index, the fouling index was disregarded for developing the prediction model.

The multiple linear regression analyses were again carried out with all tests parameters excluding the fouling index. The standardized β coefficient and p-value for each source-sensor configuration are tabulated in Table 3.8. The ranks of test parameters for the prediction models are also included in Table 3.8. The parameter with the highest absolute standardized β coefficient is assigned as the highest rank (i.e., 1), and the lowest as the lowest rank (i.e., 5). The fouling

percentage has the highest influence on the IR stiffness whereas the moisture content has the least influence for all source-sensor configuration. The other parameters have moderate influence. As the density of the specimen is directly impacted by the fouling percentage, the dry density is the other influencing parameter followed by the fouling percentage. Although the preloading force is the most influencing parameter in correlation results (see Table 3.7), it is not true for the multiple regression analysis. This is due to the simultaneous effects of several test parameters on the IR stiffness.

Table 3.8. The standardized β coefficient, p-value and rank of independent variables

Parameters	HTMT			HTMB			HBMT			HBMB		
	R*	β	p-value	R*	β	p-value	R*	β	p-value	R*	β	p-value
Preloading Force (kips)	3	0.82	0.00	2	0.66	0.00	4	0.51	0.00	4	0.53	0.00
Plasticity Index	4	0.79	0.00	3	0.46	0.01	3	0.75	0.00	3	0.63	0.01
Fouling Percentage (%)	1	-2.32	0.00	1	-0.78	0.04	1	-2.06	0.00	1	-1.18	0.02
Moisture Content (%)	5	-0.04	0.44	5	-0.32	0.00	5	-0.25	0.00	5	-0.25	0.03
Dry density (pcf)	2	2.11	0.00	4	0.33	0.35	2	1.34	0.00	2	0.75	0.12

Note: R=Rank showing the relative contributions of each of test parameter*

Using the unstandardized β coefficient, the IR stiffness prediction models are presented in Equations 3.3 to 3.6 for four source-sensor configurations. As each of the IR stiffnesses measured in each of the source-sensor configuration are different (see Figures A1 and A2 in Appendix A), the regression analyses reveal different β coefficients for each test parameter of the prediction models.

$$IR\ STIFFNESS_{HTMT} = -30.014 + 1.977 \times F_{pre} + 0.046 \times F_{PI} - 0.174 \times F_{per} - 0.004 \times MC + .295 \times \rho_{dry} \quad (R^2=0.89 \text{ and } SEE=0.45) \qquad \text{Equation 3.3}$$

$$IR\ STIFFNESS_{HTMB} = -0.874 + 1.914 \times F_{pre} + 0.033 \times F_{PI} - 0.070 \times F_{per} - 0.042 \times MC - .055 \times \rho_{dry} \quad (R^2=0.74 \text{ and } SEE=0.87) \qquad \text{Equation 3.4}$$

$$IR\ STIFFNESS_{HBMT} = -25.145 + 1.839 \times F_{pre} + 0.066 \times F_{PI} - 0.233 \times F_{per} - 0.041 \times MC + .281 \times \rho_{dry}\ (R^2=0.76\ and\ SEE=1.02) \quad \text{Equation 3.5}$$

$$IR\ STIFFNESS_{HBMB} = -15.671 + 2.029 \times F_{pre} + 0.060 \times F_{PI} - 0.142 \times F_{per} - 0.043 \times MC + .169 \times \rho_{dry}\ (R^2=0.51\ and\ SEE=1.59) \quad \text{Equation 3.6}$$

where F_{pre} = Preloading Force on tie in kips; F_{PI} = Plasticity Index of fouling agent; F_{per} = Fouling Percentage in %; MC = Moisture content of specimen in %; ρ_{dry} = Dry density of specimen in pcf; HTMT = Hit tie, measure tie; HTMB = Hit tie, measure ballast; HBMT = Hit ballast, measure tie; HBMB = Hit ballast, measure ballast

The observed and predicted IR stiffness values from the proposed models are compared in Figure 3.18. The results from the proposed models are in good agreement with the measured ones

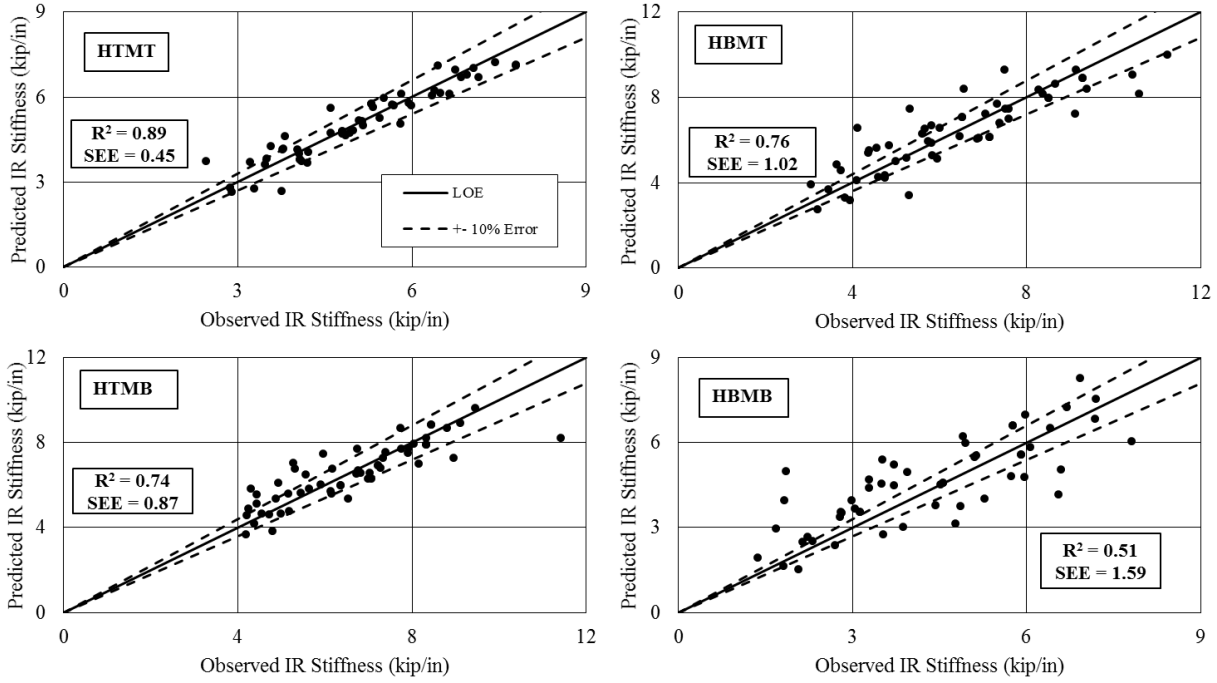

Figure 3.18. Comparison of observed and predicted IR stiffness

except for the case of HBMB. Most of the measurements for the HBMB case are outside the range of 10% error. Further, based on the R^2 and SEE values presented in Equations 3.3 through 3.6, the prediction models for the HTMT and HTMB cases seem to be better than the other two cases. In

other words, the IR test with the source impacted on the tie is more reliable than the source impacted on the ballast.

3.3.6. Comparison of Various Small-scale Experiments

This section deals with evaluating the inter-relationships among different stiffness parameters reported in the previous sections. As reflected in Appendix B, the PSPA moduli did not correlate well with the other test results simply because it is the only method that measures the property of the ballast alone.

3.3.6.1 Correlation between Load-Deformation tests and LWD

The stiffness parameters from the load-deformation tests are related to the LWD moduli for the clay- and rock dust-fouled specimens in Figure 3.19 and Figure 3.20, respectively. The permanent deformations of the clay-fouled specimens correlate well with the LWD moduli (Figure 3.19a). The permanent deformation decreases with the increase in the LWD modulus. A drastic

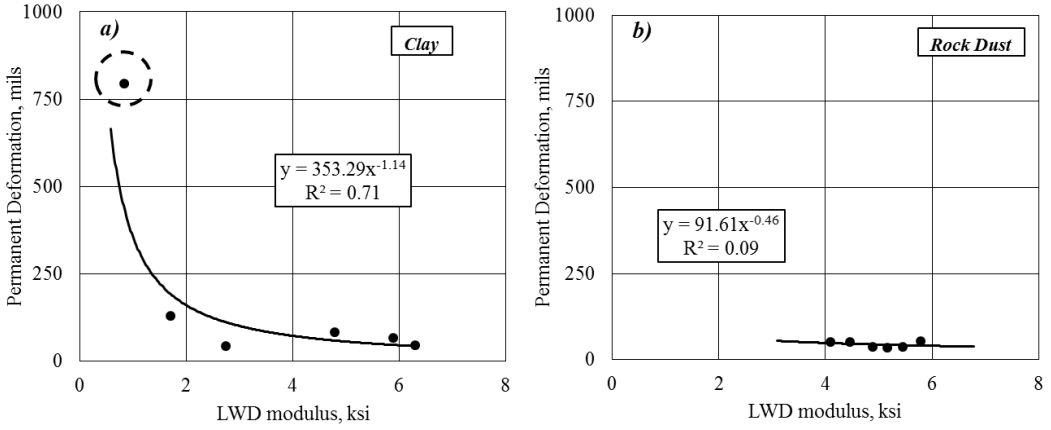

Figure 3.19. Variations in the LWD modulus and the permanent deformation of a) clay- and b) rock dust-fouled ballast specimens

increase in the permanent deformation is observed when the LWD modulus is less than 2 ksi due to excessive deformation experience by the saturated heavily-fouled specimen (Figure 3.19a). On the other hand, the permanent deformations of the rock dust-fouled specimens are independent of the LWD moduli (Figure 3.19b).

A moderate correlation (R^2=0.58) between the LD stiffness of the clay-fouled specimens and the LWD modulus can be observed in Figure 3.20a. The LD stiffness generally increases with the increase in the LWD modulus. On the other hand, the LD stiffness of the rock dust-fouled specimens does not seem to correlate with the LWD modulus at all (Figure 3.20b).

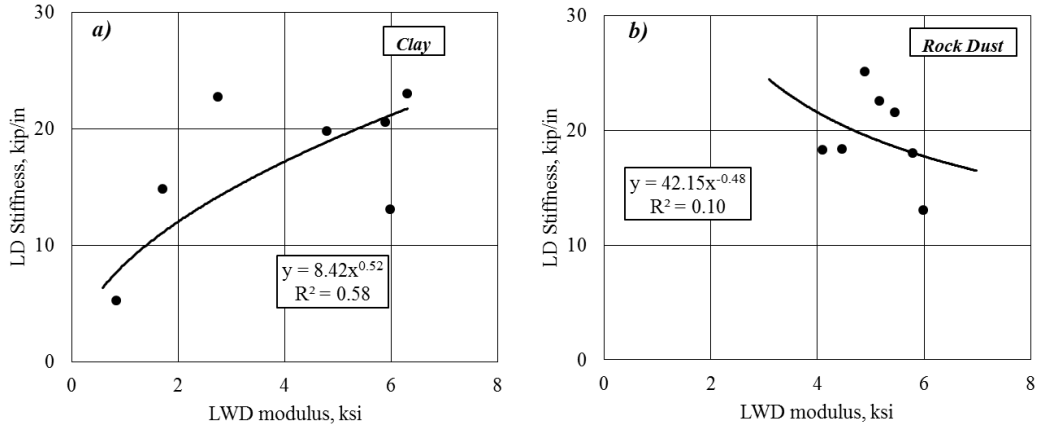

Figure 3.20. Variations in the LWD modulus and the LD stiffness of a) clay- and b) rock dust-fouled ballast specimens

3.3.6.2 Correlation between LWD and IR Tests

The nominal stress under the plate of LWD was about 34 psi. In the IR tests, the nominal stresses impacted to the medium (i.e., the tie for HTMT and HTMB cases and the ballast for HBMT and HBMB cases) with the hammer were typically 50 psi, while the nominal stresses under the tie were 5 psi, 10 psi, 14 psi and 19 psi for the preloading forces of 500 lb, 1000 lb, 1500 lb and 2000 lb, respectively. Since the nominal stress of the LWD test is more comparable with the nominal stresses associated with the highest preloading force, the results from that preloading force were used to establish correlation with the LWD modulus. Figure 3.21 shows the relationships between the LWD modulus and the IR stiffness measured with the four different source-sensor configurations of the IR tests. The fit parameters related to the power equations selected to represent the relationships, along with the associated R^2 values, are provided in Table 3.9. The clay-fouled specimens yield higher R^2 values than the rock dust-fouled specimens. The LWD modulus of the clay-fouled specimens increases with the increase in the IR stiffness. Except for

the HBMB case, the clay-fouled ballast specimens seem to have a nominal LWD modulus of 1 ksi at the IR stiffness of 4.5 kip/in. for all source-sensor configurations. The LWD modulus for the clay-fouled specimens drastically increase with the increase in the IR stiffness for the HTMT case compared with that for the HTMB and HBMT cases.

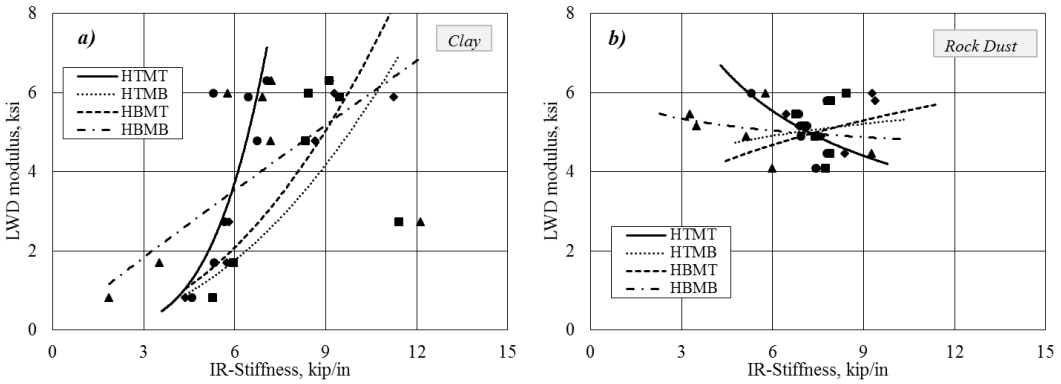

Figure 3.21. Variations in the LWD modulus and the stiffness of a) clay- and b) rock dust-fouled ballast specimens

Table 3.9. The correlation coefficients for the relationship $y=a\times x^b$ and the coefficient of determination (R^2) for the LWD test versus Impulse Response test

Fouling Agent	HTMT			HTMB			HBMT			HBMB		
	a	b	R^2	a	b	R^2	a	b	R^2	a	b	R^2
Clay	0.01	4.01	0.63	0.04	2.13	0.55	0.04	2.18	0.91	0.65	0.95	0.54
Rock Dust	15.24	-0.57	0.29	3.76	0.15	0.01	2.70	0.31	0.1	5.85	-0.08	0.05

The relationships between the LWD modulus and the IR stiffness for other preloading forces are provided in Appendix C. The LWD moduli of the clay-fouled specimens are typically correlated well with the IR stiffness for all preloading forces. On the other hand, the LWD moduli of the rock dust-fouled specimens are correlated moderately or poorly with the IR stiffness.

3.3.6.3 Correlation between Load-Deformation and IR Tests

Figure 3.22 presents the relationships between the permanent deformation and the IR stiffness of the clay- and rock dust-fouled ballast specimens for the HTMT case. The fit parameters related to the power equations selected to represent the relationships, along with the associated R^2 values, are provided in Table 3.10. The similar relationships for all other source-sensor

configurations are also provided in that table. Figure 3.22a shows that the permanent deformations of the clay-fouled specimens decrease with the increase in the IR stiffness for all preloading forces. A set of data points (marked with a dotted circle in Figure 3.22) are separated from the other measurements due to the excessive permanent deformation in the saturated heavily-fouled

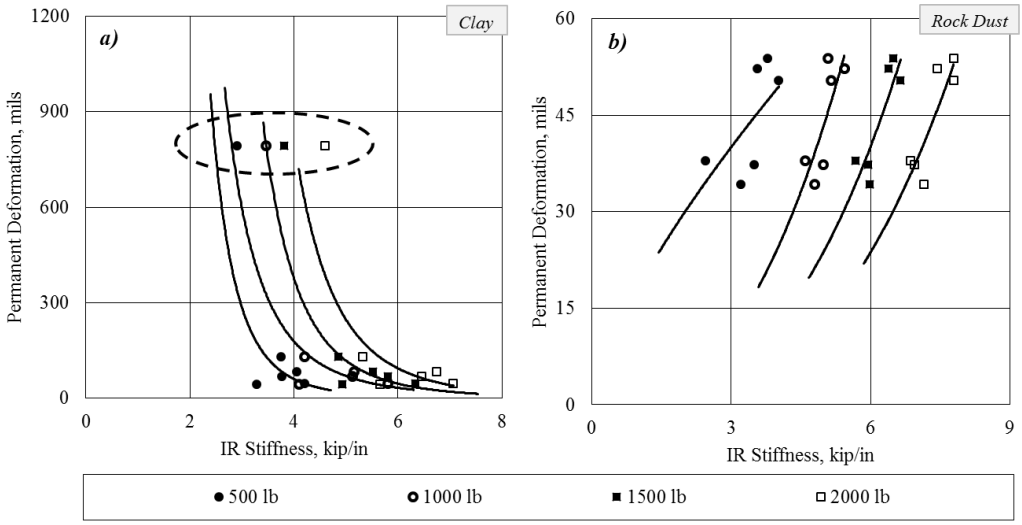

Figure 3.22. Variations in the permanent deformation and the stiffness of a) clay- and b) rock dust-fouled ballast specimens for the HTMT case

specimen. On the contrary, the permanent deformations of the rock dust-fouled specimens are minimal and increase insignificantly with the increase in the IR stiffness (see Figure 3.22b). For clay-fouled specimens, the R^2 of relationships typically increases with the increase in the preloading force for all source-sensor configurations (see Table 3.10).

Figure 3.23 shows that the LD stiffness increases with the increase in the IR stiffness for the HTMT case for all preloading forces for both clay- and rock dust-fouled specimens. Similar trends of increasing LD stiffness with the increase in the IR stiffness for other source-sensor configurations are found for clay-fouled specimens (See Table 3.11). But, for rock dust-fouled specimens, the LD stiffness decreases with the increase in the IR stiffness for other source-sensor configurations (see Table 3.11). For clay-fouled specimens, the R2 of relationships typically increases with the increase for the preloading force in all source-sensor configurations, except for the HBMB case.

For rock dust-fouled specimens, the R2 of relationships increases with the similar fashion only for the HTMT and HTMB cases (see Table 3.11).

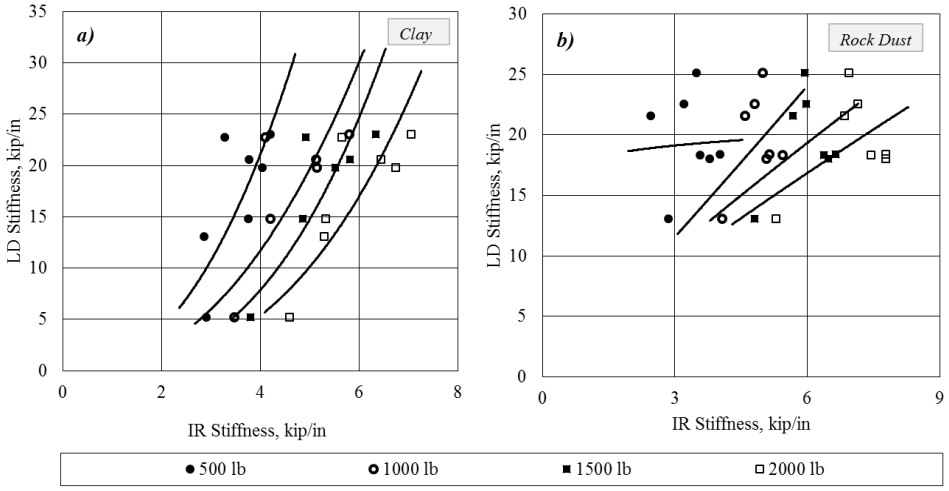

Figure 3.23. Variations in the LD stiffness and the IR stiffness of a) clay- and b) rock dust-fouled ballast specimens for the HTMT case

Table 3.10. The correlation coefficients for the relationship $y=a\times x^b$ and the coefficient of determination (R^2) for the permanent deformation and IR stiffness

Fouling Agent	Preloading force (lb)	HTMT			HTMB			HBMT			HBMB		
		a	b	R^2	a	b	R^2	a	b	R^2	a	b	R^2
Clay	500	106	-	0.48	21890.	-3.23	0.31	511.5	-1.03	0.16	1358.	-2.23	0.91
	1000	599	-	0.53	34239.	-3.17	0.66	734.7	-1.15	0.25	1555.	-1.95	0.88
	1500	505	-	0.73	204321	-3.88	0.80	2787.	-1.81	0.42	1599.	-1.72	0.90
	2000	129	-	0.64	88308.	-3.26	0.79	5749.	-2.05	0.46	1409.	-1.54	0.88
Rock Dust	500	18.1	0.72	0.39	79.80	-0.40	0.01	48.11	-0.07	0.01	24.78	0.59	0.84
	1000	0.65	2.62	0.58	0.62	2.56	0.30	2.06	1.84	0.72	23.80	0.50	0.88
	1500	0.25	2.84	0.73	0.59	2.27	0.56	2.84	1.45	0.51	20.73	0.50	0.77
	2000	0.10	3.08	0.74	0.20	2.67	0.76	4.36	1.13	0.58	21.92	0.41	0.72

Table 3.11. The correlation coefficients for the relationship $y=a\times x^b$ and the coefficient of determination (R^2) for the LD stiffness and IR stiffness

Fouling Agent	Preloading force (lb)	HTMT			HTMB			HBMT			HBMB		
		a	b	R^2	a	b	R^2	a	b	R^2	a	b	R^2
Clay	500	0.83	2.33	0.48	1.42	1.42	0.25	7.07	0.49	0.15	3.93	1.19	0.92
	1000	0.50	2.28	0.60	0.94	1.51	0.55	5.06	0.64	0.28	3.79	1.00	0.82
	1500	0.16	2.82	0.78	0.47	1.77	0.63	3.13	0.86	0.37	3.86	0.86	0.81
	2000	0.10	2.84	0.70	0.55	1.61	0.68	2.12	0.99	0.42	4.04	0.79	0.82
Rock Dust	500	17.9	0.06	0.00	96.25	-1.04	0.51	55.83	-0.68	0.45	30.78	-0.48	0.44
	1000	3.63	1.06	0.22	200.02	-1.37	0.65	242.0	-1.50	0.70	32.39	-0.41	0.51
	1500	3.98	0.88	0.21	452.66	-1.64	0.67	204.4	-1.23	0.59	34.80	-0.39	0.39
	2000	3.55	0.87	0.30	1905.7	-2.27	0.67	166.7	-1.05	0.51	29.29	-0.25	0.20

CHAPTER 4 SUMMARY AND CONCLUSION

As this dissertation is comprised of two research topics related to road base and railway ballast, the summary and conclusions of these studies are provided in the following two sections.

4.1. Summary for the Research on Base Materials

The goal of this research was to observe the mechanical responses of the contaminated base materials prepared by altering the fines content and moisture content. The specific research objectives were as follows:

- To evaluate the stiffness parameters of base materials with various fines contents and moisture contents;
- To understand the impact of the variations in fines content and moisture content of base materials on their performance;
- To develop a relationship among the stiffness parameters, fines contents and moisture content; and
- To correlate the stiffness parameters obtained from the laboratory and field methods

To achieve the stated goal and objectives, various experiments were carried out on standard (6 in. in diameter and 12 in. in height) specimens in laboratory tests and on large (36 in. in diameter and 6 in. in height) specimens in small-scale tests. The specimens for these tests were prepared with four different fines contents: 5%, 10%, 15% and 20%. The moisture contents for the tests were varied between OMC-1% and OMC+1%.

Based on the findings of the research, the following conclusions can be drawn:

- An increase in moisture content was typically detrimental to the mechanical properties of the base material. The strength and stiffness of material decreased due to increase in the moisture content. The increase in moisture content also resulted in the increase in the permanent deformation for all fines contents.

- The UCS, resilient moduli and FFRC moduli of standard specimens decreased with increase in moisture content.
- With the increase in the fines content, the UCS increased for the standard specimens prepared at OMC-1% and OMC, and the FFRC modulus increased only at OMC-1%. However, the resilient moduli were not as highly affected by the change in fines content.
- The permanent deformation of the standard specimens increased with increase in moisture content for all fines contents. The permanent deformation typically decreased with increase in fines content.
- The PSPA, LWD and cyclic moduli measured on large specimens typically decreased with increase in moisture content. The maximum PSPA moduli were achieved for specimens prepared with fines contents between 10% to 15% whereas the maximum LWD and cyclic moduli were achieved at 10% fines content.
- The cyclic moduli were also impacted by the loading area (the plate diameter) and imposed load (the peak contact pressure).
- As in the laboratory tests, the permanent deformations of the large specimens (in the small-scale tests) during cyclic stage tests increased with increase in moisture content. However, no definite pattern of deformation on the large specimens was observed.
- The stiffness values measured with the cyclic ramp load were greater than those from the continuous load.
- In the laboratory tests, the resilient moduli showed reasonably good correlation with the FFRC moduli and UCS.
- In the small-scale tests, the LWD moduli correlated reasonably well with the cyclic moduli measured with the largest plate (12 in. diameter) and highest peak contact pressure (90 psi) in the cyclic modulus tests.
- The FFRC moduli measured in the laboratory tests showed a good correlation with the PSPA moduli measured in the small-scale tests.

- The permanent deformations measured in the laboratory tests showed poor correlations with that of the small-scale tests.

4.2. Summary for the Research on Ballast

The goal of this research was to understand the behavior of clean and fouled ballast through the small-scale experiments i.e., simulated field tests in the laboratory. The specific research objectives were as follows:

- To evaluate the impacts of two types of fouling agents, clay and rock dust, on the mechanical properties of ballast;
- To measure the stiffness parameters of clean and fouled ballast at various degree of fouling and moisture contents, and;
- To understand the effects of fouling on the performance of rail tracks;

To achieve the stated goal and objectives, various experiments were carried out on the large (36 in. in diameter and 6 in. in height) specimens during the small-scale experiments. The specimens were prepared with clean and fouled ballast. The clean ballast specimens had a gradation of size number 4 as specified by the American Railway Engineering and Maintenance-of-Way. The fouled ballast specimens were prepared with two types of fouling agents: clay and rock dust. The clean ballast was mixed separately with the fouling agents in the proportion of 20% (moderately-fouled) and 50% (heavily-fouled) by weight of clean ballast to prepare fouled specimens.

Based on the findings of the research, the following conclusions can be drawn:

- The fouling agents directly impacted the physical properties of ballast by replacing the void spaces in ballast by fine particles. This resulted in reduction of the contact points in ballast. The structural integrity of ballast formed by particle interlocking and particle friction were usually disturbed by inclusion of fouling agents. Further, the increase in the moisture

content in fouled ballast, especially prepared from clay, facilitated a lubricating effect causing reduction of deformation resistance and load bearing strength.

- The high quality data, and, hence, the output for the SASW test were not available due to the limited space to place accelerometers, the intimate contact between the receivers and the ballast, and the excessive scattering of the signals from the coarse ballast particles.
- At the moderately fouled conditions, the PSPA moduli of saturated specimens prepared with clay and rock dust were less than the corresponding dry specimens. As the materials dried out to the wet condition, the moduli increased significantly. However, at the heavily fouled conditions, the PSPA moduli of both saturated and wet specimens were less than the corresponding dry specimens.
- The LWD measurements on the rock dust-fouled specimens at different degrees of fouling were almost independent of the moisture condition. The LWD moduli of the rock dust-fouled specimens were similar to that of the clean ballast. On the other hand, the LWD moduli of the heavily-fouled specimens prepared with clay measured more than half that of the clean ballast. However, the moderately-fouled specimens had moduli similar to that of the clean ballast.
- The load-deformation behaviors of clay-fouled specimens were highly sensitive to the degree of fouling and moisture content. Moreover, the heavily-fouled specimens showed significant deformation with increase in moisture content than the moderately-fouled specimens. On the other hand, the deformation of rock dust fouled specimens is essentially independent of the moisture condition. However, the moderately-fouled specimens yielded more deformation than the heavily-fouled specimens.
- The IR stiffness of ballast depended upon serval parameters such as the source-sensor configurations, the preloading forces and the index properties of ballast. Multiple linear regression analyses were carried out to understand the influences of these parameters on the IR stiffness of the specimens and develop the prediction models. The fouling

percentage has the highest influence on the IR stiffness whereas the moisture content has the least influence for all source-sensor configuration. The increase in the fouling percentage resulted in significant reduction of the IR stiffness. Based on the prediction models, the source-sensor configurations that included the sensor on the tie yielded better results than the sensor on the ballast.

- The permanent deformations and the LD stiffness correlated reasonably with the LWD moduli for clay-fouled specimens. On the contrary, the rock dust-fouled specimens had poor correlations.
- The permanent deformations decreased- and the LD stiffness increased- with the increase in the LWD moduli for clay-fouled specimens
- For the clay-fouled specimens, the LWD moduli also correlated reasonably with the IR stiffness measured for different source-sensor configurations. However, the rock dust-fouled specimens had poor correlations.
- The LWD moduli of clay-fouled specimens increased with the increase in the IR stiffness.
- The permanent deformations of the clay-fouled specimens decreased with the increase in the IR stiffness for all preloading forces. On the contrary, the permanent deformations of the rock dust-fouled specimens were minimal and increased insignificantly with the increase in the IR stiffness. For clay-fouled specimens, the R^2 of relationships typically increased with the increase in the preloading force for all source-sensor configurations.
- The LD stiffness increased with the increase in the IR stiffness for all preloading forces for clay-fouled specimens. On the hand, for rock dust-fouled specimens, the LD stiffness typically decreased with the increase in the IR stiffness for all preloading forces. For clay-fouled specimens, the R^2 of relationships typically increased with the increase of the preloading force.

REFERENCES

Alobaidi, I., and Hoare, D. J. (1996). "The development of pore water pressure at the subgrade-subbase interface of a highway pavement and its effect on pumping of fines." *Geotextiles and Geomembranes*, Elsevier, 14(2), 111–135.

Alshibli, K. A., Abu-Farsakh, M., and Seyman, E. (2005). "Laboratory Evaluation of the Geogauge and Light Falling Weight Deflectometer as Construction Control Tools." *Journal of Materials in Civil Engineering*, American Society of Civil Engineers, 17(5), 560–569.

Amiri, H. (2004). "Impact of moisture variation on stiffness response of pavements through small scale models." The University of Texas at El Paso, El Paso, TX.

Amiri, H., Nazarian, S., and Fernando, E. (2009). "Investigation of Impact of Moisture Variation on Response of Pavements through Small-Scale Models." *Journal of Materials in Civil Engineering*, American Society of Civil Engineers, 21(10), 553–560.

Anderson, J. S., and Rose, J. G. (2008). "In-Situ Test Measurement Techniques Within Railway Track Structures." *IEEE/ASME/ASCE 2008 Joint Rail Conference*, ASME, 187–207.

AREMA. (2012). *American Railway Engineering and Maintenance-of-Way Association Manual for Railway Engineering*. Lanham, Maryland.

ASCE. (2013). "Report Card for America's Infrastructure." <http://www.infrastructurereportcard.org/a/#p/rail/conditions-and-capacity> (Jan. 6, 2016).

Barskale, R. D., and Itani, S. Y. (1989). "Influence of aggregate shape on base behavior." *Transportation Research Record*, (1227), 173–182.

Bilodeau, J., Dore, G., and Pierre, P. (2009). "Pavement base unbound granular materials gradation optimization." *Bearing Capacity of Roads, Railways and Airfields. 8th International Conference*, 145–154.

De Bold, R., Connolly, D., Patience, S., and Forde, M. (2010). "Using Frequency Response Function Testing to examine a Railway Trackbed." *Transportation Research Record: Journal of the Transportation Research Board*, 1–16.

De Bold, R. P. (2011). "Non-destructive evaluation of railway trackbed ballast." The University of Edinburgh.

Brown, S. F., and Chan, F. W. K. (1996). "Reduced Rutting in Unbound Granular Pavement Layers Through Improved Grading Design." *Proceedings of the ICE - Transport*, Thomas Telford, 117(1), 40–49.

Buchanan, S. (2007). “Resilient Modulus: What, Why, and How.” *Vulcan Materials Company*, 1–13.

Calderón-Macías, C., and Luke, B. (2010). “Sensitivity studies of fundamental-and higher-mode Rayleigh-wave phase velocities in some specific near-surface scenarios.” *Advances in near-surface seismology and ground-penetrating radar*, 185–200.

Cary, C. E., and Zapata, C. E. (2010). “Enhanced model for resilient response of soils resulting from seasonal changes as implemented in mechanistic-empirical pavement design guide.” *Transportation Research Record: Journal of the Transportation Research Board*, 2170(1), 36–44.

Celaya, M., Nazarian, S., and Yuan, D. (2006). “Nondestructive Quality Control of Geo-Materials Using Seismic Methods.” *Geotechnical Special Publication*, Reston, VA; American Society of Civil Engineers; 1998, 149, 182.

Chapuis, R. P., Contant, A., and Baass, K. A. (1996). “Migration of fines in 0 20 mm crushed base during placement, compaction, and seepage under laboratory conditions.” *Canadian geotechnical journal*, NRC Research Press, 33(1), 168–176.

Cooper, K. E., Brown, S. F., and Pooley, G. R. (1985). “The Design of Aggregate Gradings for Asphalt Base courses.” *Association of Asphalt Paving Technologists Proc*, 324–346.

Dawson, A., Mundy, M., and Huhtala, M. (2000). “European research into granular material for pavement bases and subbases.” *Transportation Research Record: Journal of the Transportation Research Board*, (1721), 91–99.

Dawson, A. R., Thom, N. H., and Paute, J. L. (1996). “Mechanical characteristics of unbound granular materials as a function of condition.” *Gomes Correia, Balkema, Rotterdam*, 35–44.

DeMerchant, M. R., Valsangkar, A. J., and Schriver, A. B. (2002). “Plate load tests on geogrid-reinforced expanded shale lightweight aggregate.” *Geotextiles and Geomembranes*, 20(3), 173–190.

Ekblad, J., and Isacsson, U. (2006). “Influence of water on resilient properties of coarse granular materials.” *Road materials and pavement design*, 7(3), 369–404.

Ewins, D. J. (1984). *Modal testing: theory and practice*. Research studies press Letchworth.

Feldman, F., Nissen, D., and others. (2002). “Alternative testing method for the measurement of ballast fouling: percentage void contamination.” *CORE 2002: Cost Efficient Railways through Engineering*, Railway Technical Society of Australasia/Rail Track Association of Australia, 101.

Fleming, P., Frost, M., and Lambert, J. (2007). “Review of Lightweight Deflectometer for Routine In Situ Assessment of Pavement Material Stiffness.” *Transportation Research*

Record: Journal of the Transportation Research Board, Transportation Research Board of the National Academies, 2004, 80–87.

Fleming, P. R., Frost, M. W., Rogers, C. D. F., Thom, N. H., and Armitage, R. J. (2000). "Performance based specification for road foundation materials." *Institute of Quarrying Millennium Conference*, Bristol.

Gandara, J. A. (2004). "Characterization of Texas bases through permanent deformation testing." *University of Texas at El Paso*, El Paso, TX.

Gandara, J., and Nazarian, S. (2006). "Characterization of Rutting Potential of Texas Bases Through Laboratory and Small-Scale Tests." *Transportation Research Board 85th Annual Meeting*, 1–15.

Gautam, B., Yuan, D., Abdallah, I., and Nazarian, S. (2009). *Guidelines for using local material for roadway base and subbase*. Research Report 0-5562-1, Center for Transportation Infrastructure Systems, The University of Texas at El Paso, El Paso, TX.

Ghabchi, R., Zaman, M., Khoury, N., Kazmee, H., and Solanki, P. (2013). "Effect of gradation and source properties on stability and drainability of aggregate bases: a laboratory and field study." *International Journal of Pavement Engineering*, Taylor & Francis Group, 14(3), 274–290.

Gidel, G., Hornych, P., Chauvin, J.-J., Breysse, D., and Denis, A. (2001). "A new approach for investigating the permanent deformation behavior of unbound granular material using the Repeated Load Triaxial Apparatus." *Bulletin de Liaison des Laboratoires des Ponts et Chaussées*, 233, 5–21.

Gray, J. E. (1962). "Characteristics of graded base course aggregates determined by triaxial tests." *Engineering Research Bulletin No. 12, National Crushed Stone Association*, Alexandria, VA.

Gucunski, N., Arezoo Imani, Romero, F., Nazarian, S., Yuan, D., Wiggenhauser, H., Shokouhi, P., and Taffe, A. (2013). *Nondestructive testing to identify concrete bridge deck deterioration*. Transportation Research Board.

Habiballah, T., and Chazallon, C. (2005). "An elastoplastic model based on the shakedown concept for flexible pavements unbound granular materials." *International Journal for Numerical and Analytical Methods in Geomechanics*, 29(6), 577–596.

Han, X., and Selig, E. T. (1997). "Effects of fouling on ballast settlement." *Proc., 6th International Heavy Haul Railway Conference*.

Hicks, R. G., and Monismith, C. L. (1971). "Factors influencing the resilient response of granular materials." *Highway research record*, (345), 15–31.

Huang, C.-W., Al-Rub, R. K. A., Masad, E. A., and Little, D. N. (2010). "Three-dimensional simulations of asphalt pavement permanent deformation using a nonlinear viscoelastic and viscoplastic model." *Journal of Materials in Civil Engineering*, 23(1), 56–68.

Huang, H., Tutumluer, E., and Dombrow, W. (2009). "Laboratory Characterization of Fouled Railroad Ballast Behavior." *Transportation Research Record: Journal of the Transportation Research Board*, Transportation Research Board of the National Academies, 2117, 93–101.

Huang, Y. H. (2004). *Pavement design and analysis*. Pearson/Prentice Hall, Upper Saddle River, NJ.

Indraratna, B., Nimbalkar, S., and Tennakoon, N. (2010). "The behaviour of ballasted track foundations: track drainage and geosynthetic reinforcement." *ASCE Annual GI Conf. GeoFlorida 2010*, 2378–2387.

Ishihara, K. (1996). *Soil behaviour in earthquake geotechnics*. Oxford University Press, Oxford, UK.

Jorenby, B. N., and Hicks, R. G. (1986). "Base Course Contamination Limits." *Transportation Research Record*, (1095), 86–101.

Kaewunruen, S., and Remennikov, A. (2006). "Non-destructive testing (NDT): A tool for dynamic health monitoring of railway track structures." *Materials Australia*.

Kamal, M. A., Dawson, A. R., Farouki, O. T., Hughes, D., and Sha'at, A. A. (1993). "Field and laboratory evaluation of the mechanical behavior of unbound granular materials in pavements." *Transportation Research Record*, (1406), 88–97.

Karasahin, M., Dawson, A. R., and Holden, J. T. (1993). "Applicability of resilient constitutive models of granular material for unbound base layers." *Transportation Research Record*, (1406), 98–107.

Kaya, Z., Cetin, A., Cetin, B., Aydilek, A. H., and others. (2012). "Effect of Compaction Method on Mechanical Behavior of Graded Aggregate Base Materials." *GeoCongress 2012@ State of the Art and Practice in Geotechnical Engineering*, 1486–1494.

Kolisoja, P. (1997). "Resilient deformation characteristics of granular materials." University of Technology, Tampere, Finland.

Konrad, J.-M., and Lemieux, N. (2005). "Influence of fines on frost heave characteristics of a well-graded base-course material." *Canadian geotechnical journal*, NRC Research Press, 42(2), 515–527.

Lekarp, F. (1999). "Resilient and permanent deformation behavior of unbound aggregates under repeated loading." Royal Institute of Technology, Stockholm, Sweden.

Lekarp, F., Isacsson, U., and Dawson, A. (2000). "State of the art. I: Resilient response of unbound aggregates." *Journal of Transportation Engineering*, 126(1), 66–75.

Li, T., and Baus, R. L. (2005). "Nonlinear Parameters for Granular Base Materials from Plate Tests." *Journal of Geotechnical and Geoenvironmental Engineering*, American Society of Civil Engineers, 131(7), 907–913.

Malla, R. B., and Joshi, S. (2008). "Subgrade resilient modulus prediction models for coarse and fine-grained soils based on long-term pavement performance data." *International Journal of Pavement Engineering*, 9(6), 431–444.

Mazari, M., Navarro, E., Abdallah, I., and Nazarian, S. (2014). "Comparison of numerical and experimental responses of pavement systems using various resilient modulus models." *Soils and Foundations*, 54(1), 36–44.

Nazarian, S. (2012). "Shear Wave Velocity Profiling with Surface Wave Methods." *Geotechnical Engineering State of the Art and Practice@ sKeynote Lectures from GeoCongress 2012*, ASCE, 221–240.

Nazarian, S., Mazari, M., Abdallah, I. N., Puppala, A. J., and Mohammad, L. N. (2014). *Modulus-based construction specification for compaction of earthwork and unbound aggregate. Transportation Research Board, Draft Interim Report for NCHRP Project 10-84.*

Nazarian, S., and Reddy, S. (1996). "Study of Parameters Affecting Impulse Response Method." *Journal of Transportation Engineering*, American Society of Civil Engineers, 122(4), 308–315.

Nazarian, S., Reddy, S., and Baker, M. (1994). "Determination of voids under rigid pavements using impulse response method." *STP*, 1198, 473–487.

Nazarian, S., and Stokoe, K. H. (1985). "In Situ Determination of Elastic Moduli of Pavement Systems by Spectral-analysis-of-surface-waves Method." (Federal Highway Administration), 1–190.

Nazarian, S., Yuan, D., and Williams, R. R. (2003). "A simple method for determining modulus of base and subgrade materials." *ASTM Special Technical Publication*, 1437, 152–164.

Nohl, J., and Domnick, B. (2000). "Stockpile Segregation." *Technical Paper T-551, Superior Industries*, Morris, Minnesota.

NTSB. (2013). "National Transportation Safety Board Railroad Accident Brief: Metro-North Railroad Derailment." <http://www.ntsb.gov/investigations/AccidentReports/Reports/RAB1411.pdf> (Jun. 1, 2016).

Pan, T., Tutumluer, E., and Anochie-Boateng, J. (2006). "Aggregate morphology affecting resilient behavior of unbound granular materials." *Transportation Research Record: Journal of the Transportation Research Board*, (1952), 12–20.

Parsons, R., Rahman, A., and Han, J. (2012). *Properties of Fouled Railroad Ballast*. Washington D.C.

Piratheepan, J., Gnanendran, C. T., and Lo, S.-C. R. (2010). "Characterization of Cementitiously Stabilized Granular Materials for Pavement Design Using Unconfined Compression and IDT Testings with Internal Displacement Measurements." *Journal of Materials in Civil Engineering*, American Society of Civil Engineers, 22(5), 495–505.

Von Quintus, H. L., Rao, C., Minchin, R. E., Nazarian, S., Maser, K. R., and Prowell, B. (2009). *NDT technology for quality assurance of HMA pavement construction*. Transportation Research Board.

Von Quintus, H., and Killingsworth, B. (1998). *Analyses relating to pavement material characterizations and their effects on pavement performance*. Federal Highway Administration, McLean, VA.

Raad, L., Minassian, G. H., and Gartin, S. (1992). *Characterization of saturated granular bases under repeated loads*. Transportation Research Record 1369, Washington, D.C.

Rauch, A. F., Haas, C. T., Kim, H., and Browne, C. (2000). "Rapid Test to Establish Grading of Unbound Aggregate Products: Evaluation of Potential Aggregate Grading Technologies." *ICAR Technical Reports*.

Richart, F. E., Hall, J. R., and Woods, R. D. (1970). "Vibrations of soils and foundations."

Richter, C. A. (2006). "Seasonal variations in the moduli of unbound pavement layers." Report No. FHWA-HRT-04-079, Federal Highway Administration, U.S. Department of Transportation.

Roberts, R., Rudy, J., and Gssi, S. (2006). "Railroad ballast fouling detection using ground penetrating radar. A new approach based on scattering from voids." *European Conference on Nondestructive Testing*, 1(5).

Saeed, A., Hall, J. W., and Barker, W. (2001). "NCHRP Report 453: Performance-Related Tests of Aggregates for Use in Unbound Pavement Layers." *Transportation Research Board, National Research Council, Washington, DC*, 1–56.

Salehi, R., Little, D., and Masad, E. (2008). "Material Factors That Influence Anisotropic Behavior of Aggregate Bases." *Transportation Research Record: Journal of the Transportation Research Board*, Transportation Research Board of the National Academies, 2059, 20–30.

Santha, B. (1994). "Resilient modulus of subgrade soils: comparison of two constitutive equations." *Transportation Research Record*, (1462), 79–90.

Sawangsuriya, A., Bosscher, P. J., and Edil, T. B. (2006). "Alternative Testing Techniques for Modulus of Pavement Bases and Subgrades." *13th Great Lakes Geotechnical and Geoenvironmental Conference*, 108–121.

Schnaid, F., Prietto, P. D. M., and Consoli, N. C. (2001). "Characterization of Cemented Sand in Triaxial Compression." *Journal of Geotechnical and Geoenvironmental Engineering*, American Society of Civil Engineers, 127(10), 857–868.

Selig, E. T., and Waters, J. M. (1994). *Track geotechnology and substructure management*. Thomas Telford.

Stokoe, K. H., Wright, S. G., Bay, J. A., and Roesset, J. M. (1994). "Characterization of geotechnical sites by SASW method." *Geophysical characterization of sites*, 15–25.

Sweere, G. T. H. (1990). "Unbound granular bases for roads." TU Delft, Delft University of Technology.

Thom, N. H., and Brown, S. F. (1988). "The effect of grading and density on the mechanical properties of a crushed dolomitic limestone." *Australian Road Research Board (ARRB) Conference, 14th, 1988, Canberra*, 94–100.

Thompson, M. R., and Smith, K. L. (1990). "Repeated triaxial characterization of granular bases." National Research Council, Washington, D.C., 7–17.

Tian, P., Zaman, M., and Laguros, J. (1998). "Gradation and moisture effects on resilient moduli of aggregate bases." *Transportation Research Record: Journal of the Transportation Research Board*, (1619), 75–84.

Tutumluer, E. (2013). *Practices for unbound aggregate pavement layers*. NCHRP Synthesis 445, National Cooperative Highway Research Program, Transportation Research Board, Washington, D.C.

Tutumluer, E., and Seyhan, U. (2000). "Effects of fines content on the anisotropic response and characterization of unbound aggregate bases." *Proceedings of the Unbound Aggregates in Roads (UNBAR5) Symposium, University of Nottingham, England*.

USACE. (2014). *U.S. Army Corps of Engineers Railroad Design and Rehabilitation Manual*. Washington, DC.

Wen, H., Warner, J., Edil, T., and Wang, G. (2010). "Laboratory Comparison of Crushed Aggregate and Recycled Pavement Material With and Without High Carbon Fly Ash." *Geotechnical and Geological Engineering*, 28(4), 405–411.

White, D. J., Morris, M., and Thompson, M. (2006). “Power-Based Compaction Monitoring Using Vibratory Padfoot Roller.” *GeoCongress 2006*, 1–6.

Williams, R. R., and Nazarian, S. (2007). “Correlation of Resilient and Seismic Modulus Test Results.” *Journal of Materials in Civil Engineering*, American Society of Civil Engineers, 19(12), 1026–1032.

Yau, A., and Quintus, H. L. Von. (2002). “Study of LTPP laboratory resilient modulus test data and response characteristics.” Report No. FHWA-RD-02-051, Federal Highway Administration, Austin, TX.

Yideti, T. F., Birgisson, B., Jelagin, D., and Guarin, A. (2014). “Packing theory-based framework for evaluating resilient modulus of unbound granular materials.” *International Journal of Pavement Engineering*, Taylor & Francis, 15(8), 689–697.

Yuan, D., and Nazarian, S. (1992). “Rapid Determination of Layer Properties of Pavements from Surface Wave Method.” *Transportation Research Record*, (1377), 159–166.

Yuan, D., and Nazarian, S. (2003). “Variation in moduli of base and subgrade with moisture.” *Transportation Research Board 82nd Annual Meeting, Washington, DC*, 12–16.

APPENDIX

Appendix A: Impulse Response Test

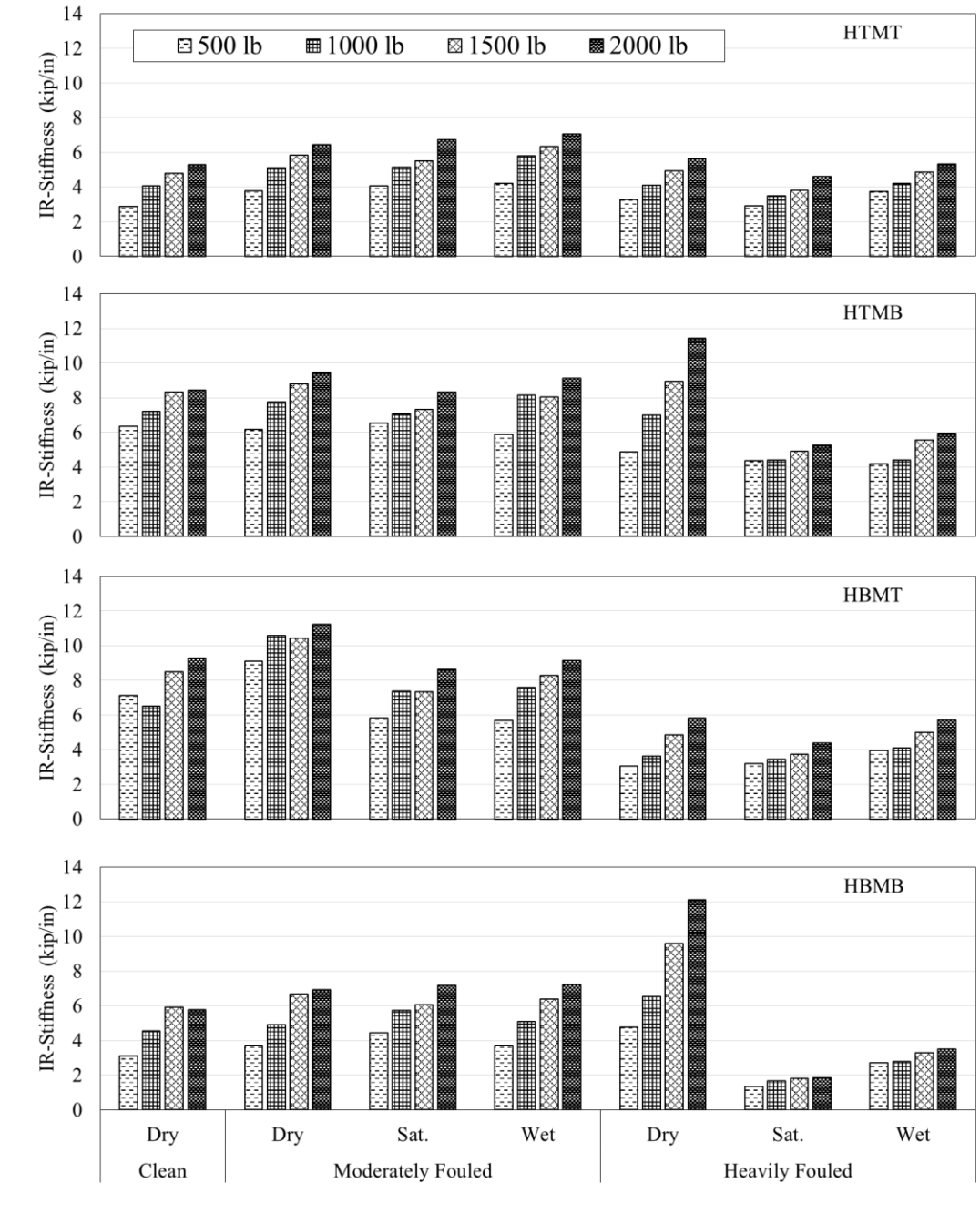

Figure A1. Stiffness measured from Impulse Response tests of clay-fouled ballast

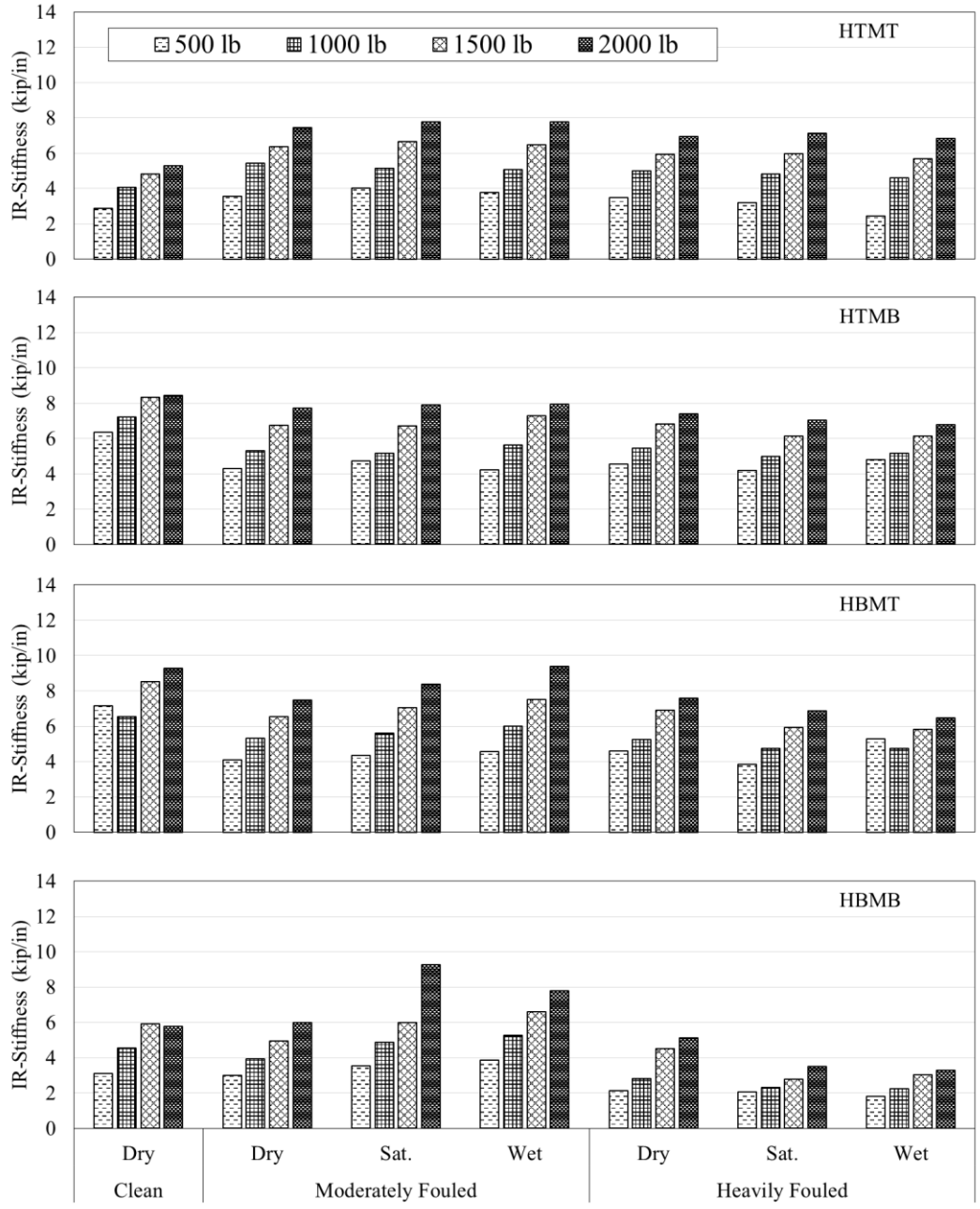

Figure A2. Stiffness measured from Impulse Response tests for rock dust-fouled ballast

Table A1. The standardized β coefficient, p-value and rank of independent variables (with all test parameters)

Parameters	HTMT			HTMB			HBMT			HBMB		
	R*	β	p-value	R*	β	p-value	R*	β	p-value	R*	β	p-value
Preloading Force (kips)	3	0.82	0.00	4	0.66	0.00	5	0.51	0.00	5	0.53	0.00
Fouling Agent PI	4	0.77	0.00	5	0.48	0.00	4	0.78	0.00	4	0.60	0.01
Fouling Percent, %	1	-2.98	0.00	1	1.31	0.15	2	1.55	0.03	1	-3.65	0.01
Fouling Index, %	5	0.32	0.22	3	-1.01	0.01	1	-1.74	0.00	3	1.19	0.04
Moisture Content (%)	6	-0.04	0.34	6	-0.29	0.00	6	-0.20	0.00	6	-0.28	0.01
Dry density (pcf)	2	2.58	0.00	2	-1.15	0.09	3	-1.21	0.02	2	2.49	0.01

Note: R= Rank showing the relative contributions of each of test parameter*

Appendix B: Comparison of PSPA Test with Other Tests

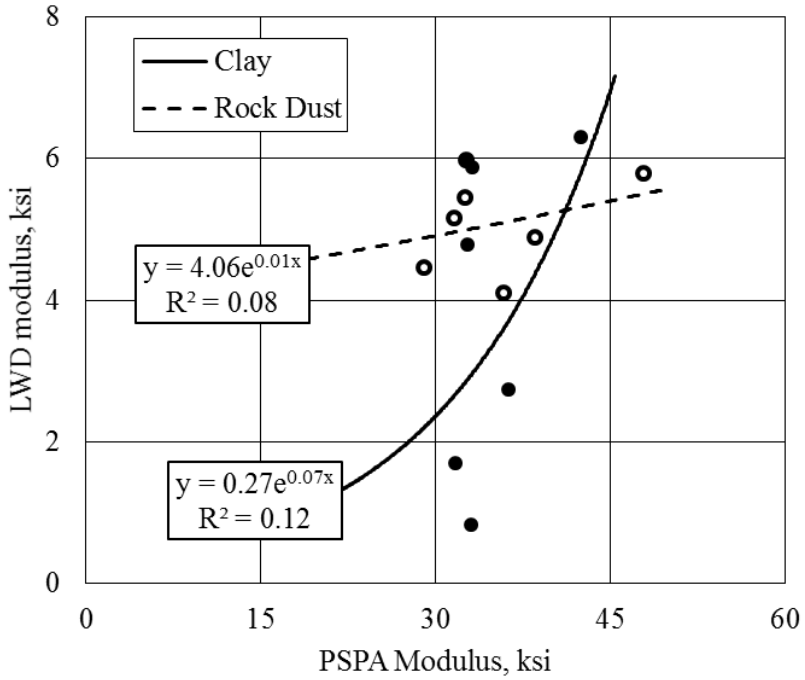

Figure B1. Variations in the LWD and PSPA moduli of clay- and rock dust-fouled ballast specimens

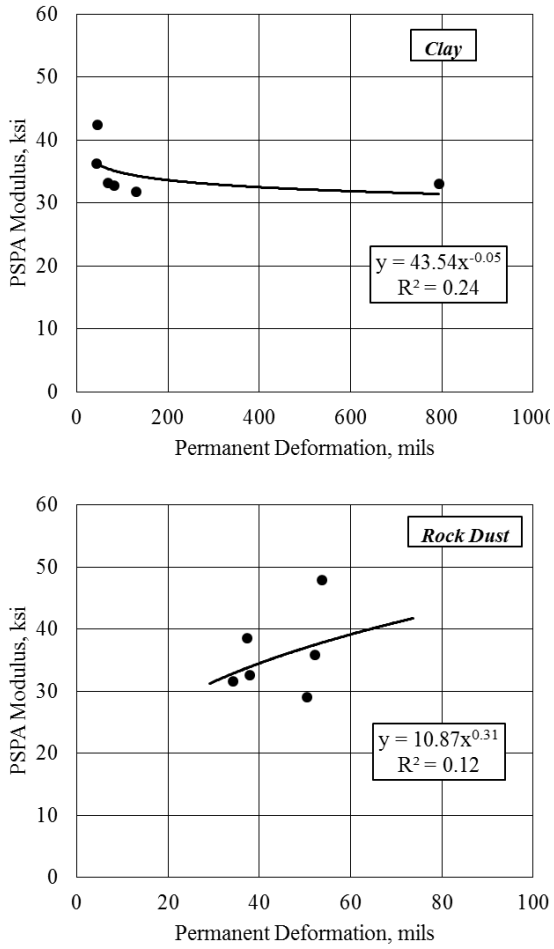

Figure B2. Variations in the PSPA modulus and the Permanent deformation of clay- and rock dust-fouled ballast specimens

Table B1. The correlation coefficients for the relationship $y=a\times x^b$ and the coefficient of determination (R^2) for the PSPA and Impulse Response tests

Fouling Agent	Preloading Force (lb)	HTMT			HTMB			HBMT			HBMB		
		a	b	R2	a	b	R2	a	b	R2	a	b	R2
Clay	500	24.78	0.26	0.16	29.49	0.09	0.03	35.07	-0.01	0.01	31.56	0.07	0.1
	1000	21.77	0.30	0.29	23.58	0.20	0.27	32.34	0.04	0.02	30.76	0.08	0.14
	1500	20.11	0.33	0.29	24.90	0.16	0.14	31.43	0.05	0.03	30.63	0.07	0.15
	2000	18.72	0.35	0.28	24.03	0.17	0.21	30.89	0.05	0.03	30.55	0.07	0.17
Rock Dust	500	25.42	0.27	0.08	64.30	-0.39	0.12	39.19	-0.07	0.01	29.51	0.17	0.09
	1000	16.17	0.49	0.08	27.98	0.13	0.01	18.23	0.39	0.08	29.58	0.13	0.09
	1500	18.48	0.36	0.06	16.11	0.40	0.07	18.80	0.32	0.07	26.36	0.19	0.14
	2000	18.85	0.32	0.06	16.86	0.36	0.03	13.88	0.45	0.15	29.53	0.10	0.05

Appendix C: Comparison of LWD and Impulse Response Tests

Table C1. The correlation coefficients for the relationship $y=a\times x^b$ and the coefficient of determination (R^2) for the LWD and Impulse Response tests

Fouling Agent	Preloading Force (lb)	HTMT			HTMB			HBMT			HBMB		
		a	b	R2	a	b	R2	a	b	R2	a	b	R2
Clay	500	0.20	2.21	0.19	0.01	3.78	0.81	0.28	1.52	0.65	0.64	1.41	0.58
	1000	0.02	3.41	0.61	0.02	2.78	0.85	0.22	1.54	0.73	0.49	1.34	0.67
	1500	0.01	4.01	0.71	0.01	2.82	0.73	0.08	1.96	0.88	0.53	1.13	0.63
	2000	0.01	4.01	0.63	0.04	2.13	0.55	0.04	2.18	0.91	0.65	0.95	0.54
Rock Dust	500	8.22	-0.40	0.23	2.55	0.45	0.22	2.62	0.43	0.41	5.17	-0.02	0.01
	1000	29.94	-1.12	0.59	1.78	0.62	0.31	2.56	0.40	0.12	5.10	0.00	0.01
	1500	20.32	-0.78	0.38	1.78	0.55	0.17	2.47	0.37	0.13	5.06	0.00	0.01
	2000	15.24	-0.57	0.29	3.76	0.15	0.01	2.70	0.31	0.1	5.85	-0.08	0.05

VITA

Prajwol earned his Bachelor degree in Civil Engineering from Pulchowk Campus, Institute of Engineering, Tribhuvan University, Nepal in 2006. After graduation, he worked in private companies and Government of Nepal for designing buildings and micro-hydro power structures. Later he came to the US in 2009 to purse his Master's degree in Civil Engineering from the University of Nevada Las Vegas. During his Master's degree, Prajwol worked as a Teaching Assistant and Research Assistant and researched on the areas of Geotechnical engineering and Geophysics. He also worked as a research engineer at the Dissert Research Institute, Las Vegas, Nevada in summer of 2010. Prajwol earned his Master's degree in 2011 and returned back home. He was involved in teaching and administrative jobs, and running an engineering consulting firm. In August 2013, he joined the doctoral program in Civil Engineering at The University of Texas at El Paso (UTEP) under the supervisory of Prof. Soheil Nazarian. Prajwol has had the opportunity to work as a graduate research associate on several research projects at the Center for Transportation Infrastructure Systems (CTIS). Throughout his academic career at UTEP, Prajwol maintained 4.0 GPA and honored with International Road Federation (IRF) Fellowship in 2015 from IRF and Anita Mochen Loya Scholarship in 2015 and 2016 from College of Engineering, UTEP. Prajwol is the founding president for Transportation Leadership Council (TLC) and Nepalese Student Association (NSA) at UTEP. He is also a member of American Society of Civil Engineers, Golden Key International Honors Society and more. His dissertation mainly focused on the impacts of contamination on the road base and railway ballast.

Contact Information: ptamrakar@miners.utep.edu | prajwol.tamrakar@gmail.com

This dissertation was typed by Prajwol Tamrakar